

Nonlinear Finite Element Analysis of Thin-Walled Cylindrical  
Shells  
Subject to Pure Bending

by

Douglas J. Petrick

A thesis  
presented to the University of Manitoba  
in partial fulfillment of the  
requirements for the degree of  
Master of Science in Civil Engineering  
in  
Department of Civil Engineering

Winnipeg, Manitoba

(c) Douglas J. Petrick, 1985

NONLINEAR FINITE ELEMENT ANALYSIS OF THIN-WALLED  
CYLINDRICAL SHELLS SUBJECT TO PURE BENDING

BY

DOUGLAS J. PETRICK

A thesis submitted to the Faculty of Graduate Studies of  
the University of Manitoba in partial fulfillment of the requirements  
of the degree of

MASTER OF SCIENCE

© 1985

Permission has been granted to the LIBRARY OF THE UNIVER-  
SITY OF MANITOBA to lend or sell copies of this thesis, to  
the NATIONAL LIBRARY OF CANADA to microfilm this  
thesis and to lend or sell copies of the film, and UNIVERSITY  
MICROFILMS to publish an abstract of this thesis.

The author reserves other publication rights, and neither the  
thesis nor extensive extracts from it may be printed or other-  
wise reproduced without the author's written permission.

## ABSTRACT

The local buckling of thin-walled fabricated steel cylinders loaded in pure flexure is investigated. Analyses to predict inelastic buckling of these shells are conducted using the finite element technique. The program used, NISABO, includes both material and geometric nonlinearities in the prediction of the limit load.

A rational technique is developed to incorporate initial imperfections into the analyses. A previous experimental investigation conducted at the University of Alberta in 1981, provided the initial data base for this investigation.

The investigation here in involved a series of nonlinear analysis on various mesh configurations. Results from these analyses are compared with the University of Alberta testing of two flexurally loaded cylinders fabricated from 3.4-mm and 5-mm plate and approximately 1525 mm in diameter.

On the basis of the limited amount of test evidence available for the flexurally loaded fabricated cylinders, the results of the nonlinear analysis are acceptable. The nonlinear finite element technique incorporating initial imperfections, is a reliable means of predicting the limit point load of a flexurally loaded fabricated cylinder.

Further experimental study is required to establish a larger data base for the flexural buckling strength of fabricated steel tubes. Additional testing is required to determine the effects of residual stresses on the buckling strength of thin-walled tubes with large  $R/t$  ratios.

## ACKNOWLEDGEMENTS

The author would like to express his sincere thanks and appreciation to his advisor, Dr. R. B. Pinkney. The guidance, encouragement, and friendship provided by Dr. Pinkney are gratefully acknowledged and will long be remembered.

The author would like to thank Professor J. Glanville and Professor A.B. Thornton-Trump for their comments and suggestions during the preparation of this thesis. He expresses his thanks to Mrs. M. Innes for her typing of the manuscript. He would like to thank Mr. H. Laube for his assistance in computer programming.

The financial assistance provided by the Natural Science and Engineering Research Council of Canada is gratefully acknowledged.

The author wishes to thank his colleagues Harold, Bruce and Alan, for their advice and assistance throughout the thesis. He also wishes to express his sincere appreciation to Dean Brandt, Marge Brandt, and Richard Parsons of Jacobson Elevator Builders Ltd. Their thoughtfulness, and assistance in completing this thesis are gratefully acknowledged.

Finally the author wishes to express his deepest thanks and gratitude to his parents, grandmother Petrick, and

brother Richard. Their encouragement, guidance and unselfish sacrifices over the past six years have made this all possible.

## CONTENTS

ABSTRACT . . . . .	iv
ACKNOWLEDGEMENTS . . . . .	vi

<u>Chapter</u>	<u>page</u>
I. INTRODUCTION . . . . .	1
Thin-walled Tubular Members . . . . .	1
Statement of the Problem . . . . .	3
Objectives . . . . .	4
II. REVIEW OF LOCAL INSTABILITY . . . . .	5
Introduction . . . . .	5
Local Buckling in Cylindrical Shells . . . . .	6
Bending Stability . . . . .	8
Inelastic Buckling . . . . .	11
Residual Stresses . . . . .	12
Large Displacement Theory . . . . .	14
Summary . . . . .	17
III. NONLINEAR FINITE ELEMENT ANALYSIS . . . . .	21
Introduction . . . . .	21
Nonlinear F.E.M. From A Linear Perspective . . . . .	21
NISA80 Program . . . . .	27
Shell Modelling . . . . .	30
IV. INITIAL IMPERFECTIONS . . . . .	40
Introduction . . . . .	40
Available Experimental Data . . . . .	41
Introduction . . . . .	41
Experimental Data . . . . .	41
Measurement Procedure . . . . .	42
Adjustment to Define the Perfect Cylinder . . . . .	43
Development of the Interpolated Surface . . . . .	50
Introduction . . . . .	50
Spline Model . . . . .	51
End Region Imperfections . . . . .	52
Introduction . . . . .	52
End Region Extrapolation . . . . .	53
Incorporation of the Weld Depressions . . . . .	54
Developed Plots of the Interpolated Surface . . . . .	55

V.	GEOMETRIC IMPERFECTIONS . . . . .	61
	Introduction . . . . .	61
	Incorporation of Initial Imperfections . . . . .	62
	Eccentric Junctions of the Shells . . . . .	64
VI.	RESULTS OF THE NONLINEAR FINITE ELEMENT ANALYSIS . . . . .	67
	Introduction . . . . .	67
	Eigenvalue Solutions . . . . .	67
	Eccentric Junctions . . . . .	69
	Mesh Refinements . . . . .	70
	Nonlinear Imperfect Shell Solution . . . . .	72
	Magnitude of Initial Imperfections . . . . .	74
VII.	DISCUSSION . . . . .	86
	Introduction . . . . .	86
	Initial Imperfections . . . . .	86
	Achieving the Limit Point Load . . . . .	88
VIII.	CONCLUSIONS AND RECOMMENDATIONS . . . . .	91
	Conclusions . . . . .	91
	Recommendations . . . . .	92
<u>Appendix</u>		<u>page</u>
A.	MOMENT-CURVATURE . . . . .	93
B.	SUPPORTING COMPUTER PROGRAMS . . . . .	108
	Cylinder . . . . .	109
	Gen . . . . .	117
	Seam . . . . .	122
	Graph . . . . .	124
	Plotsur . . . . .	125
	Model . . . . .	127
	Adddisp . . . . .	135
	Loads . . . . .	139
	Nisaplot . . . . .	142
	BIBLIOGRAPHY . . . . .	150

## LIST OF TABLES

<u>Table</u>	<u>page</u>
6.1. Eigenvalue Solutions . . . . .	76
6.2. Nonlinear Solutions of Specimen B1 . . . . .	76
6.3. Effect of Increased Nodal Imperfections on the Buckling Moment . . . . .	84
6.4. Effect of Increased Nodal Imperfections on the Buckling Moment . . . . .	85
A.1. Moment vs Curvature B1S3.N1 . . . . .	94
A.2. Moment vs Curvature B1S3.N2 . . . . .	95
A.3. Moment vs Curvature B1S3.N3 . . . . .	96
A.4. Moment vs Curvature B1S3.N4 . . . . .	97
A.5. Moment vs Curvature B1S4.N1 . . . . .	98
A.6. Moment vs Curvature B1S5.N1 . . . . .	99
A.7. Moment vs Curvature B1S7.N1 . . . . .	100
A.8. Moment vs Curvature B1S7.N2 . . . . .	101
A.9. Moment vs Curvature B1S7.N3 . . . . .	102
A.10. Moment vs Curvature B2S3.N1 . . . . .	103
A.11. Moment vs Curvature B2S7.N1 . . . . .	104
A.12. Moment vs Curvature B2S7.N2 . . . . .	105
A.13. Moment vs Curvature B2S7.N3 . . . . .	106
A.14. Moment vs Curvature B2S7.N4 . . . . .	107

## LIST OF FIGURES

<u>Figure</u>	<u>page</u>
2.1. Correlation Factor . . . . .	19
2.2. Correlation Factor . . . . .	19
2.3. Comparison of Buckling Strength . . . . .	20
3.1. Constant-Arc-Length Method after Ramm (28) . . . . .	33
3.2. Shell Model . . . . .	33
3.3. Mesh Configuration S3 . . . . .	34
3.4. Mesh Configuration S4 . . . . .	35
3.5. Mesh Configuration S5 . . . . .	36
3.6. Mesh Configuration S6 . . . . .	37
3.7. Mesh Configuration S7 . . . . .	38
3.8. Mesh Configuration S8 . . . . .	39
4.1. Experimental Prototype . . . . .	56
4.1. Axis Rotation and Translation . . . . .	56
4.3. Adjusted Data Points in Central Region . . . . .	57
4.4. Extrapolated Straight-Line Generators . . . . .	57
4.5. Cicumferential Weld Imperfection . . . . .	58
4.6. Interpolated Surface Map B1 . . . . .	59
4.7. Interpolated Surface Map B2 . . . . .	60
5.1. Shell Junctions of Different Wall Thickness . . . . .	66
5.2. Eccentric Shell Intersections . . . . .	66
6.1. Mode Shape 1 B1S3.E1 . . . . .	77
6.2. Mode Shape 1 B1S5.E1 . . . . .	77

6.3.	Mode Shape 1	B1S4.E1	. . . . .	78
6.4.	Mode Shape 1	B1S6.E1	. . . . .	78
6.5.	Mode Shape 1	B1S7.E1	. . . . .	79
6.6.	Mode Shape 1	B1S8.E1	. . . . .	79
6.7.	Mode Shape 1	B2S3.E1	. . . . .	80
6.8.	Mode Shape 1	B2S7.E1	. . . . .	80
6.9.	Shell Alignment		. . . . .	81
6.10.	Local Buckling of	B1S4.N1	. . . . .	82
6.11.	Buckled Region of	B1S4.N1	. . . . .	82
6.12.	Failure Deformations of	B1S7.N1	. . . . .	83
6.13.	Failure Deformations of	B2S7.N1	. . . . .	83
6.14.	Scale Factor vs Moment	B1S3	. . . . .	84
6.15.	Scale Factor vs Moment	B2S7	. . . . .	85
A.1.	Moment vs Curvature	B1S3.N1	. . . . .	94
A.2.	Moment vs Curvature	B1S3.N2	. . . . .	95
A.3.	Moment vs Curvature	B1S3.N3	. . . . .	96
A.4.	Moment vs Curvature	B1S3.N4	. . . . .	97
A.5.	Moment vs Curvature	B1S4.N1	. . . . .	98
A.6.	Moment vs Curvature	B1S5.N1	. . . . .	99
A.7.	Moment vs Curvature	B1S7.N1	. . . . .	100
A.8.	Moment vs Curvature	B1S7.N2	. . . . .	101
A.9.	Moment vs Curvature	B1S7.N3	. . . . .	102
A.10.	Moment vs Curvature	B2S3.N1	. . . . .	103
A.11.	Moment vs Curvature	B2S7.N1	. . . . .	104
A.12.	Moment vs Curvature	B2S7.N2	. . . . .	105
A.13.	Moment vs Curvature	B2S7.N3	. . . . .	106
A.14.	Moment vs Curvature	B2S7.N4	. . . . .	107

## LIST OF SYMBOLS

$a, b, c$	estimate of the unknown curve-fitting parameters
$a_0, b_0, c_0$	next available approximation of curve-fitting parameters
$a_1$	extracted scale factor
$E$	modulus of elasticity
$E$	secant modulus of elasticity
$E$	tangent modulus of elasticity
$F$	condition equation
$F$	reduced condition equation
$l$	length of the cylinder
$r$	radius of gyration
$R$	radius of the shell wall
$S$	sum of the squares of the residuals
$t$	thickness of the shell wall
$v$	displacement vector of the nodal imperfections
$x, y$	global reference axes of the cylinder cross section
$z$	global reference axis of the cylinder's longitudinal direction
$x', y'$	reference axes adjusted for tilt about the global $z$ axis
$z'$	reference axis same as the global $z$ axis
$x'', y'', z''$	reference axes of the perfect cylinder
$x_i, y_i$	adjusted $x, y$ coordinate
$X_i, Y_i$	measured $x, y$ coordinate
$V_{x_i}, V_{y_i}$	residual $x$ & $y$ component

$w_{x_1}, w_{y_1}$  weight of the x & y coordinate  
X, Y surface coordinate in direction 1, direction 2  
XL, YL surface coordinate of interpolated value in direction 1, direction 2  
NX number of observed points in direction 1  
NY number of observed points in direction 2  
NXY number of interpolated points in direction 1  
NYL number of interpolated points in direction 2  
FL interpolated function value  
S approximating spline function  
S' first derivative of the approximating spline  
S'' second derivative of the approximating spline  
 $\alpha$  angle between the global x axis and the adjusted x' axis  
 $\beta$  angle between the global z axis and the adjusted z'' axis  
 $\gamma$  correlation factor  
plasticity correction term  
 $\phi$  eigenvector

Chapter I  
INTRODUCTION

1.1 THIN-WALLED TUBULAR MEMBERS

The use of thin-walled tubular members constructed from steel sheets is growing in application in civil engineering structures. The need for increased knowledge concerning the complex structural stability of these shells is in direct response to this growth. Exhaustive investigation by Yamaki (1) has provided a complete solution to the problem of buckling in cylindrical shells subjected to compression, torsion, and pressure. However, to date only a few investigations have focussed attention on the interaction of pure bending and the buckling phenomenon. In this investigation an analysis is conducted into the stresses produced by pure bending and their effect on the local buckling of thin-walled tubular members.

Thin-walled structures fabricated from cold-formed steel plates consist of stiffened and unstiffened cylinders with small thickness-to-radius ratios  $t/R$ . Tubular steel structures, in most cases, are space-type structures. Cylindrical forms of such structures with large diameter-to-thickness ratios  $D/t$  are most often referred to as shells.

Tubular shells offer several advantages, as explained by Troitsky (2):

1. Structurally, the shell is very efficient:

- a continuous medium which permits a high portion of the material to be used to capacity;
- material is distributed along the perimeter providing a large radius of gyration;
- stability of a circular cylinder is optimum in all directions compared to other available sections;
- substantially smaller aerodynamic and hydrodynamic resistances;
- minimal perimeter of contact leading to reduced maintenance against corrosion compared to a section of equal cross sectional area, such as a wide-flange beam

2. The cylindrical shell has the capacity to perform technological functions and simultaneously to serve as a carrying structure:

- conveyor galleries and pipelines both act in this manner.

3. Ease of Fabrication:

- the advantages are numerous but the introduction of sophisticated welding techniques provided a benchmark in their extensive use.

The most difficult area in the design of tubular shells is the assessment of stability requirements. Thin-walled cylindrical shells may fail either by the instability of the shell as a whole, involving bending of the axis, or by the local instability of the wall of the shell. This report will deal with the latter type of failure, commonly called local buckling or wrinkling.

## 1.2 STATEMENT OF THE PROBLEM

Current North American code specifications (3),(4),(5). base design recommendations on empirical local-buckling-strength equations established from tests on sharp-yielding mild steel cylinders. Recently, a distinction has been made (Baker et al. (6)) between local buckling strength of cylindrical members subjected to uniform axial compression and that of such members subjected to flexural loading. Unfortunately these formulations do not predict the response of the structure in the plastic range of analysis. Furthermore these formulations are based on limited data available for flexurally loaded tubular steel members. These data show a large degree of scatter, and to date no unified theory exists to explain the observed experimental behaviour (Baker et al. (6)). Hence there exists a great deal of uncertainty in the prediction of local buckling behaviour of thin-walled cylindrical shells subjected to flexure.

### 1.3 OBJECTIVES

The objective of this study is to predict analytically the nonlinear response of cylindrical shell specimens subjected to pure bending, tested in a previous experimental investigation at the University of Alberta (7). By comparing the limit point load of the experimental investigation with the analytical response, it is hoped that the analytical procedure may be extended to predict the nonlinear response of any cylinders subjected to bending with large  $R/t$  ratios.

Chapter II  
REVIEW OF LOCAL INSTABILITY

2.1 INTRODUCTION

A structure subjected to a compressive load which, after an infinitesimal increase in the load, undergoes a large change in its equilibrium configuration is said to have reached its buckling load. According to linear theory, displacements are proportional to the applied loads. However the buckling phenomenon denotes a disproportionate increase in displacement resulting from a small increase in the load. Therefore a nonlinear shell theory is required (Troitsky (2)).

A thin-walled cylindrical shell subjected to compressive forces may fail either due to the instability of the entire shell, resulting in bending of the longitudinal axis, or due to local instability of the thin wall, which may or may not involve lateral distortion of the axis. The former type of failure, known as overall buckling, was investigated by Euler and is directly related to the ratio of length to radius of gyration ( $L/r$ ). The latter, known as local buckling or wrinkling, is of primary concern in the design of thin-walled cylindrical shells since it is often the govern-

ing consideration. Furthermore, since the criterion is one of stability, failure may initiate at load levels corresponding to nominal stresses well below the yield strength.

## 2.2 LOCAL BUCKLING IN CYLINDRICAL SHELLS

Local instability is a function of the ratio of the thickness to the radius of the shell wall ( $t/R$ ). As implied in its name, it is local in nature and results in characteristic bulges or wrinkles. Initiation of failure depends on the combined compressive stresses at the specific point in question and is independent of the length of the shell.

In the case of columns and flat plates it is possible to use the classical small-deflection theory to predict the buckling load. In general, however this method of analysis may not be used for shell structures. As early as 1940, Von Karman (8) and his collaborators showed the significant difference in results between the buckling stress predicted by linear theory and that predicted by nonlinear theory. This was attributed to the fundamental nonlinear nature of the buckling process in thin-walled shells. Following these findings and continuing to the present, numerous testing programs have been conducted to verify the proposed nonlinear shell theories that followed.

The buckling load for some types of shell may be much lower than the load predicted by classical small-deflection

theory. In addition, the scatter of test data may be quite large. For example, if a set of ten nominally identical thin-walled cylinders of the same geometry were fabricated from a particular metal, none of the cylinders would fail at the same load. In fact, the scatter of results may range to 500 percent and the average buckling load may be one-eighth of the theoretical buckling load (Baker (6)). The dependence of the cylindrical shell buckling load on small deviations from the perfect circular cylindrical shape, as well as local edge conditions, have resulted in severe discrepancies between theoretical and experimental failure loads.

Current methods of establishing design data tend to treat both initial imperfections and edge conditions as random events. Available test results are lumped together without regard to specimen construction or method of testing. Results are analyzed to yield lower bounds or statistical correction factors to be applied to simplified versions of theoretical results. When using a lower-bound correction factor, data which do not seem typical are left out.

Statistical correction factors are determined by calculating a best-fit curve for a given set of data (Baker (6)). After establishing the standard deviation of the test data, small-sample theory is used to formulate a design curve for certain probability limits. For a 90% probability level, the chances are about 9 out of 10 that a shell subject to the critical buckling load will not buckle. The proposed formulations are only approximate.

### 2.3 BENDING STABILITY

A solution to local buckling induced by pure flexure was first introduced in 1932 by Flugge (9). His method utilized a linearly elastic stability theory which incorporated an assumed buckle wavelength-to-radius ratio. A later paper by Timoshenko (10) cited Flugge's calculation and the theory stood for some time. Flugge's calculation predicted a buckling stress that was 1.3 times the corresponding axial compressive buckling stress. Experimental work at that time supported those findings.

Work by Seida and Weingarten (11) in 1961 pointed out Flugge's assumed critical wavelength was incorrect. Their results indicated that, although the ratio of bending and compressive stresses can vary widely with wavelength, when the wavelength is minimized, the critical buckling stress due to flexure is approximately the same as the compressive buckling stress. At this point the small-displacement theory was abandoned as a basis for differentiating between critical buckling stresses caused by bending and compression.

A fundamental difference between uniformly compressed cylinders and flexurally loaded ones is the limit-point buckling mode inherent to the latter. Compressed cylinders display a distinct bifurcation-type buckling mode as discussed by Stephens et al. (7). Bifurcation-type buckling

is characterized by a load curve which displays a distinct bifurcation point in which the load path separates into stable and unstable branches.

Flexurally loaded tubes display the so-called "Brazier Effect" in response to the applied load. First investigated by Brazier (12) in 1927, this effect is characterized by the cylinder assuming an oval shape due to the applied load. Any member subjected to bending will assume a curvature. This curvature results in components of the longitudinal tensile and compressive forces that are directed toward the neutral surface of the tube. These forces in turn squeeze the tube into an oval shape, thereby decreasing the moment of inertia. This results in a reduction of the stiffness and, eventually, a loss of stability. Based on the geometry of the undeformed cross section, Brazier predicted the critical buckling stress as

$$\sigma_{cr} = 0.33 E t/R \quad (2.1)$$

As reported by Troitsky (2) in a state-of-the-art treatise, the current consensus among various investigators is that bending tests of cylinders similar to those tested in axial compression show that buckling occurs over the compression side of the cylinders in the same wave form, and with approximately the same wavelengths, as in axially-loaded cylinders. Also similar to axially-loaded cylinders,

pure-bending test results show exactly the same decrease of load with an increase of the ratio  $R/t$ . For moderately long cylinders Baker et al. (6) reports, the critical buckling stress is

$$\sigma_{cr} = \eta \gamma C E t/R \quad (2.2)$$

where  $t$  = thickness

$R$  = mean radius of the shell

$E$  = modulus of Elasticity

$$C_b = \frac{1}{\sqrt{3(1 - \nu^2)}}$$

$\gamma$  = correlation factor for unstiffened  
unpressurized circular cylinders

= plasticity correction term

The factor  $\gamma_1$  is included to account for the difference between the theoretical and experimental results for cylinders subjected to axial compression. The classical theoretical value for the buckling coefficient is  $\gamma_1=1$ .  $\gamma_1$  may be obtained from figure 2.1. For elastic buckling the value of  $\eta = 1$  is used.

The critical buckling stress for cylinders subjected to bending may be obtained from the above equation but  $\gamma_1$  is replaced by the bending correlation factor,  $\gamma_2$ , as shown in figure 2.2. The critical buckling stress will represent the maximum stress due to the bending moment (i.e., the outer

fiber stress). For inelastic buckling, the critical stress  $\sigma$  may be found by using the plasticity correlation term suggested for axial compression.

#### 2.4 INELASTIC BUCKLING

If the buckling stress is below the proportional limit then the compressive modulus of the material may be assumed constant. However, if the stresses are in the inelastic range the modulus of the material becomes a function of the stresses. Under inelastic stress conditions, the modulus of the material decreases, resulting in a decrease of the stiffness and a corresponding decrease of the buckling load.

The effect of plasticity on the buckling of shells can be accounted for by the use of the plasticity correction term. This reduction factor reflects the variation of the material stiffness with the stress level and may be defined as

$$n = \sigma_{cr} / \sigma_e \quad (2.3)$$

where  $\sigma_{cr}$  = actual inelastic buckling stress

$\sigma_e$  = elastic buckling stress

According to the NASA shell stability design guide (12), for inelastic local buckling the recommended plasticity correction term is;

$$n = \sqrt{(E_s E_t)} / E \quad (2.4)$$

where  $E$ ,  $E_s$  and  $E_t$  are the elastic, secant and tangent modulus, respectively. Equation (2.4) implies a homogeneous material with gradual-yielding stress-strain curves. A more general factor is suggested by Gerrard (14) for other material behaviour. Nonhomogenous material behaviour can result from residual stresses introduced during fabrication of most structural steel. This behaviour causes localized regions of the cylinder to deform plastically before the nominal stress reaches the yield point. Theoretically-based reduction factors do not account for this type of behaviour and reduction factors must therefore be determined empirically.

## 2.5 RESIDUAL STRESSES

Residual stresses are those stresses that would exist in a body if all external loads were removed. Divided into macro- and micro-scales, the latter is concerned with the microscopic properties of the metal at the time of crystal formation. Concerns in this report deal with macroscopic residual stresses.

Residual stresses in metal structures are usually produced during the manufacturing stages. Common processes causing residual stresses are:

- rolling, casting, and forging;

- forming and shaping of parts by such fabrication processes as bending, shearing, machining, and grinding;
- welding and riveting;
- heat treatments during manufacture.

Residual stresses caused by welding are of special concern to the study of thin-walled cylindrical shells. Due to localized heating by the welding arc and subsequent rapid cooling, welds always have residual stresses. Maximum values in regions near the weld can reach the yield strength of the material being welded. These residual stresses also cause distortion of the welds. The residual stresses and distortion cause complex effects, which maybe harmful to the structural integrity of the welded structure. High tensile residual stresses in regions near the weld may promote brittle fracture, fatigue, or stress corrosion cracking. Compressive residual stresses and initial distortion may reduce the buckling strength.

To analyze residual stresses and distortion in welds Masubuchi (15) suggests a four part procedure:

Step 1: Analysis of heat flow

Step 2: Analysis of transient thermal stresses during welding

Step 3: Determination of incompatible displacements after the weldment cools to the initial temperature

Step 4: Determination of residual stresses and distortion due to the enforcement of strain compatibility.

Step 3 of this process is the most important. If transient thermal stresses were completely elastic, no incompatible strain would be produced and the structure would remain unchanged when it cooled to the initial temperature. However, in real materials incompatible strains are produced as a combined effect of strain due to plastic deformation, solidification of the weld metal, and strain changes caused by phase transformations. Once the distribution of incompatible strains is determined, it is then possible to determine analytically the residual stresses and distortion by an elastic analysis.

A unique characteristic of residual stresses in welds is that incompatible strains are typically confined to small regions near the weld zone. Therefore, analyses based on relatively simple distributions of incompatible strains often provide results which are reasonably accurate.

Computer programs have been developed to analyze heat flow, transient thermal stresses, distortion and resulting residual stresses in welded structures (Masubuchi (15)).

## 2.6 LARGE DISPLACEMENT THEORY

Present developments of the large-displacement theory for shell buckling have not advanced to include cylindrical shells in bending Stephens et al. (7). Contrary to the classical small-displacement theory, which predicts compara-

tively equal buckling stresses for compression and bending, experimental results repeatedly indicate a higher buckling stress for flexurally loaded members (16),(17). Although not directly applicable to cylindrical shells in bending, the large displacement theory for axial compression does assist in understanding of the concepts of the theory.

An approximate numerical analysis, based on the elastic nonlinear finite-displacement theory developed by Donnell (18), provided important progress towards understanding nonlinear buckling behaviour. Von Karman and Tsien (19) showed in 1941 that asymmetric or diamond-shaped buckling configuration is unstable. These results indicated that equilibrium states involving large displacements can be maintained by loads far smaller than the critical bifurcation load obtained from classical small displacement theory. Thus the appreciable difference of observed load values ranging from  $1/2$  to  $1/3$  of those predicted by classical linear theory were rationalized.

Considerable insight was also gained into the effects of transverse membrane stresses that develop after buckling starts. For a thin cylinder, the inward buckling of the asymmetric diamond shaped mode generates superimposed transverse compression membrane stresses, and the initial buckled form is therefore unstable. Consequently, buckling is coincident with failure and is followed by a considerable drop in the load-carrying capacity of the cylinder.

In 1945, Koiter (20) recognized the imperfection sensitivity of shells and incorporated finite initial imperfections into a general nonlinear stability theory. Koiter's theory related the maximum load to the size of the imperfection which causes premature buckling. In addition to providing a path for the transition from the unbuckled to buckled state at loads lower than the classical value, the inclusion of initial imperfections serves as an additional factor to explain the large amount of scatter observed in test results.

Further studies into axisymmetric and asymmetric modes were performed by Almroth (21), and Tennyson and Muggeridge (22). The studies modified and extended the basic axisymmetric imperfection theory previously proposed by Koiter. Later studies by Koiter (23) showed that the interaction between various axisymmetric and asymmetric modes results in a pronounced reduction in strength.

In the absence of a large-displacement theory for the buckling of cylindrical shells subjected to pure flexure, there is conjecture as to the possible reasons for the difference in behaviour. Observed buckle patterns for cylinders in bending are similar to those found in axial compression. This suggests that the response of both loading cases is similar and that initial imperfections are important to both. A preferred region of buckling is characteristic for cylinders in bending since the stress distribution varies

circumferentially. Statistically this results in a lower probability of imperfections occurring within the critical buckling region. Nevertheless it is expected that some bend-buckling stresses would approach the corresponding compression values. Experimental results have not supported this postulate, as illustrated by Fig. 2.3. A ratio of the flexural-buckling strength to the compression-buckling strength is plotted against increasing values of the dimensionless parameter  $R/t$ . Results indicate that the flexural-buckling strength is significantly higher. There remain unresolved questions as to why this behaviour exists. Currently it is believed that the strain gradient resulting from the circumferentially varying bending stress is responsible for the increased buckling strength.

## 2.7 SUMMARY

The analysis of cylindrical shell buckling requires a nonlinear shell theory. Local instability is often the governing criterion in the design of thin-walled tubular structures.

The classical small-deflection theory leads to inconsistencies in shell buckling theory. A rigorous large-deflection theory has not yet been developed for cylindrical shells subjected to flexure. Important observations on the behaviour of these members has led to the consensus among investigators that edge effects, imperfections, and nonli-

near response to loading are the major factors contributing to the large discrepancy with classical theories.

During inelastic buckling the compressive modulus of the material decreases resulting in a loss of stiffness and subsequently a lower buckling load. Plasticity reduction factors may be incorporated to account for this effect.

Residual stresses are inherent in welded structures. In thin-walled cylindrical shells, bending fabrication and welding are regarded as the major source of these stresses. Residual stresses and distortion cause complex effects which result in a reduction of the buckling strength.

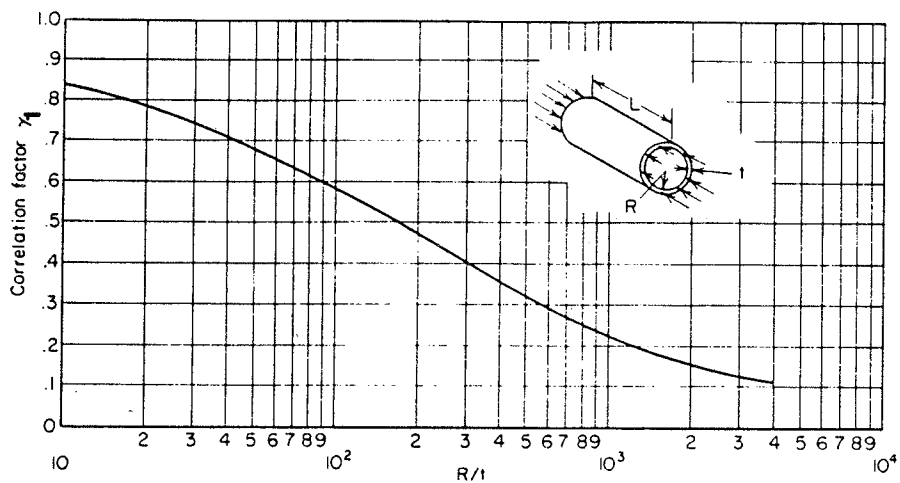


Figure 2.1: Correlation Factor Axial Compression after Baker (5)

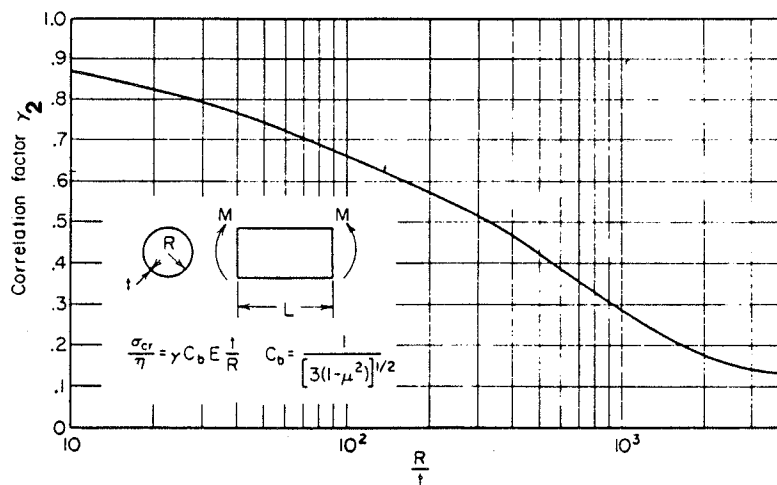


Figure 2.2: Correlation Factor Pure bending after Baker (5)

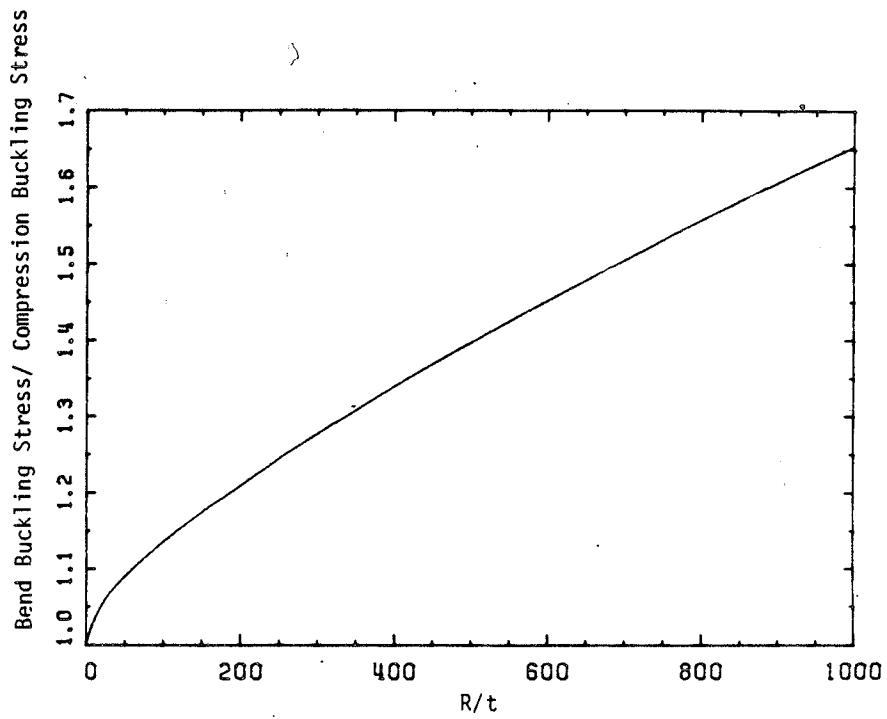


Figure 2.3: Comparison of Buckling Strength  
Flexural vs Compressive

Chapter III  
NONLINEAR FINITE ELEMENT ANALYSIS

3.1 INTRODUCTION

The shell buckling problem requires nonlinear shell theory analysis. If a finite element formulation is to be used in this analysis, the essence of the problem requires the formulation to be nonlinear. The analytical criteria require the system to include both material and geometric nonlinearities. The objective of the nonlinear analysis is to estimate the maximum load that a structure can support prior to structural instability or collapse.

3.2 NONLINEAR F.E.M. FROM A LINEAR PERSPECTIVE

The fundamental linear finite element equations may be used as a basis for understanding the nonlinear finite element formulation. A physical argument may be made as to why the nonlinear response is appropriately predicted using the linear formulation. This approach is instructive and yields insight into the process. However, when considering a more complex solution, a consistent continuum mechanics-based approach should be employed.

In a linear finite element formulation the displacements of the finite element assemblage are infinitesimally small and the material is linearly elastic. Under these conditions the F.E.M. equilibrium equations for the static analysis are

$$\mathbf{KU}=\mathbf{R} \quad (3.1)$$

where  $\mathbf{U}$ = displacement response  
 $\mathbf{R}$ = applied load vector  
 $\mathbf{K}$ = stiffness matrix

The system of equations is said to be linear since  $\mathbf{U}$  is a linear function of  $\mathbf{R}$  i.e. an increment of load  $\alpha\mathbf{R}$  will result in an proportionate increment of displacement  $\alpha\mathbf{U}$ .

The constraint that the displacement must be small enters into the evaluation of both the stiffness matrix  $\mathbf{K}$  and the load vector  $\mathbf{R}$ . Both terms are integrated over the original volume, which is assumed to be constant for infinitesimal displacements. The strain-displacement matrix of each element is assumed to be constant and independent of the element displacements. Also, the use of a constant stress-strain matrix implies a linearly elastic material.

From the above discussion, it can be seen that the basic assumptions used in a linear analysis define what is meant by a nonlinear analysis. It also suggests two main categories of nonlinearity, material nonlinearity, and kinematic nonlinearity.

The most general case is one in which the material is subjected to large translations and rotations as well as large strains. This results in, fibre extensions and angle changes between fibres which are large, fibre translations and rotations which may also be large, and a stress-strain relationship which may be linear or nonlinear. Bathe (24) states the Total Lagrangian (T.L.) or Updated Lagrangian Jaumann (U.L.J.) formulation are typically used. In the Total Lagrangian formulation all static and kinematic variables are referred to the initial configuration at time 0. The Updated Lagrangian formulation is based on the same procedures that are used in the T.L. formulation, but in the solution all static and kinematic variables solved at time  $t+\Delta t$ , are referred to the last calculated configuration at time  $t$ . Bathe and Bolourchi (25) state, "the only advantage of using one formulation rather than the other is the fact that it may yield a more effective numerical solution." Consistent with the T.L. formulation the second Piola-Kirchhoff stress (26) and Green-Lagrange (27) strain derivations are used.

The basic problem in a static analysis is to find the state of equilibrium of a body corresponding to the applied loads. The general equilibrium conditions of a system of finite elements can be expressed as

$${}^t\mathbf{R} - {}^t\mathbf{F} = 0 \quad (3.2)$$

where

${}^t\mathbf{R}$  = externally applied nodal point forces  
at time  $t$

${}^t\mathbf{F}$  = nodal point forces corresponding to the  
element stress in this configuration.

In the general case of large deformations, the volume of the body, as well as the stresses, are both unknown at time  $t$ . Equation 3.2 must express equilibrium of the system in the deformed shape, taking account of all nonlinearities. In a static analysis without time effects other than the definition of load level (i.e. no creep effects), time is only a convenient variable which denotes different intensities of load applications and correspondingly different configurations. If the interests of analysis include path-dependent nonlinear geometric or material conditions, the equilibrium condition of equation 3.2 must be solved by a step-by-step incremental analysis.

The basic approach in an incremental step-by-step solution is to assume that the solution of a discrete point in loading (time  $t$ ) is known and that the solution for discrete time  $t+\Delta t$  is required. Hence, the equilibrium conditions of (3.2) require

$${}^{t+\Delta t}\mathbf{R} - {}^{t+\Delta t}\mathbf{F} = 0 \quad (3.3)$$

Knowing the solution step  $t$  we can write

$${}^{t+\Delta t}\mathbf{F} = {}^t\mathbf{F} + \mathbf{F} \quad (3.4)$$

where

$\mathbf{F}$  = increment in nodal point force corresponding to the increment in element displacements and stresses from time  $t$  to time  $t+\Delta t$

This incremental vector  $\mathbf{F}$  can be approximated using the tangent stiffness matrix,  ${}^t\mathbf{K}$  ;

$$\mathbf{F} = {}^t\mathbf{K} \mathbf{U} \quad (3.5)$$

where

${}^t\mathbf{K}$  = tangent stiffness matrix for the known geometric and material conditions at time  $t$

$\mathbf{U}$  = vector of incremental nodal point displacements.

Substituting (3.5) & (3.4) into (3.3);

$${}^t\mathbf{K} \mathbf{U} = {}^{t+\Delta t}\mathbf{R} - {}^t\mathbf{F} \quad (3.6)$$

Solving (3.6) for an approximation for the displacements of time  $t+\Delta t$  is obtained;

$${}^{t+\Delta t}\mathbf{U} = {}^t\mathbf{U} + \mathbf{U} \quad (3.7)$$

The exact solution for the displacements at the time  $t+\Delta t$  corresponds to the applied load  ${}^{t+\Delta t}\mathbf{R}$  but since  ${}^{t+\Delta t}\mathbf{K}$  was assumed approximately equal to  ${}^t\mathbf{K}$ , equation (3.7) is only an approximation.

After evaluating the expression for the displacements at time  $t+\Delta t$ , the corresponding expressions for the stresses (approximate) and their associated nodal point forces may be found. Since the solution is only approximate and a function of the load step size, it will be necessary to iterate until the solution of (3.3) is obtained to sufficient accuracy.

Although the Modified Newton Iteration technique is most often used, a closer study of the so-called Modified Riks-Wempner Method, with constant arc length (28), is investigated in the following section.

The previous discussion is valuable in identifying the components that form the basis of the equilibrium iteration method. The various nonlinearities which together form the basic finite element equations used to predict the nonlinear response of a structural system have been reviewed. However, the governing finite element equation for a more complex system should be developed from a consistent continuum mechanics approach.

A displacement-based finite element solution developed from the governing continuum mechanics equations uses the principle of virtual work. Nonlinear analysis requires equilibrium of the body being considered to be established in its current configuration. Considering the motion of a general body in a stationary Cartesian Coordinate system,

the possibility exists that the body may experience large displacements, large strains and a nonlinear constitutive response. The solution process evaluates equilibrium positions at discrete points repeatedly until the complete solution path has been solved for. The analysis follows all particles of a body in their motion, from the original to the final configuration of the body. Thus, a Lagrangian (or material) formulation of the problem is adopted.

### 3.3 NISA80 PROGRAM

The NISA80 program is a nonlinear incremental structural analysis multipurpose program for geometrically and materially nonlinear systems. The program was written in Germany at the Institut fuer Baustatik Universitaet Stuttgart in 1977.

The analysis of shell structures using the finite element method lead to the development of a number of different finite elements. In these developments, basically two approaches have been followed. Firstly, a classical approach and, secondly, an approach in which displacement/rotation isoparametric elements are employed.

The NISA80 shell elements are developed from the second approach in which independent rotational and displacement degrees of freedom are employed. This procedure was originally applied to the nonlinear analysis of shells by Ramm

(29) and Krakeland (30). These elements differ from the usual displacement isoparametric elements in two ways. Firstly, it is assumed that the normal to the shell middle surface remains straight and that there is no change in thickness. Secondly, the normal stresses in the direction of the shell thickness are ignored in the element formulation, thus eliminating erroneous strain energy corresponding to these stresses. The first assumption reduces the number of degrees of freedom per cross section from six to five. The second compensates for the increase in bending stiffness by the factor  $1/(1-\nu^2)$ .

This concept is referred to as 'degeneration' of elements. The advantage of these displacement/rotation isoparametric elements is their inherent generality, permitting ease of application to various analysis. The geometry and the displacement field of the structure are directly discretized and interpolated as in the analysis of continuum problems. The numerical analysis leads to the displacement solution from which the stresses can be derived without using the resultants. Importantly, the element provides high accuracy without reduced integration.

The NISA80 program employs the "constant-arc-length method" of Riks (31)(32) and Wempner (33) to trace the nonlinear response from the pre-limit to the post-limit range. The limit point may be defined as the maximum load observed on the load deformation response curve. Although postcritical

states cannot be tolerated in a design, a prediction of the response is valuable in understanding the complete structural behaviour. Typically, a static analysis can trace the postcritical range, allowing for a better judgement of the overall structural response. The usual solution techniques that are effective in the prebuckling range are not very efficient in the post-critical stage and often diverge before a solution is reached.

Recently the work of Ramm (29) and Crisfield (34) has shown that a modified Riks/Wempner method can be especially recommended for postcritical states. These modifications permit an efficient iterative technique throughout the entire range of loading and not only near the critical point.

Riks and Wempner independently introduced the constant-arc-length iterative technique. The basis of their model was to limit the load step size by satisfying a constraint equation. That is, the generalized arc length of the tangent at the previous equilibrium position  $m$  of the load displacement response curve, is fixed to a prescribed value as shown in Figure 3.1. Then the iteration path follows a plane normal to the tangent. The constraint equations originally were added to the incremental stiffness expression destroying symmetry and the banded nature of the stiffness matrix.

Ramm cited Wessels work (35) and used his results as a basis for further modification which permitted the removal of these difficulties. The modifications were based on geometrical considerations and required only two additional steps. The modified iterative technique was found to be very efficient in the entire load range, particularly when automatic load incrementation is used. The additional storage requirements were only minor, and the extra computer time was negligible.

In addition to constraining the arc length, Ramm (28) suggests the load step size may also be scaled for each load step. The program is modified to recall the number of iterations  $n$  required for equilibrium in the previous step. The load step is then adjusted in size by multiplying the load increment by a factor  $\sqrt{\hat{n}_1 / n}$ , where  $\hat{n}_1$  (a constant) represents a value for the number of desired iterations.

The use of this scaling technique reduces oscillations near the limit point. This procedure aids in the prevention of divergence near the limit point.

#### 3.4 SHELL MODELLING

Generally, the cost of analysis of a complete shell configuration is prohibitive. Thus only a portion of the cylinder is modelled. The principle of symmetry is used and only one quarter of the experimental shell is analyzed.

This does however, restrict the analysis to assume that the initial imperfections are also symmetrical, which obviously is not the case.

The geometry of the tube is referred to a polar coordinate system  $x, R, \theta$  in which the  $x$ -axis follows the centerline of the undeformed tube. The NISA80 program immediately transfers these coordinates to an orthogonal Cartesian system  $x, y, z$  in which the  $x$ -axis follows the centerline of the undeformed tube. The external loading is assumed to be symmetric about the  $x$ - $z$  plane, as also are the geometric imperfections. Due to this symmetry only one quarter of the tube need be considered (see figure 3.2). Further, at end 1 (midpoint of the shell) the plane  $y$ - $z$  remains unwarped after deformations; at end 2 truss elements prevent deformation of the shell at the point of load application. This simulated the solid plates welded to the ends of the experimental shells to prevent deformation at the the point of loading. All boundary conditions are given in figure 3.2.

Figures 3.3 to 3.8 show the selected mesh patterns used in this investigation. Rectangular shell elements are used both for the central test section and end regions. Sixteen-node bicubic elements are used to model the shell with the exception that the transition elements between the central and end portions are reduced four-node bilinear elements. A finer element mesh is used in the thinner central test region. Figures 3.3 to 3.8 view the projected mesh pattern

from the inside of the cylinder. Boundary conditions, element and node numbering are shown in these figures. The symbols XT, YT, ZT, XR, YR, ZR stand for translation in the global x-direction, translation in the global y-direction, translation in the global z-direction, rotation about the global x-axis, rotation about the global y-axis, and rotation about the global z-axis respectively.

The different mesh configurations and analyses are identified by the following notation. "B" signifies bending in conformance with the experimental shell specimen B1 or B2. "S" identifies the particular mesh configuration performed in a segment of the investigation. "E" indicates that the eigenvalue solution is being performed, and "N" identifies the nonlinear solutions. A given analysis consists of a particular "B" and "S" combination that is analyzed first by the eigenvalue solution and then the nonlinear solution.

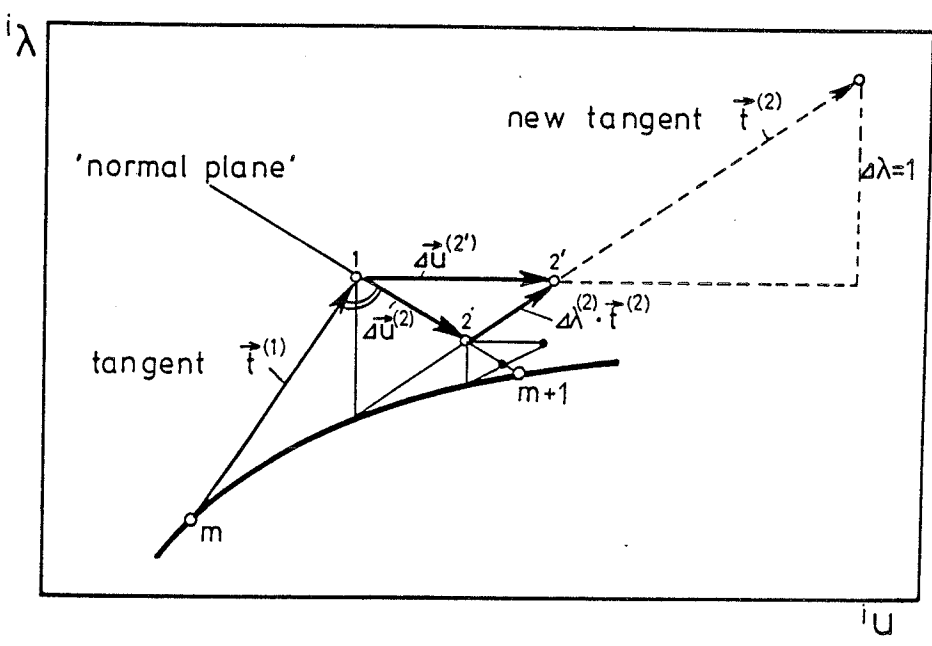


Figure 3.1: Constant-Arc-Length Method after Ramm (28)

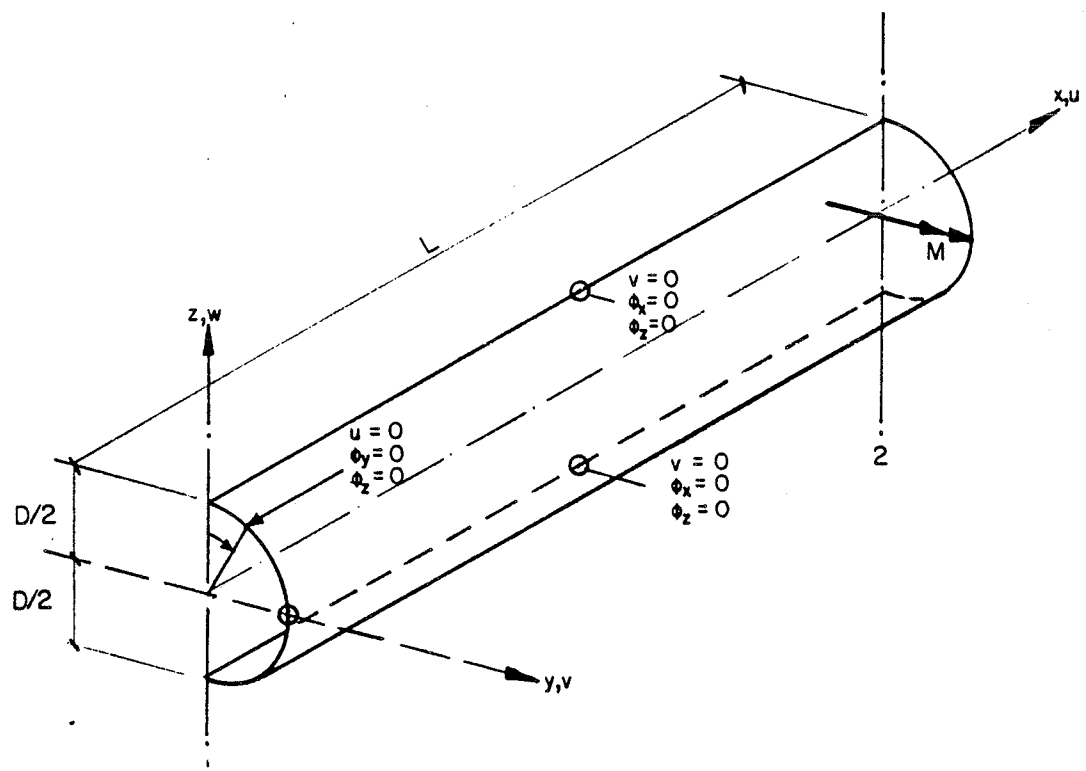
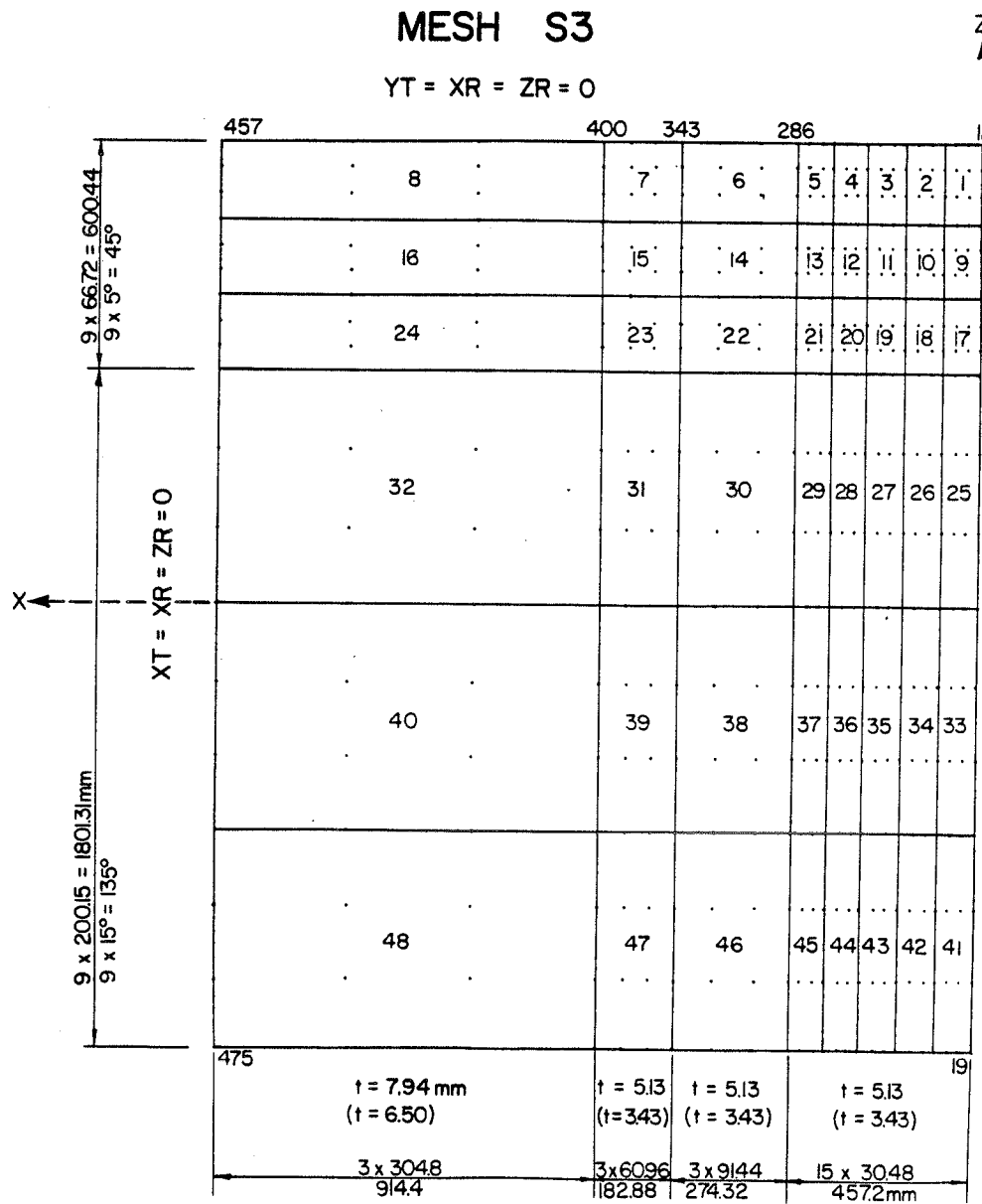


Figure 3.2: Shell Model



Radius  
 B1 = 764.5 mm  
 B2 = 761.7 mm

494 NODES  
 48 - 16 Node Shell Elements  
 0 - 4 Node Shell Elements  
 19 - Truss Elements

Figure 3.3: Mesh Configuration S3

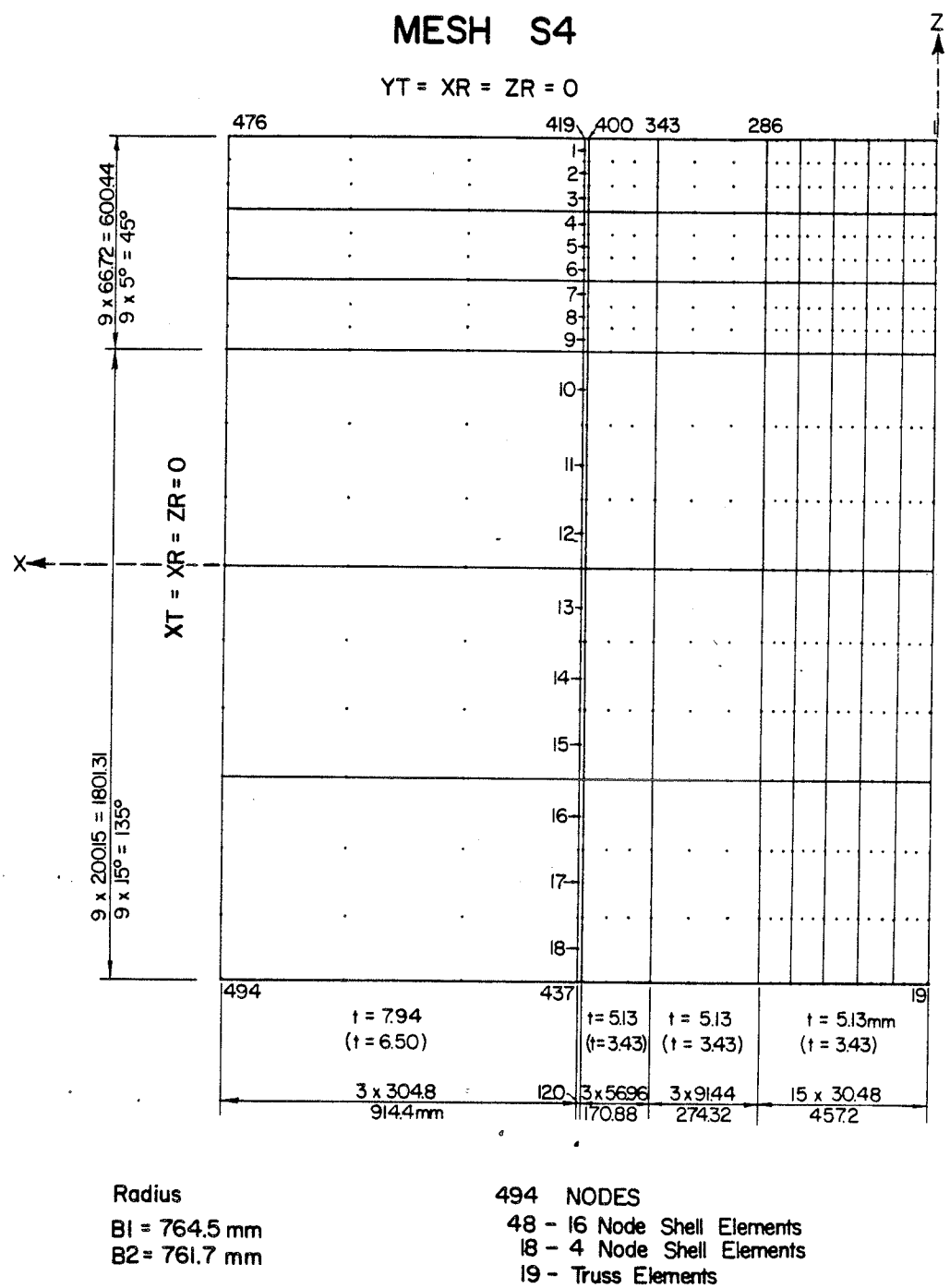
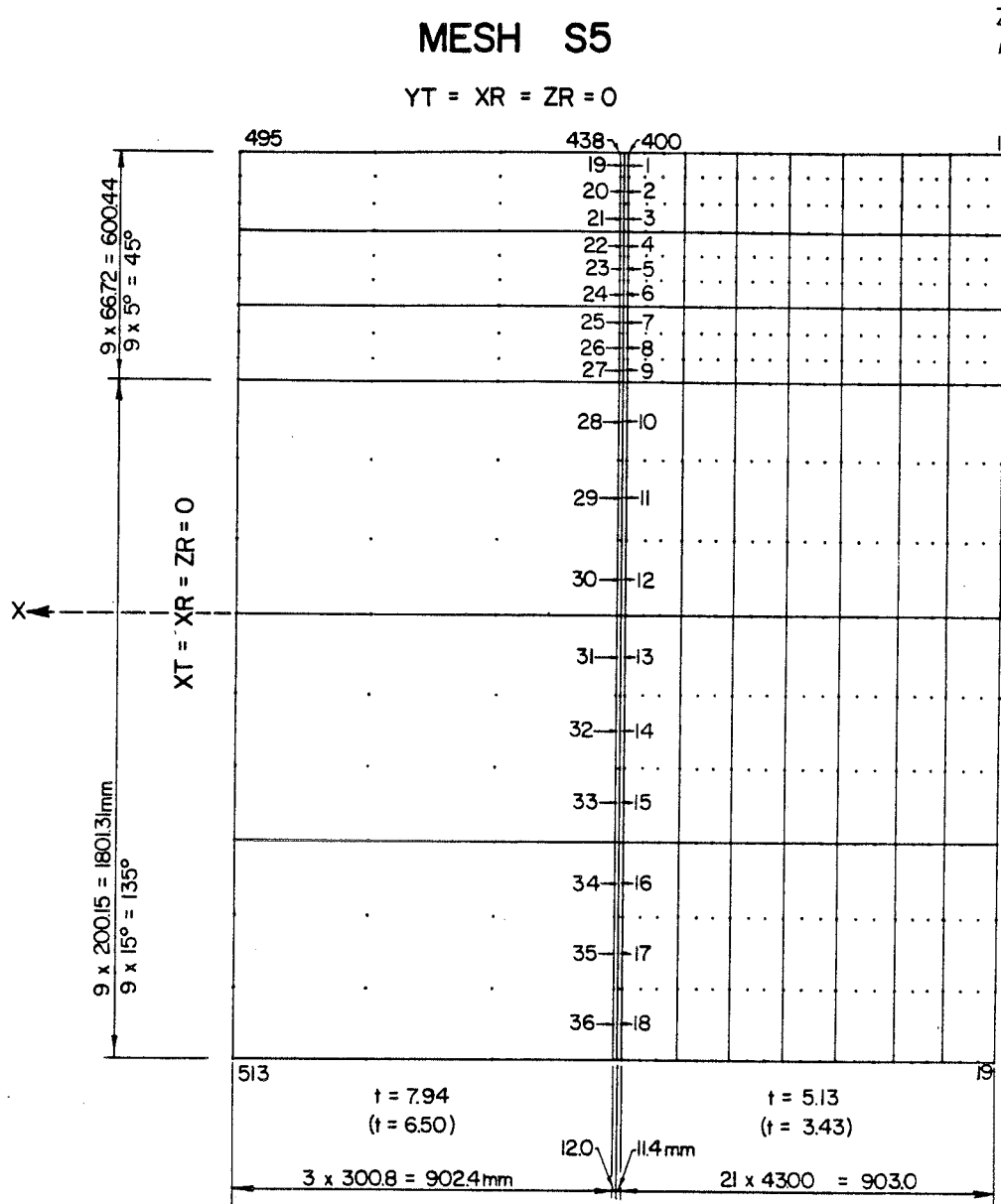


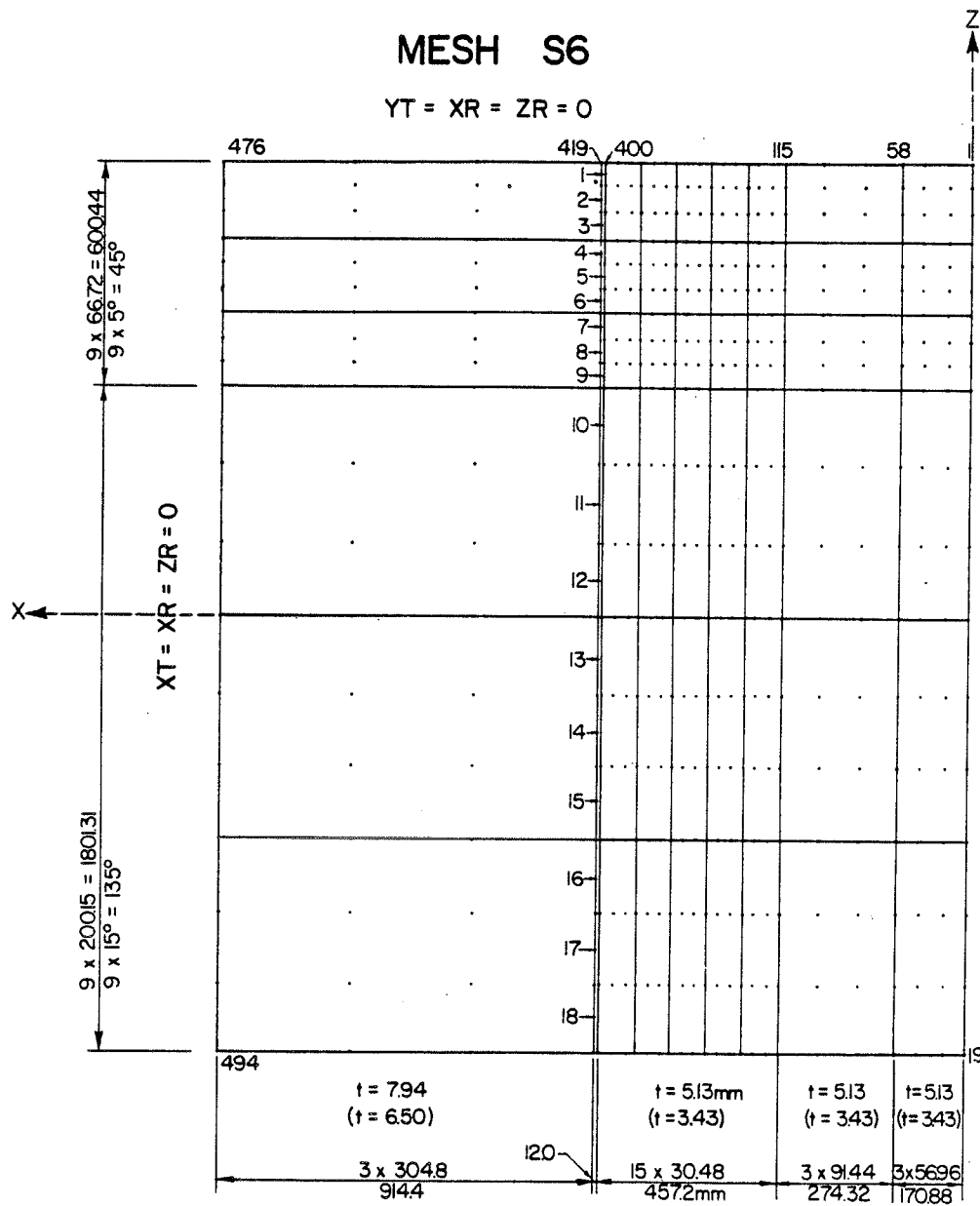
Figure 3.4: Mesh Configuration S4



Radius  
B1 = 764.5 mm  
B2 = 761.7 mm

532 NODES  
48 - 16 Node Shell Elements  
36 - 4 Node Shell Elements  
19 - Truss Elements

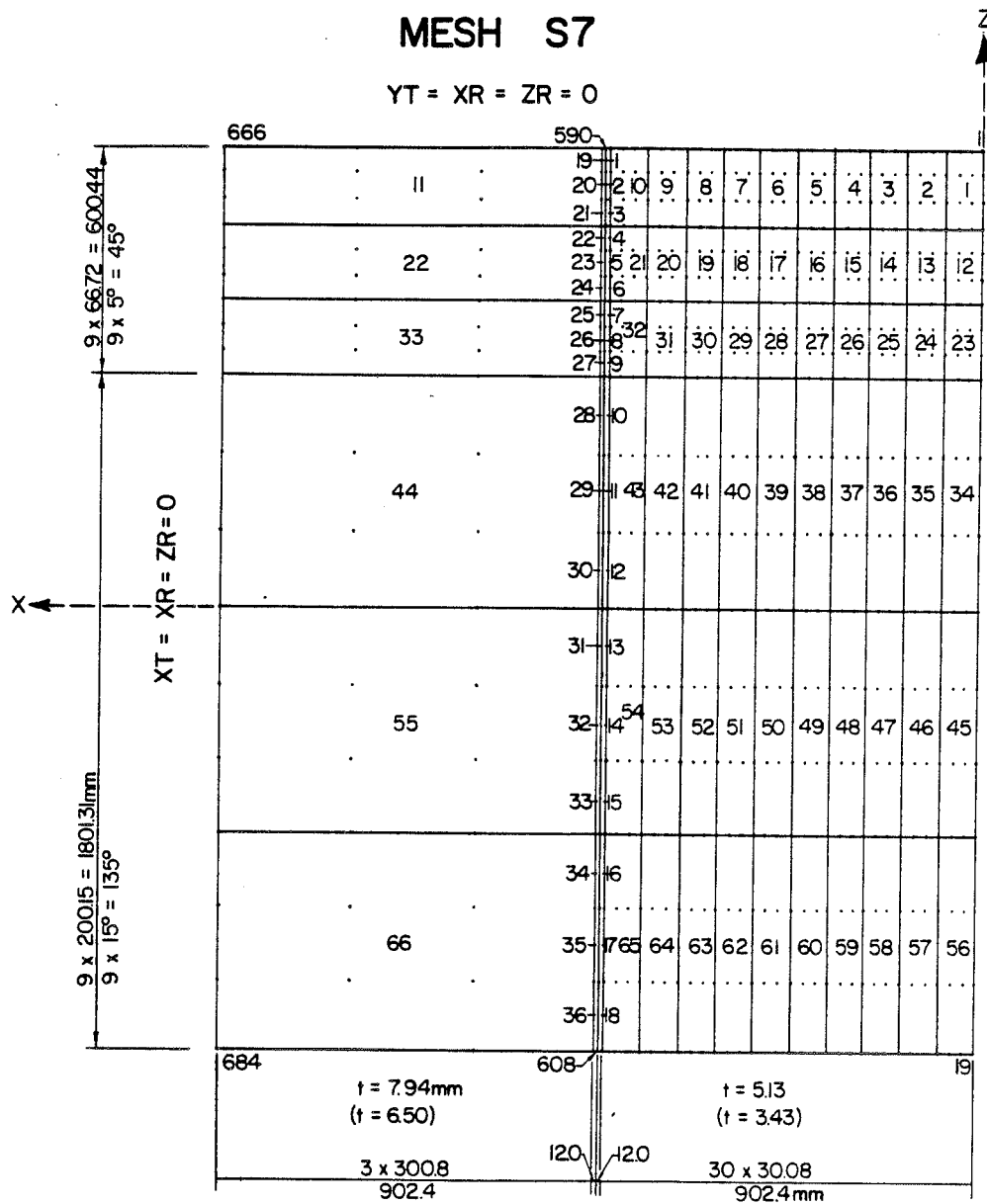
Figure 3.5: Mesh Configuration S5



Radius  
 B1 = 764.5 mm  
 B2 = 761.7 mm

513 NODES  
 48 - 16 Node Shell Elements  
 18 - 4 Node Shell Elements  
 19 - Truss Elements

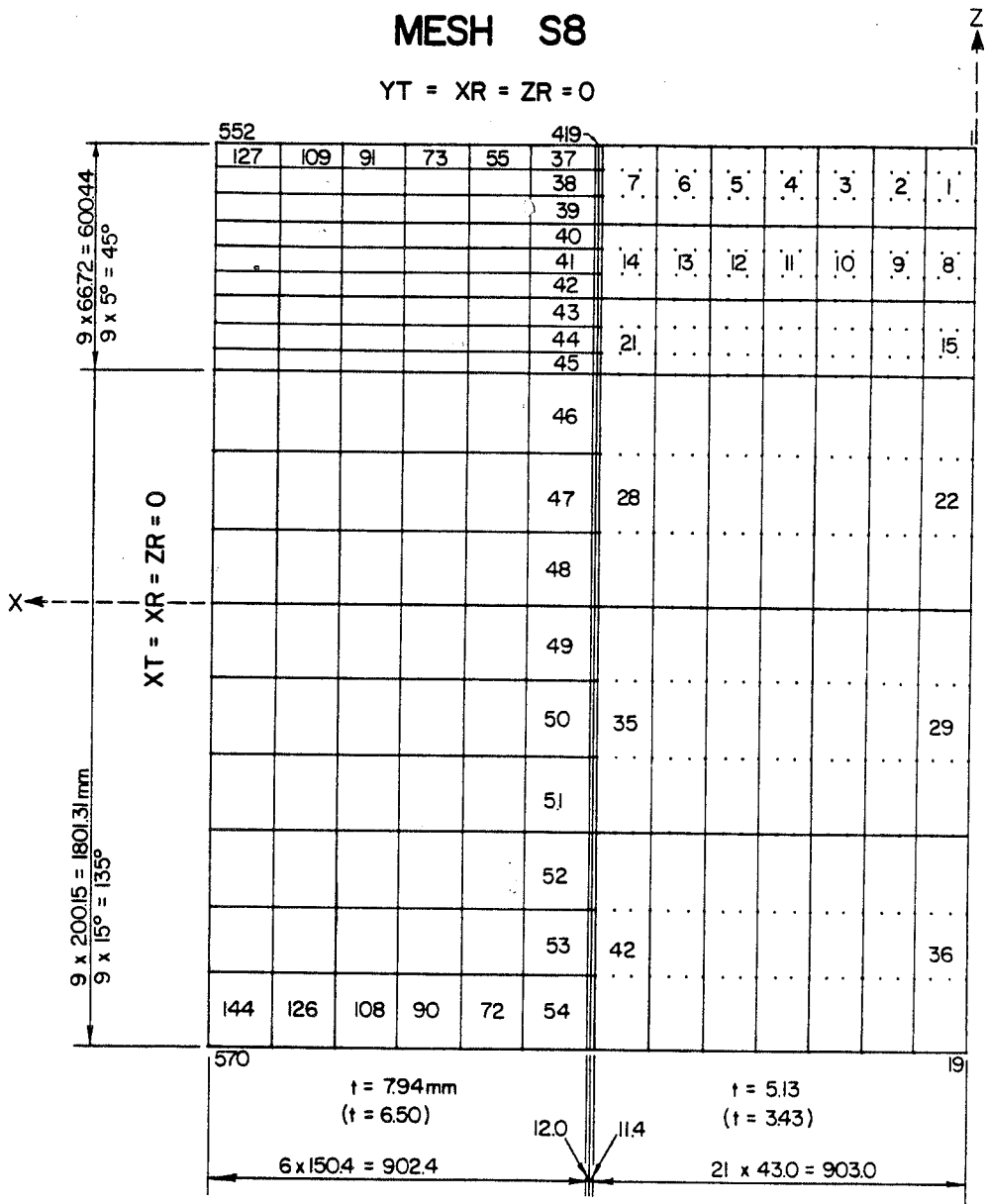
Figure 3.6: Mesh Configuration S6



Radius  
B1 = 764.5 mm  
B2 = 761.7 mm

703 NODES  
66 - 16 Node Shell Elements  
36 - 4 Node Shell Elements  
19 - Truss Elements

Figure 3.7: Mesh Configuration S7



Radius

B1 = 764.5 mm

B2 = 761.7 mm

589 NODES

42 - 16 Node Shell Elements

144 - 4 Node Shell Elements

19 - Truss Elements

Figure 3.8: Mesh Configuration S8

Chapter IV  
INITIAL IMPERFECTIONS

4.1 INTRODUCTION

Initial imperfections in thin-walled cylindrical shells are inevitable under normal fabrication. If the purpose of engineering analysis is to predict the true behaviour of a structure under normal conditions then these conditions must be incorporated into the analysis.

A modern phase of investigation, beginning in 1940 with the work of von Karman (8), has identified initial imperfections as one of the main factors leading to serious disagreement between classical buckling analysis and experimental data.

Subsequent investigations by Hutchinson (36), Almroth (21), and Koiter(20) showed that thin-walled circular cylindrical shells subjected to axial compression are very sensitive to small deviations from the exact circular cylindrical shape. Koiter's analysis indicated that initial imperfection amplitudes equal to the thickness of the shell, were sufficient to reduce the critical buckling load to 20 percent of the load corresponding to the perfect shell.

Therefore, not only is the inclusion of an initial imperfection pattern necessary, but the determination must be both accurate and representative of the initial displacement configuration at the time of loading.

## 4.2 AVAILABLE EXPERIMENTAL DATA

### 4.2.1 Introduction

Experimental procedures often provide initial imperfection values only at discrete points and not a scan of the total surface. In order to incorporate the imperfections of the prototype into the theoretical analysis model, an interpolation of the total surface must be established from the discrete measurements. Development of the surface pattern permits subsequent interpolation at any desired points, such as the nodal points of a finite element approximation.

### 4.2.2 Experimental Data

An experimental program into thin-walled cylinder behaviour was conducted at the the University of Alberta by M.J. Stephens et al. in 1981. The program was designed to investigate the local buckling behaviour of large diameter thin-walled fabricated cylinders loaded in either uniform axial compression or pure flexure. The results from the latter case were subsequently used in this investigation.

The experimental prototype structures were made to approximately one-half of their commonly used full scale diameter. Tests on the large diameter cylinders involved two specimens, both fabricated from three subsections. A complete tube consisted of a thin central test section 1525 mm in diameter and 1830 mm long, and two thicker end sections each 1525 mm in diameter and 915 mm long. All subsections were welded together with a full-penetration groove weld along the circumference as shown in Figure 4.1. For specimen B1, the central section was fabricated from CSA 40.21 300W steel plate with a mean thickness of 5.13 mm and end sections of similar material with a mean thickness of 7.93 mm. Specimen B2 was fabricated from ASTM A36 steel plate comprising a central section with a mean thickness of 3.43 mm and end sections with a mean thickness of 6.50 mm.

The initial geometry of the large diameter specimens was carefully measured to permit the determination of initial imperfections in the cylinder walls. The recorded observations of the Stephens et al. experiment were used as a data base for the surface interpolation.

#### 4.2.3 Measurement Procedure

Measurements (at discrete points on the cylinder wall) of specimen radii were obtained with a device that established radial measurements with respect to an assumed longitudinal axis. By rotating this device through 22.5 degree inter-

vals, 16 radial measurements were taken at seven locations on the longitudinal generator. A total of 112 measurements were taken for each cylinder. In addition, circumferential weld-seam depressions at the intersection of the central and end shell connections were measured at the same 16 intervals for both ends of the shell.

#### 4.2.4 Adjustment to Define the Perfect Cylinder

Before approximating the true initial imperfections it is necessary to define the perfect cylinder. In the Stephens et al. experiment radial deviations from an imaginary cylindrical reference axis were measured. The "best" location and orientation of the perfect axis needed to be determined analytically. From this determination the measured values could be adjusted to use the perfect cylinder as a datum. This requires both a rigid body rotation of the two principal axis as well as a rigid body translation to determine the true axis centre. Referring to figure 4.2, the translation and the rotations may be calculated as follows;

Rotate about the z axis

$$\begin{Bmatrix} x' \\ y' \\ z' \end{Bmatrix} = \begin{bmatrix} \cos \beta & \sin \beta & 0 \\ -\sin \beta & \cos \beta & 0 \\ 0 & 0 & 1 \end{bmatrix} \begin{Bmatrix} x-x_0 \\ y-y_0 \\ z \end{Bmatrix} \quad (4.1)$$

Rotate about the  $y'$  axis

$$\begin{Bmatrix} x'' \\ y'' \\ z'' \end{Bmatrix} = \begin{bmatrix} \cos \alpha & 0 & -\sin \alpha \\ 0 & 1 & 0 \\ \sin \alpha & 0 & \cos \alpha \end{bmatrix} \begin{Bmatrix} x' \\ y' \\ z' \end{Bmatrix} \quad (4.2)$$

Substitute (4.1) into (4.2) and multiply

$$\begin{aligned} x'' &= (x-x_0)\cos \alpha \cos \beta + (y-y_0)\cos \alpha \sin \beta - z \sin \alpha \\ y'' &= -(x-x_0)\sin \beta + (y-y_0)\cos \beta \end{aligned} \quad (4.3)$$

Since the experimental imperfections were measured in terms of the polar coordinates  $(R, \phi)$  it is necessary to transform these initial observations into  $(x, y, z)$  coordinates. Assuming a reference cylinder aligned with a fixed global frame:

$z$  - axis of cylinder

$x, y$  - axis of cross section

$\phi$  - angle between observation arm and  $x$ -axis

$r$  - measured observations

$$x = r \sin \phi$$

$$y = r \cos \phi \quad (4.4)$$

To determine the "best" perfect cylinder, a statistical adjustment of data was performed on the measured observations based on the principle of least squares.

Examining the general problem of least squares Deming (37) states "that as a result of any experiment there will be observations, and when the adjustment is completed, to each observed value there will be a corresponding adjusted value." Repeating an experiment a large number of times will produce a set of observed values. Deming suggests taking the average of these random values results in a "true value." The statistical adjustment may be performed by examining the relationship between the observed, calculated (or adjusted), and true coordinates. The method of least squares calculates the value of the residuals. From these values the error values may be calculated. The best results are obtained when this error is minimized.

In formulating the problem of the following quantities are used:

Observed values	$X_i, Y_i$	$i \in (1, 2, \dots, n)$
Adjusted values	$x_i, y_i$	$i \in (1, 2, \dots, n)$
(Calculated values)		
Weights	$w_{x_i}, w_{y_i}$	
True values		
Residuals	$V_{x_i}, V_{y_i}$	$V_{x_i} = X_i - x_i$ $V_{y_i} = Y_i - y_i$

The principle of least squares requires that the sum of the weighted squares of the residuals

$$S = \sum w V^2 \quad (4.5)$$

shall be a minimum with respect to the "adjusted values."

In curve fitting the adjusted values are required to satisfy a set of conditions. In the general case, suppose that the adjusted values  $x, y$  are subject to  $\nu$  conditions;

$$F^h(x, y; a, b, c) = 0 \quad h \in (1, 2, \dots, \nu) \quad (4.6)$$

where  $a, b, c$  are estimates of the unknown curve fitting parameters  $\alpha, \beta, \gamma$ . Equations (4.6) are referred to as the condition functions.

By the principle of least squares the equations are all handled alike, namely by the minimizing of  $S$ . The functions must be chosen such that when equated to zero, they force the conditions that are to be imposed on the adjusted coordinates. This development is based on the fact that the "true" coordinates would exactly satisfy the conditions.

Using the notation;

$$F_{xi} = \frac{\partial F^h}{\partial x_i}$$

$$F_{yi} = \frac{\partial F^h}{\partial y_i} \quad (4.7)$$

$$F_a^h = \frac{\partial F^h}{\partial a}$$

etc.

the derivatives of the condition functions may be evaluated. Numerical values of these derivatives are needed, and for most purposes it suffices to evaluate them with the observed values  $X_i, Y_i$  with the next available approximations  $a_0, b_0, c_0$ .

Making the condition equations (4.6) linear in the residuals by expanding in Taylor's series and neglecting higher order terms, while noting

$$\begin{aligned} X_i &= X_i - V_{x_i} \\ Y_i &= Y_i - V_{y_i} \\ a &= a_0 - A \\ b &= b_0 - B \\ c &= c_0 - C \end{aligned} \tag{4.8}$$

the so-called "reduced equations" then become

$$\sum_i^n [F_{x_i}^h V_{x_i} + F_{y_i}^h V_{y_i}] + F_a^h A + F_b^h B + F_c^h C = F_0^h \tag{4.9}$$

$$\text{where } F_0 = F^h(X, Y, a_0, b_0, c_0) \quad h \in (1, 2, \dots, v) \tag{4.10}$$

and is, in fact, the amount by which the condition  $F^h = 0$  fails to be satisfied by the observed values  $X_i, Y_i$  and the approximations  $a_0, b_0, c_0$ .

Thus in the present case the condition equation is

$$F(x_i, y_i, z_i; x_0, y_0, \beta, \alpha, R) = (x'')^2 + (y'')^2 - R^2 = 0 \tag{4.11}$$

To linearize, expand in the Taylor series;

$$F(x + \Delta x, y + \Delta y, z + \Delta z, x_0 + \Delta x_0, y_0 + \Delta y_0, \beta + \Delta \beta, \alpha + \Delta \alpha, R + \Delta R) = \quad (4.12)$$

$$F(x_i, y_i, z_i; x_0, y_0, \beta, \alpha, R) + \frac{\partial F}{\partial y_0} \Delta x_i + \frac{\partial F}{\partial y_i} \Delta y_i + \frac{\partial F}{\partial z_i} \Delta z_i \\ + \frac{\partial F}{\partial x_0} \Delta x_0 + \frac{\partial F}{\partial y_0} \Delta y_0 + \frac{\partial F}{\partial \beta} \Delta \beta + \frac{\partial F}{\partial \alpha} \Delta \alpha + \frac{\partial F}{\partial R} \Delta R$$

$$\frac{\partial F}{\partial x_i} = 2x_i'' \frac{\partial x_i}{\partial x_i} + 2y_i'' \frac{\partial y_i''}{\partial x_i}$$

$$\frac{\partial F}{\partial y_i} = 2x_i'' \frac{\partial x_i}{\partial y_i} + 2y_i'' \frac{\partial y_i''}{\partial y_i}$$

$$\frac{\partial F}{\partial z_i} = 2x_i'' \frac{\partial x_i}{\partial z_i} + 2y_i'' \frac{\partial y_i''}{\partial z_i}$$

$$\frac{\partial F}{\partial x_0} = 2x_i'' \frac{\partial x_i}{\partial x_0} + 2y_i'' \frac{\partial y_i''}{\partial x_0}$$

$$\frac{\partial F}{\partial y_0} = 2x_i'' \frac{\partial x_i}{\partial y_0} + 2y_i'' \frac{\partial y_i''}{\partial y_0}$$

$$\frac{\partial F}{\partial \beta} = 2x_i'' \frac{\partial x_i}{\partial \beta} + 2y_i'' \frac{\partial y_i''}{\partial \beta}$$

$$\frac{\partial F}{\partial \alpha} = 2x_i'' \frac{\partial x_i}{\partial \alpha} + 2y_i'' \frac{\partial y_i''}{\partial \alpha}$$

$$\frac{\partial F}{\partial R} = -2R$$

(4.13)

where

$$x'' = (x - x_0) \cos \sigma \cos \beta + (y - y_0) \cos \alpha \sin \beta - z \sin \alpha$$

$$y'' = - (x - x_0) \sin \beta + (y - y_0) \cos \beta$$

$$\frac{\partial x''}{\partial x} = \cos \alpha \cos \beta$$

$$\frac{\partial x''}{\partial y} = \cos \alpha \sin \beta$$

$$\frac{\partial x''}{\partial z} = \sin \alpha$$

$$\frac{\partial x''}{\partial x_0} = \cos \alpha \cos \beta$$

$$\frac{\partial x''}{\partial y_0} = \cos \alpha \sin \beta$$

$$\frac{\partial x''}{\partial \phi} = - (x - x_0) \cos \alpha \sin \beta + \cos \alpha \cos \beta$$

$$\frac{\partial x''}{\partial \alpha} = - (x - x_0) \sin \alpha \cos \beta - (y - y_0) \sin \alpha \cos \beta = z \cos \alpha$$

$$\frac{\partial y''}{\partial x} = - \sin \beta$$

$$\frac{\partial x''}{\partial y} = \cos \beta$$

$$\frac{\partial y''}{\partial z} = 0$$

$$\frac{\partial y''}{\partial x_0} = \sin \beta$$

$$\frac{\partial x''}{\partial y} = \cos \beta$$

$$\frac{\partial y''}{\partial \beta} = - (x - x_0) \cos \alpha - (y - y_0) \sin \beta$$

$$\frac{\partial y''}{\partial \alpha} = 0$$

Equation (4.12) may be substituted into equation (4.11) and, using the observed values  $X_i, Y_i$ , numerical values may be obtained. A computer program, CYLINDER (Appendix B) was written to evaluate this expression. The output of the program produced the adjusted (calculated) values  $x, y$ .

#### 4.3 DEVELOPMENT OF THE INTERPOLATED SURFACE

##### 4.3.1 Introduction

A precise interpolation model is required to map the initial imperfection configuration. The criteria dictate that the model interpolate in two orthogonal directions, with one direction having a function of periodicity  $2\pi$ .

Previous investigations have frequently used models which incorporate a Fourier Series summation to approximate the imperfect surface. Using the measured discrete points as input the coefficients of the Fourier Series are calculated. This method is restrictive since neither a sine series nor a cosine series is capable of representing the imperfect shape completely. The sine series results in zero imperfections along the upper and lower circumferences, whereas the cosine series produces zero slopes at these positions.

In this investigation bicubic splines were used to approximate the imperfect surface.

### 4.3.2 Spline Model

Given a set of discrete  $(X,Y)$  values and their corresponding function values, the objective of the spline model is to interpolate a set of  $XL$  &  $YL$  values anywhere on the surface.  $XL, YL$  represent the coordinates of any point on the surface. A two-dimensional interpolation function using bicubic splines in orthogonal directions satisfies this objective. In order to perform the shell analysis, a mesh of discrete function values containing  $NXL$  by  $NYL$  nodal points must be developed from an initial set of  $NX$  by  $NY$  function values. The values in the  $X$ -direction (circumferential) must be periodic with period  $2\pi$ .

To accommodate these conditions the following procedure was used:

1. A cubic spline interpolation function with periodic end conditions was accessed from the University of Manitoba IMSL Library (38). `ICSPLN` was called  $NY$  times to interpolate in the  $X$ -direction at the points

$$(XL_i, Y_j) \quad \begin{array}{l} i \in (1, 2, \dots, NXL) \\ j \in (1, 2, \dots, NY) \end{array}$$

2. A cubic spline interpolation function `ICSCCU` was called  $NXL$  times to interpolate in the  $Y$  direction to determine values of the natural bicubic spline at the points

$$(XL_i, YL_j) \quad i \in (1, 2, \dots, NXL)$$

$$j \in (1, 2, \dots, \text{NYL})$$

Note that in calculating the initial cubic splines with periodic end conditions, spline functions are found at only the original NY intervals since the program has no function values for the NYL points at this time.

Both the above procedures utilize a common routine ICSEVU to calculate the coefficients of the spline and to evaluate the cubic splines output.

The routine ICSPLN creates a cubic spline with periodic end conditions. That is, if  $S(X)$  is the approximating spline then,  $S(X_1) = S(X_{\text{NX}})$ ,  $S'(X_1) = S'(X_{\text{NX}})$  and  $S''(X_1) = S''(X_{\text{NX}})$ , where the prime denotes differentiation.  $S(X)$  is written as a linear combination of periodic basis splines. The cubic spline calculated passes through each data point producing  $FL(X, Y) = f(X, Y)$ , i.e. an exact fit. The sub-routines used to calculate the spline algorithm are based on work done by de Boor (39).

#### 4.4 END REGION IMPERFECTIONS

##### 4.4.1 Introduction

In the Stephens et al. experimental program, measurements of radial imperfections were taken only for the thinner central portion of the cylinder. At the circumferential weld seams connecting the central portion to the end portions the observed weld depressions were measured with re-

respect to shell surface. Therefore no reference was provided of the overall shell imperfections with respect to the assumed longitudinal axis. The theoretical analysis requires that the surface be mapped to produce an initial displacement configuration at the discrete nodal points.

#### 4.4.2 End Region Extrapolation

Since there were no measured points for the end region of the shell, extrapolated straight-line generators were used to predict the initial configuration of these sections. Better results are obtainable by extrapolating the generators to produce sample data points before the spline approximation of the imperfect surface. Eliminating this extrapolation tends to produce amplified imperfections in the end regions due to the oscillatory nature of bicubic splines between distant data points. The straight-line generators were calculated from least-squares fits in the the central section. Initially the "adjusted data points" (as derived in section 4.2.4) were calculated to produce the adjusted cylinder as shown in Figure 4.3. This procedure was performed in order to remove any bias from the original data before extrapolating the generators. The generators were then calculated to coincide with the  $\pi/8$  measurement intervals of the observed data points and were oriented parallel to the longitudinal axis of the cylinder (Figure 4.4). A total of sixteen generators were fitted, from which imper-

fections were estimated at the circumferential welds, extreme ends, and two points arbitrarily chosen at the quarter points so as to prevent violent oscillation of the bicubic splines between the distant points. A program, GEN (Appendix B), was written for these calculations.

#### 4.4.3 Incorporation of the Weld Depressions

Since the measurements taken at the circumferential welds were not referred to the assumed longitudinal axis, the only remaining reference points were the straight line generators. Thus the initial imperfections at the circumferential weld locations are represented by the generator-calculated imperfection minus the measured circumferential weld depression (see Figure 4.5). The derivation of these imperfections was further complicated by the fact that the measured depressions were only taken at  $\pi/4$  intervals. This was overcome by first fitting the eight observed values with a periodic bicubic spline and then interpolating the remaining eight values. Once all the depressions were calculated a FORTRAN program, SEAM (Appendix B), was written to incorporate their effects into the end-region imperfections.

Combining the adjusted central-region imperfections and the end-region imperfections produced a map of the total cylinder surface. This map of imperfection function values, consisting of 15 intervals in the longitudinal direction (assumed as y-values), containing 16 data points in the cir-

cumferential direction (assumed x-direction), produces 240 function values  $F(X,Y)$ . These values were used as input for the development of the interpolated surface. A FORTRAN program, GRAPH (Appendix B), performed the numerical computation of the surface interpolation. The program yielded a mesh of interpolated values at 50-mm intervals in the longitudinal direction and 5 degree intervals in the circumferential direction.

#### 4.5 DEVELOPED PLOTS OF THE INTERPOLATED SURFACE

The output from GRAPH was plotted using the Versatec plotting library. Although functionally 2-dimensional, the resulting plot appears as a 3-dimensional image. This effect is achieved by offsetting the coordinate axes after each successive interval is plotted. The generators from which the original data were measured are plotted parallel to the cylinder axis. Figures 4.6 and 4.7 represent the the final interpolated surface map for specimen B1 and B2 respectively.

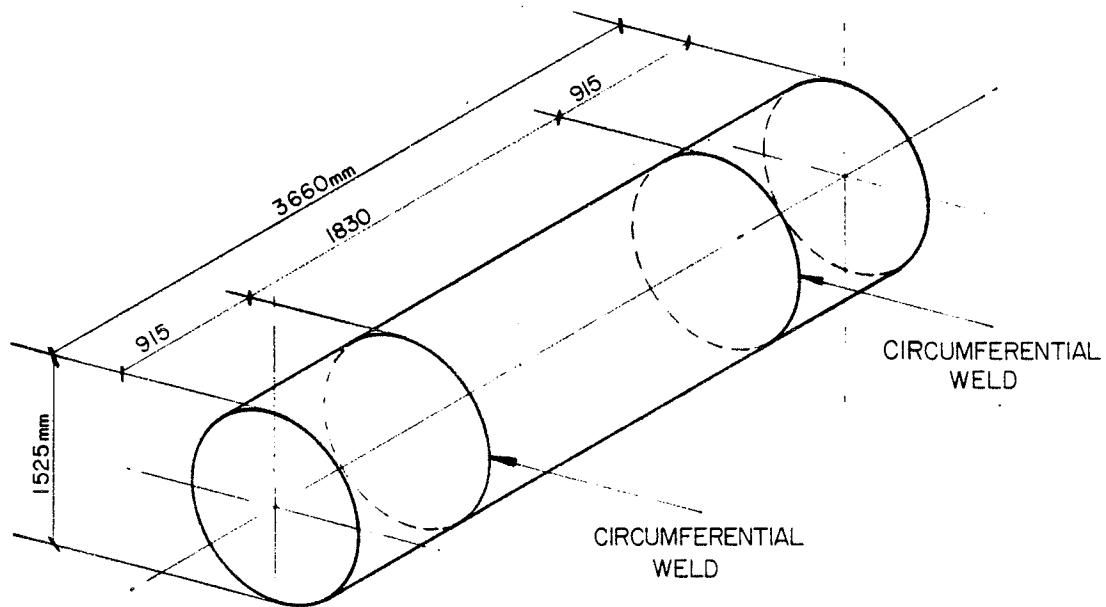


Figure 4.1: Experimental Prototype Tested at the University of Alberta

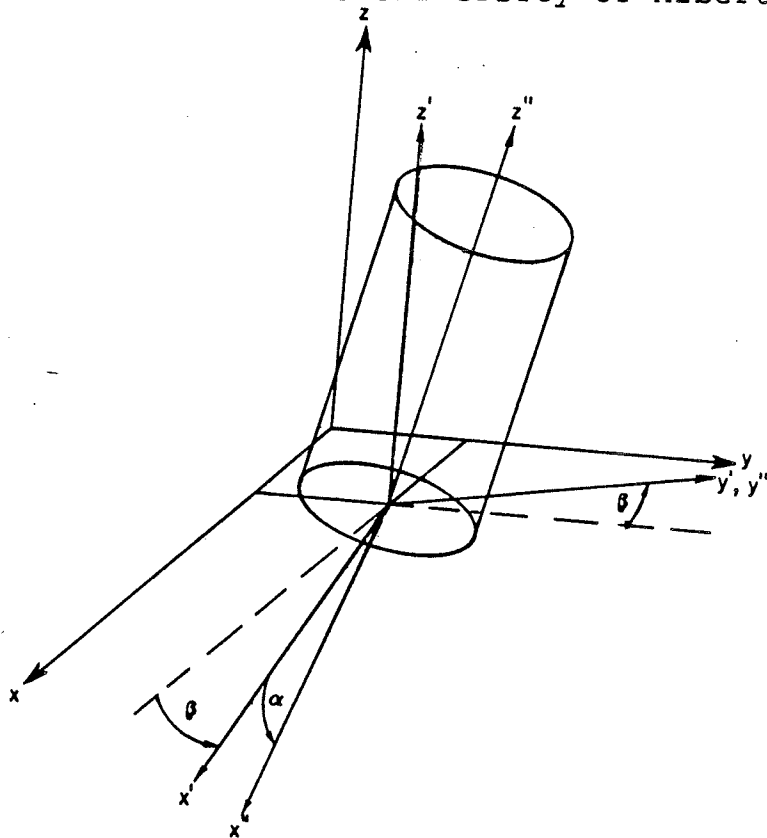


Figure 4.2: Axis Rotation and Translation

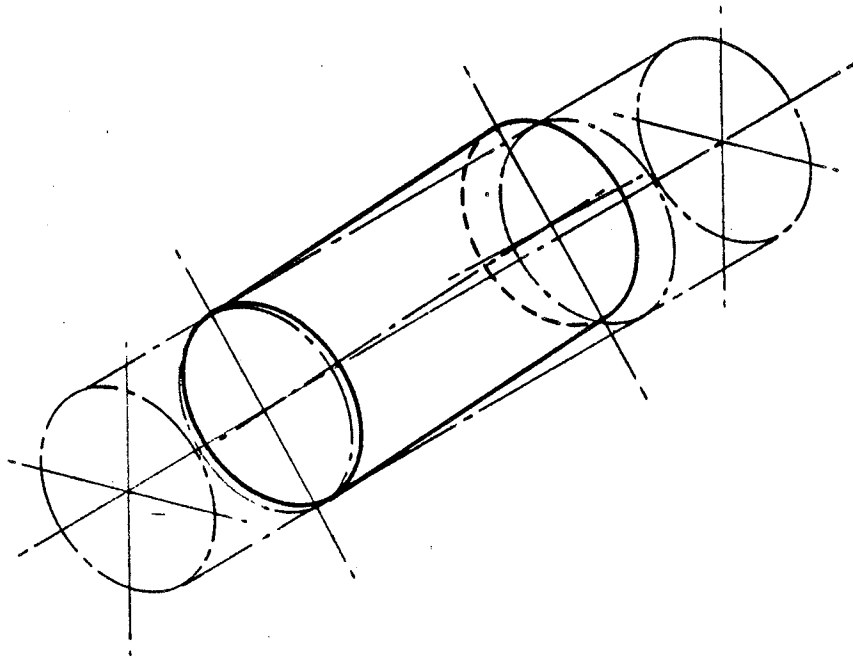


Figure 4.3: Adjusted Data Points in Central Region

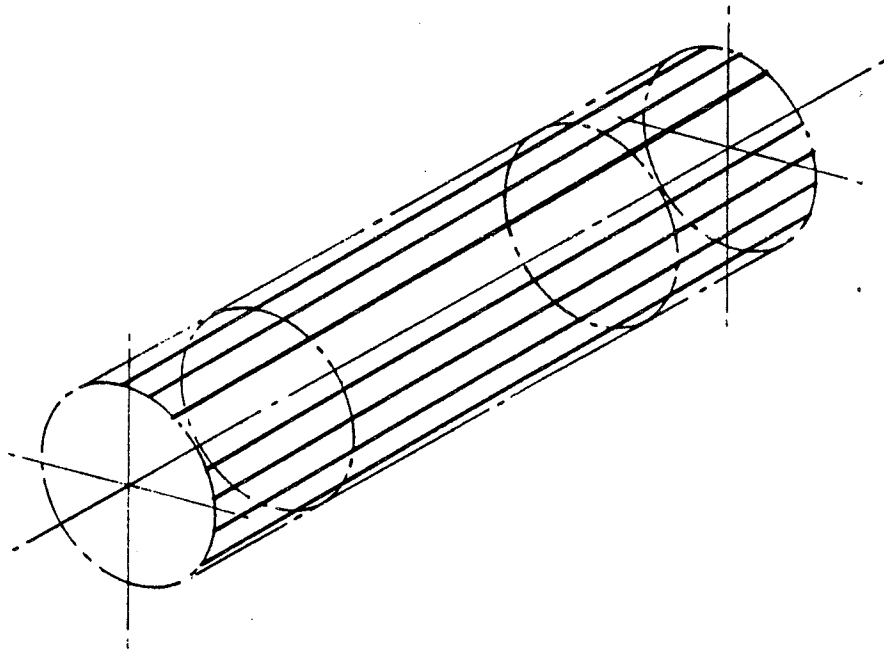


Figure 4.4: Extrapolated Straight-Line Generators

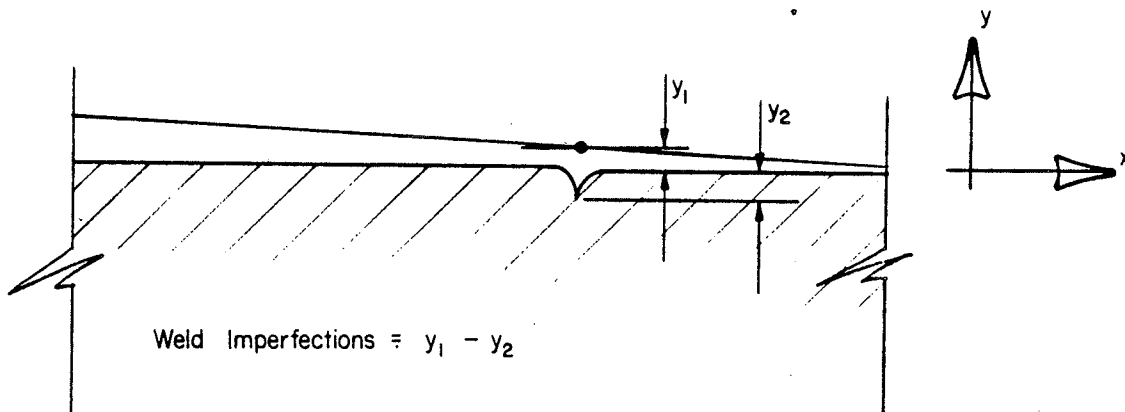


Figure 4.5: Cicumferential Weld Imperfection

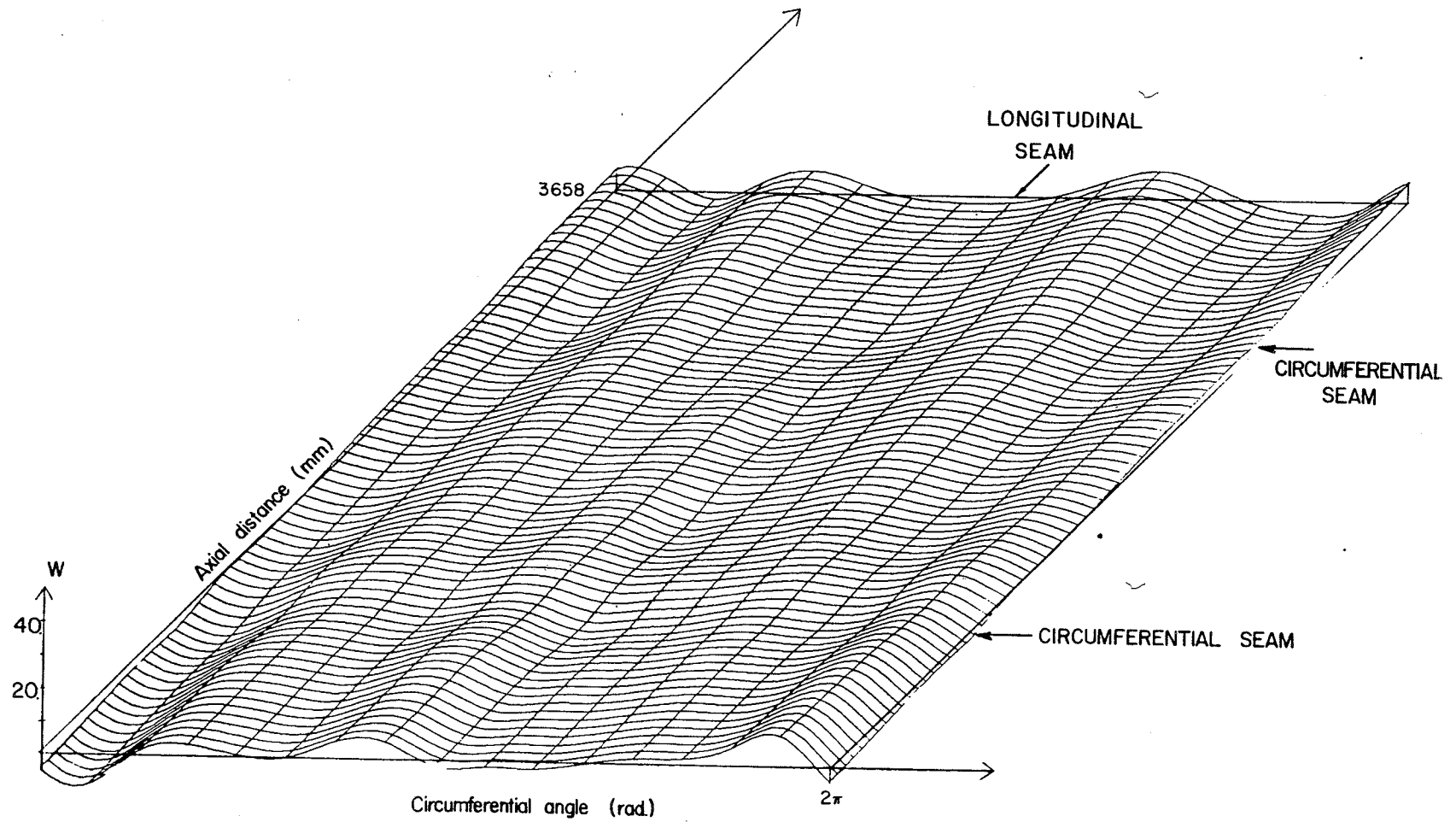


Figure 4.6: Interpolated Surface Map B1

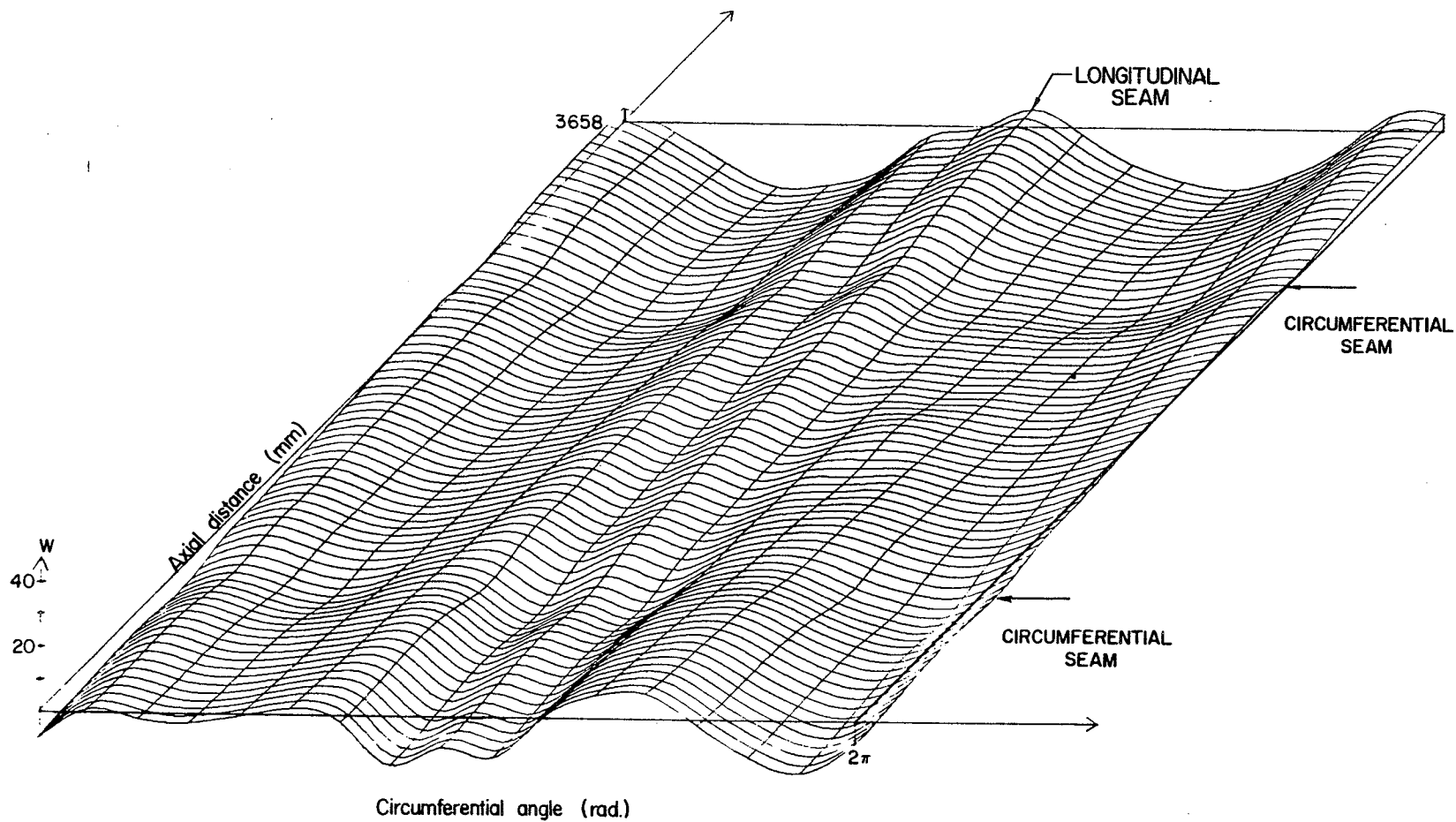


Figure 4.7: Interpolated Surface Map B2

Chapter V  
GEOMETRIC IMPERFECTIONS

5.1 INTRODUCTION

The incorporation of initial imperfections into a nonlinear analysis is usually restrictive since it requires some advance knowledge of the geometric imperfections of the structure being considered. In a prototype, the imperfections can be carefully measured experimentally and then incorporated into an analysis. For shells manufactured in normal production, this approach is impractical. The optimum procedure is to establish the characteristic initial imperfection distribution which a given fabrication process is likely to produce. All such available data would be combined statistically to predict the most probable occurrence.

Other geometric irregularities introduced in the manufacturing process may cause additional localized stresses in the loaded shell. For example, localized forces are introduced at the junction of eccentric shells. The abrupt change of the generator results in a discontinuous resultant force at the junction.

## 5.2 INCORPORATION OF INITIAL IMPERFECTIONS

It is presumed that the smallest initial imperfections that would result in a lower bound for the ultimate load would be those corresponding to the theoretical first mode (i.e., critical mode) shape for a perfect shell. Since a real shell would not have precisely this initial configuration, it is necessary to estimate the first mode amplitude that would predict the same ultimate load as the true initial configuration.

For the type of structure under consideration it was decided that the most reliable way to incorporate geometric imperfections was to scale the corresponding eigenvector components obtained from the theoretical eigenvalue analysis. For design purposes the scale factor would be derived from a statistical procedure as a function of the fabrication process and the dimensions of the shell. However, where there is available experimental data, a scale factor proportional to the actual initial imperfections may be extracted. For the analysis of experimental data, the given displacement pattern, discretized at the nodal points to give vector  $\{v\}$ , can be represented by superposition of the eigenvectors  $\{\phi\}$  of the same discretization. Hence we may write

$$\{v\} = \sum a \{\phi\} \quad (5.1)$$

and, by orthogonality, the contribution of the first mode to the initial displacement pattern is

$$a_1 = \frac{\{\phi\}_1 \{v\}}{\{\phi\}_1^T \{\phi\}_1} \quad (5.2)$$

The eigenvector of expression (5.2) includes radial and axial translations as well as rotations of each node, whereas only radial initial imperfections were measured. Therefore the eigenvectors  $\{\phi\}_1$  of equation (5.1) must be restricted to comprise only the radial components of displacement. The vectors obtained are not strictly orthogonal, resulting in only an approximate value of the scaling factor  $a_1$ . Nevertheless, since the neglected terms are much smaller in magnitude, the approximation is close. The restricted eigenvectors  $\{\phi\}_1$  of the radial displacements are now of order equal to the number of nodes.

The resulting imperfections incorporated into the nonlinear analysis are represented by

$$\{v\} = a_1 \{\phi\}_1 \quad (5.3)$$

A computer program, MODEL (Appendix B), was written to perform the numerical calculation of the scaling factor " $a_1$ ." The preliminary subroutines interpolate the initial radial imperfections at the discrete nodal points using the surface interpolation technique described in chapter 4. Subsequent to this, the x-y components of these imperfections are extracted, based on the orientation of the individual node with respect to the global axis. The x-y contributions of

the chosen eigenvector previously stored from the eigenvalue analysis are then called from memory. Substitution of the above values into equation 5.2 then produces the scaling factor  $a_1$ . The field of imperfections is measured for the complete cylinder, but for cost effectiveness, the model takes advantage of symmetry and only selects one quarter of the cylinder. Therefore it was necessary to revolve the shell about its longitudinal axis in  $\pi/8$  intervals and select one of the sixteen cases. In attempting to establish a common basis for repeated investigation, the worst case was selected.

Knowing the scale factor  $a_1$ , the value of the applied nodal imperfection may be determined. A program, ADDDIDP (Appendix B), calls the x-y contribution of the eigenvector and using simple trigonometric relations calculates the radial component at each corresponding node. The radial component is then multiplied by the factor  $a_1$  to produce the scaled imperfection value. This value is then added to the radial coordinate of that specific node, thus incorporating the scaled imperfections into the nonlinear analysis.

### 5.3 ECCENTRIC JUNCTIONS OF THE SHELLS

Sections having abrupt changes in geometry develop additional forces, stresses and deformations which are commonly termed edge effects. Due to the elastic resistance of the adjoining parts, the edge effect does not spread far and acts upon relatively narrow zones.

The physical cause of the edge effects are:

1. An absence of free deformation of the shell;
2. Sudden changes or eccentricity of the generator, which lead to additional meridional forces or local moments due to its eccentricity.

Cylindrical shells having different wall thicknesses and eccentric junctions contribute two causes to the origin of edge effects. In the first case, although there is no break of the generator the deformations are restricted due to the different thicknesses of the walls, as shown in figure 5.1. This results in unequal values of the free deformations. In the second case, figure 5.2 illustrates that an eccentric junction causes a break in the longitudinal generator, resulting in local moments and subsequent bending of the shell. This bending results in shear forces and additional meridional and circumferential forces. These additional forces produce local deformations which, in the case of shell buckling, could be instrumental in initiating local failure.

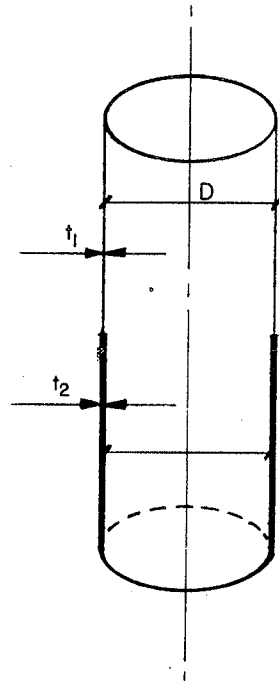


Figure 5.1: Shell Junctions of Different Wall Thickness

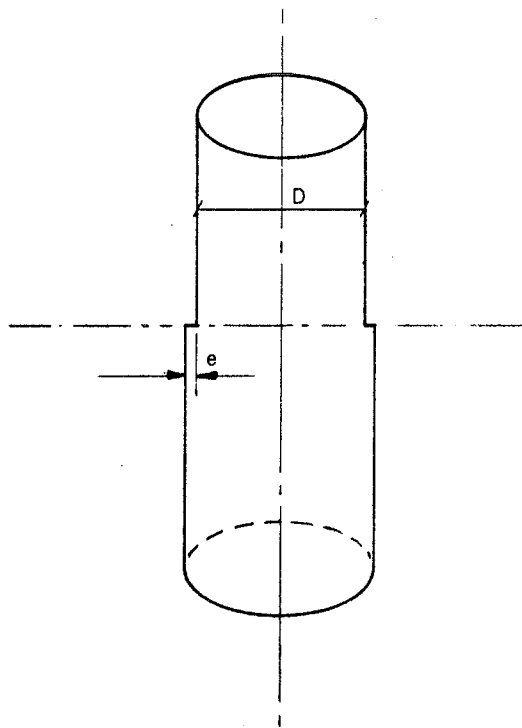


Figure 5.2: Eccentric Shell Intersections

## Chapter VI

### RESULTS OF THE NONLINEAR FINITE ELEMENT ANALYSIS

#### 6.1 INTRODUCTION

The analytical program attempted to isolate various factors affecting the ultimate buckling load predicted by the NISA80 program. Consideration was given to the magnitude of initial imperfections, mesh refinement, eccentric junctions, and weld depressions. Each successive step led to a closer idealization of the true structure. Ultimately the analysis refinements should predict limit loads close to the experimental values of 2143 kN-m for specimen B1, and 1030 kN-m for specimen B2.

#### 6.2 EIGENVALUE SOLUTIONS

An eigenvalue solution of the perfect configuration was obtained for each of the mesh layouts. In each analysis the theoretical first mode (i.e., the critical mode) shape was determined. The corresponding eigenvalues were calculated and are tabulated in Table 6.1. Critical moments are obtained by multiplying the applied moment times the eigenvector.

It has been shown (Timoshenko and Gere 1961(10)) that the critical uniform axial stress for a geometrically perfect, elastic, circular thin cylinder is

$$\sigma_{cr} = \frac{Et}{r\sqrt{3(1-\nu^2)}} \quad (6.1)$$

where  $\sigma_{cr}$  = critical stress; E = Young's modulus; t = wall thickness; r = mean radius;  $\nu$  = Poisson's ratio. The critical moment may be obtained from

$$M_{cr} = \frac{\sigma_{cr} I}{r} \quad (6.2)$$

where I = moment of inertia. From equations 6.1, 6.2 the critical moments for the geometrically perfect, elastic cylinders are 7779 kN-m and 3491 kN-m for B1 and B2, respectively. Comparing this to the critical moments obtained in the eigenvalue solutions, 7946 kN-m and 3541 kN-m for model B1S7 and B2S7, respectively, a good correlation is achieved. This indicates that the modelling and mesh refinement chosen are a good representation of the prototype.

The resulting indeterminate radial components of mode shape 1 were used in conjunction with the corresponding initial imperfections to determine the scale factor  $a_1$  of equation 5.2. Once determined, the first mode radial components could be extracted to produce the initial displacement pattern for the nonlinear analysis. The mode shape 1 displace-

tern for the nonlinear analysis. The mode shape 1 displacement patterns for all eigenvalue solutions may be found in figures 6.1 through 6.8. It should be noted that all of the displacement pattern figures are somewhat deceiving since the plotting routine does not differentiate between inner node links and the shell element boundaries. This results in typical 16-node elements appearing as 9 4-node elements.

### 6.3 ECCENTRIC JUNCTIONS

It was discovered that, although original design specifications called for the centerline alignment of the central and end shell sections, fabrication techniques resulted in a 1.6-mm. offset of the middle surfaces as shown in Figure 6.9. Physically, the magnitude of this offset seems very small, but compared to a shell thickness of 5.13 mm for specimen B1 (3.43 mm for B2) the result is a significant eccentricity. Introducing a small 4-node element at the junction of the two shells permitted the incorporation of this eccentricity into the analysis (model S4, Figure 6.3). The resulting eigenvalue solution for the eccentric junction configuration of mesh S4 remained relatively unchanged, compared to the original centerline alignment configuration of mesh S3.

Interesting results were obtained for the S4 configuration when a nonlinear analysis for the perfect shell was performed. Figures 6.10 and 6.11 show that local buckling

of the shell took place within close proximity to the circumferential weld, a result consistent with the experimental results. However, the limit load obtained, 3485 kN-m, was only slightly different from the 3534 kN-m result obtained without incorporating the eccentric junction, and much higher than the experimental result of 2143 kN-m. Because of the insignificant difference, it was determined that a non-linear analysis of S4 incorporating the initial imperfections would yield no further useful information. Table A.5 and Figure A.5 of Appendix A show the Moment vs Curvature relationship for the S4 analysis.

#### 6.4 MESH REFINEMENTS

In order to confirm the results of configurations S3 and S4, a coarse, uniformly spaced mesh S5 (Figure 6.2) was analyzed. Model S5 also incorporated an abrupt weld depression at the junction of the end and central sections. The effect of the latter adjustment was to provide a sharp pinching of the adjoining sections.

The eigenvalue solution for S5 had a significant change from that for the previous mesh. Figures 6.1 and 6.2 indicate that, compared to S3, the general pattern of mode shape 1 had extended across the central test section. Severe doubts were placed on the validity of the previous mesh. Although the technique was valid, it was evident further tuning of the model was necessary.

In order to determine what effects the mesh refinement had on a typical eigenvalue solution a fourth mesh pattern, S6 was introduced. The pattern of S6 was identical to that of S4 except that the refinement was interchanged from the centre-most section, to a section adjoining the circumferential weld.

Results of the eigenvalue solution for S6 again revealed a dramatic shift of the mode shape 1 pattern. Figures 6.3, 6.4 compare the new pattern S6, with S4. It was concluded that a nonuniform mesh was inappropriate to the loading conditions and any further analysis would require a uniform mesh configuration.

The S7 configuration used the finest mesh refinement in the central test portion of the cylinder. The pattern of small uniform elements yielded equal element stiffnesses along the longitudinal axis. Two rows of 4-node elements with coincident normals were used to transfer forces from the offset middle surfaces. The net effect of the mesh refinement and incorporation of the eccentric junction at the circumferential weld produced a smooth eigenvalue displacement pattern with a maximum peak at the centerline section damping to a minimum at the shell junction. Figure 6.5 illustrates the smooth transition as the stiffer end portions are approached.

In a final step, the thicker end shell portion was refined from 6 16-node elements to 108 4-node elements. The basic configuration of the S5 mesh was retained for the central portion. The eigenvalue solution of configuration S8 produced only minor displacements in the end section, as shown in Figure 6.6. It was concluded that the coarse mesh details of the previous patterns were not affecting the resulting displacement patterns to any significant degree.

Specimen B2 was analyzed for the S3 and S7 configurations. Results show a pattern consistent with the results of specimen B1. Figures 6.7, 6.8 display the eigenmode shape 1 displacement patterns.

#### 6.5 NONLINEAR IMPERFECT SHELL SOLUTION

Nonlinear solutions were obtained for the S3, S4, S5, and S7 configurations of specimen B1. Similar solutions were obtained for the S3, and S7 configurations of B2. For specimen B1, all nonlinear solutions except for the S4 configuration incorporated scaled initial imperfections. Specimen B2 was analyzed under only two configurations since it was assumed the results of testing B1 would indicate which configurations would yield the most valuable information.

The B1S3.N1, B1S5.N1, and B1S7.N1 investigations were analyzed under similar conditions by extracting a scaling factor from their corresponding eigenvalue solution and

using this factor to determine the initial imperfections of the shell surface. This permitted a comparison of their results as shown in Table 6.2. The most refined solution, B1S7.N1, had a limit moment of 2545 kN-m, 18.7% higher than that obtained experimentally. In the analysis of the B1S7 configuration two solutions, N2 and N3, were performed with a scale factor equal in magnitude but opposite in sign. A negligible difference in the limit load was observed, as shown in Tables A.7 and A.8 of Appendix A.

The first analysis of specimen B2 (B2S3.N1) used an arbitrary scale factor which was 3.36 times larger than the extracted scale factor. This analysis predicted a limit moment very close to the experimental value. However, these results can not be extended to a general case since the scale factor was arbitrary. The B2S7.N1 analysis produced a critical moment of 1201 kN-m, 16.6% higher than the maximum experimental moment of 1030 kN-m.

Moment-curvature relationships for all B1 and B2 analyses may be found in Appendix A. A considerable difference in load path may be observed comparing specimen B1 and B2. Specimen B2 displays a gradual failure pattern while B1 indicates a sharp peaking at maximum load.

The deformed configuration of B1S7 and B2S7 are found in the Figures 6.12, 6.13. Wrinkling of the cross section may be observed for each specimen.

## 6.6 MAGNITUDE OF INITIAL IMPERFECTIONS

A series of nonlinear analyses was performed to determine the effect of arbitrarily increasing the extracted scale factor and thus the corresponding first mode contributions to the initial displacement pattern. In the initial investigations four such analyses were conducted on model B1S3. Increasing scale factors were applied until a lower bound critical buckling load close to the experimental value was determined. Table 6.3 compares the scale factors to the critical buckling load. Figure 6.14 shows the reduction of the limit load with increase in nodal imperfections. While the general trend of these results was instructive, the uncertain nature of the S3 mesh configuration precluded further analysis to be performed on the final mesh configuration, S7.

The B2S7 configuration was analyzed with scale factors magnified 4, 8, and 16 times as large as the extracted mode-1 contribution. Table 6.4 compares the scale factors to the critical buckling load. Figure 6.15 indicates the reduced buckling load with increasing nodal imperfections. It can be seen that initially an increase in the scale factor results in a significant decrease of the critical load. However, further increases in the scale factor result in a smaller decrease of the the limit load. This suggests that the imperfection sensitivity of thin-walled tubes is not linear, i.e. an incremental increase in the initial imper-

fections results in a disproportionate reduction in the limit load. The B1S3 results suggest that at some value, further incremental increases result in no significant decrease of the limit load, a limit to imperfection sensitivity is indicated. Moment vs curvature tables and corresponding graphs of the series B1S3, and B2S7 tests may be found in Tables A.1 to A.4, A.12 to A.14 and Figures A.1 to A.4, A.12 to A.14 of Appendix A.

TABLE 6.1  
Eigenvalue Solutions

Analysis	Eigenvalues	Critical Moment (kN-m)
B1S3.E1	8.04959 X10 <sup>6</sup>	8050
B1S4.E1	8.03930 X10 <sup>6</sup>	8039
B1S5.E1	8.09969 X10 <sup>6</sup>	8100
B1S5.E1	8.09969 X10 <sup>6</sup>	8100
B1S7.E1	7.94626 X10 <sup>6</sup>	7946
B1S8.E1	8.19115 X10 <sup>6</sup>	8191
B2S3.E1	3.59704 X10 <sup>6</sup>	3597
B2S7.E1	3.54069 X10 <sup>6</sup>	3541

TABLE 6.2  
Nonlinear Solutions of Specimen B1

Analysis	Limit Moment (kN-m)
B1S3.N1	3057
B1S5.N1	2950
B1S7.N1	2761
Experimental	2143

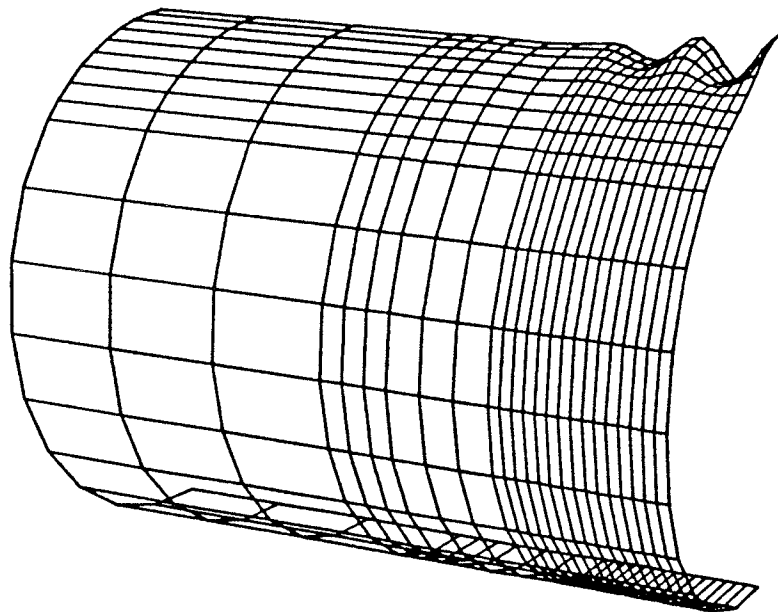


Figure 6.1: Mode Shape 1 B1S3.E1

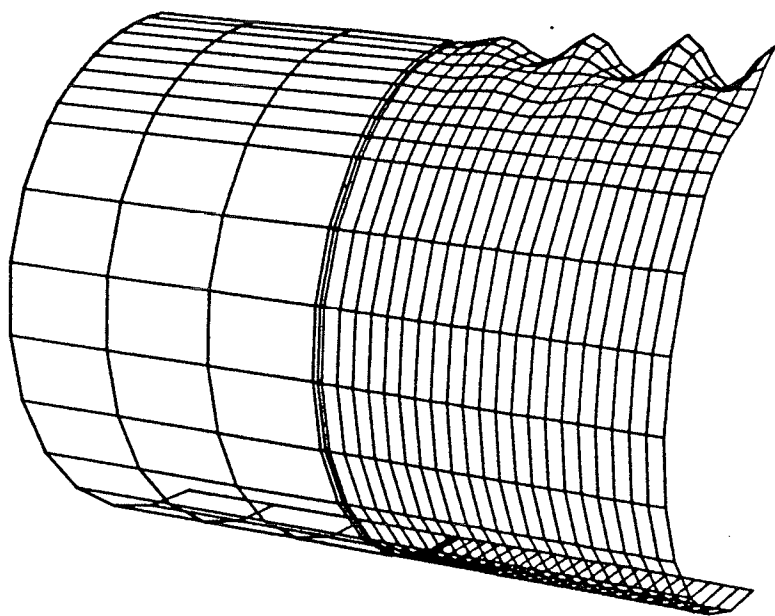


Figure 6.2: Mode Shape 1 B1S5.E1

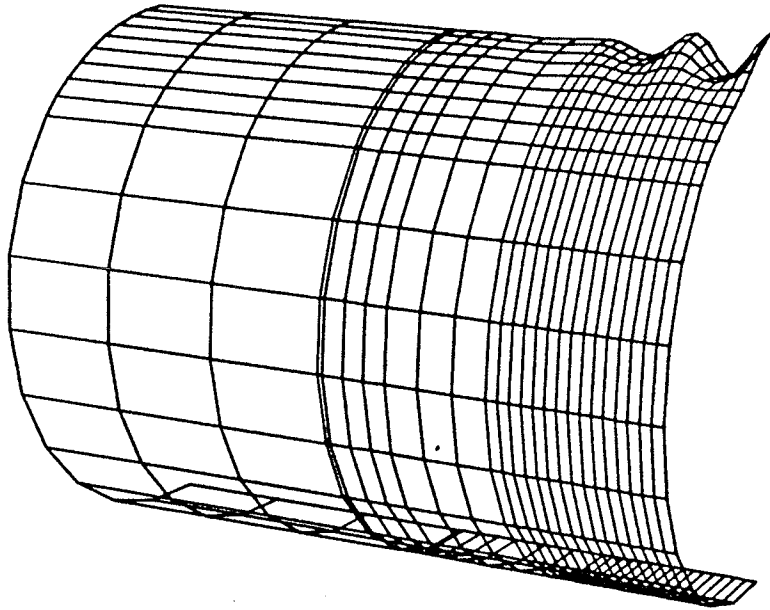


Figure 6.3: Mode Shape 1 B1S4.E1

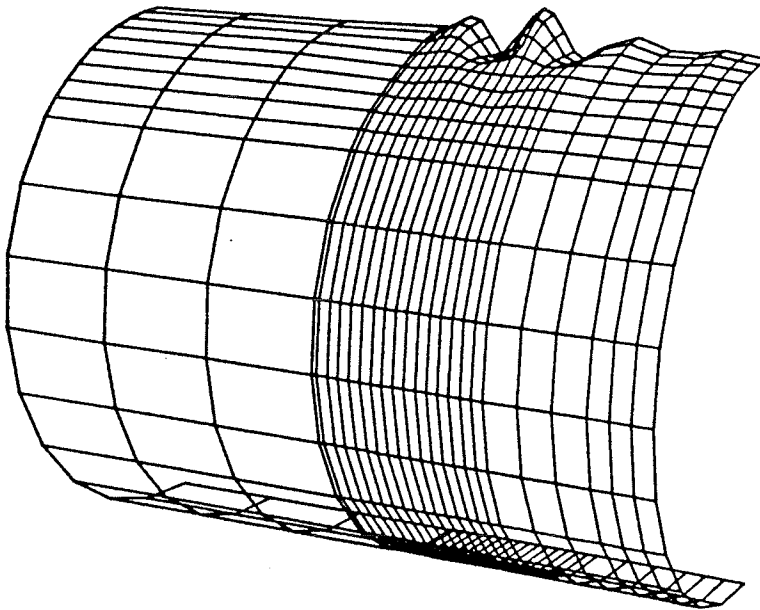


Figure 6.4: Mode Shape 1 B1S6.E1

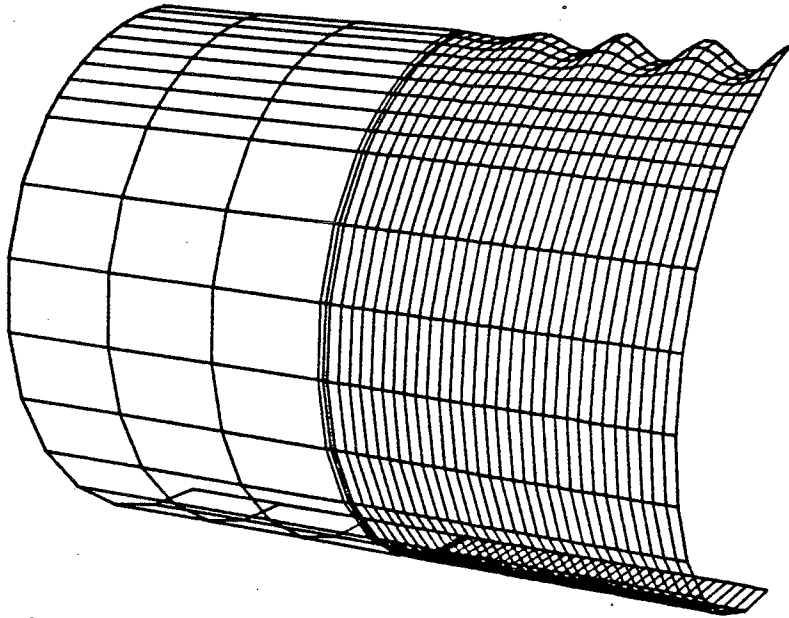


Figure 6.5: Mode Shape 1 B1S7.E1

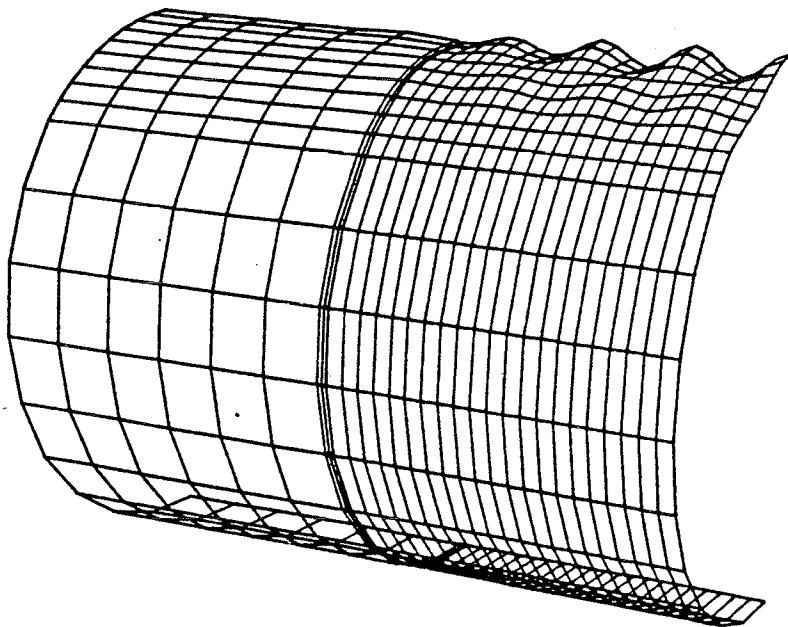


Figure 6.6: Mode Shape 1 B1S8.E1

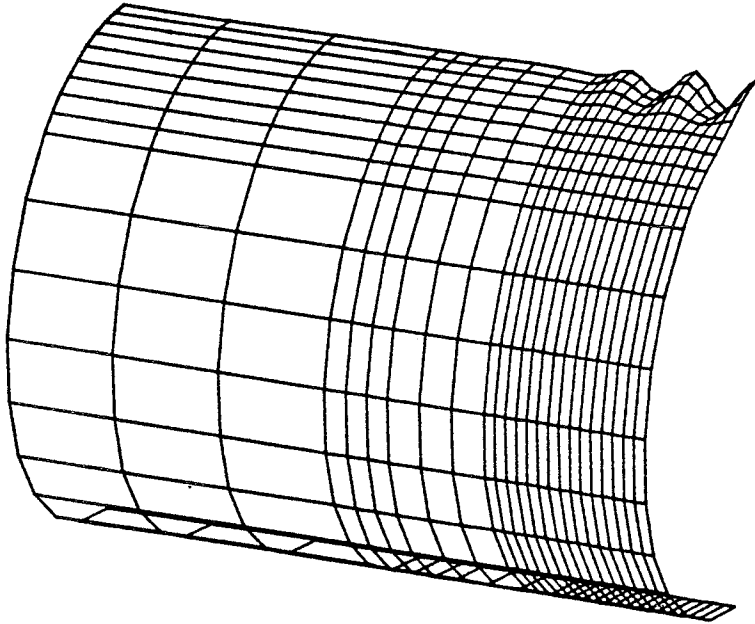


Figure 6.7: Mode Shape 1 B2S3.E1

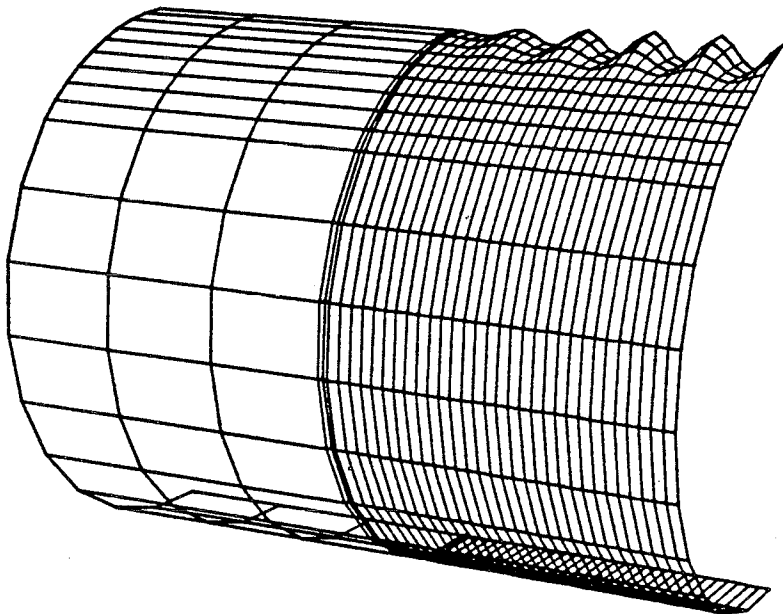
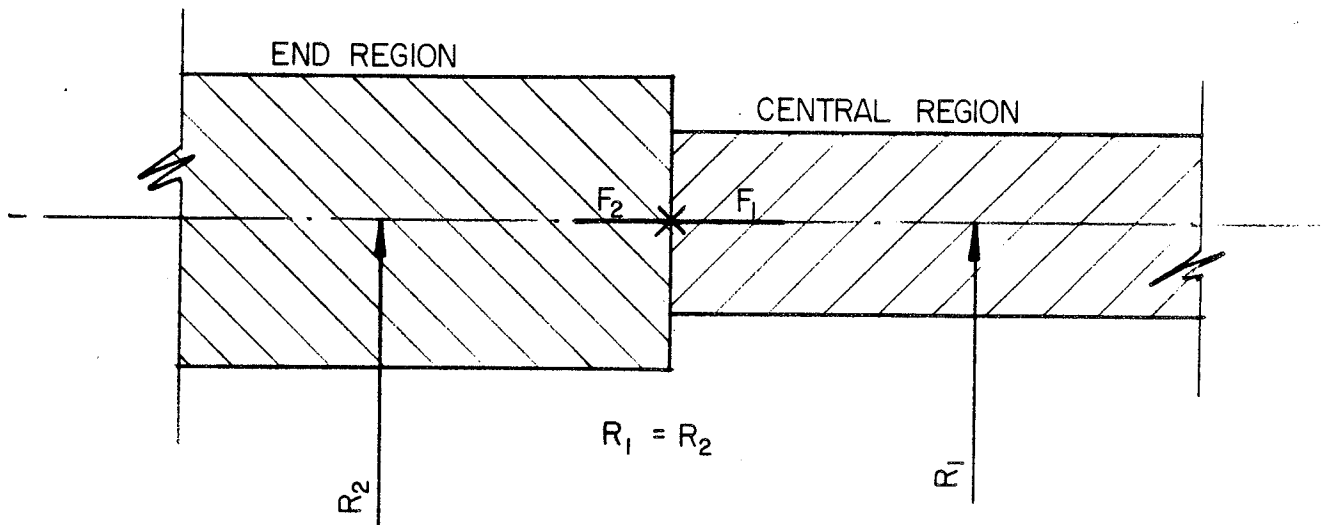
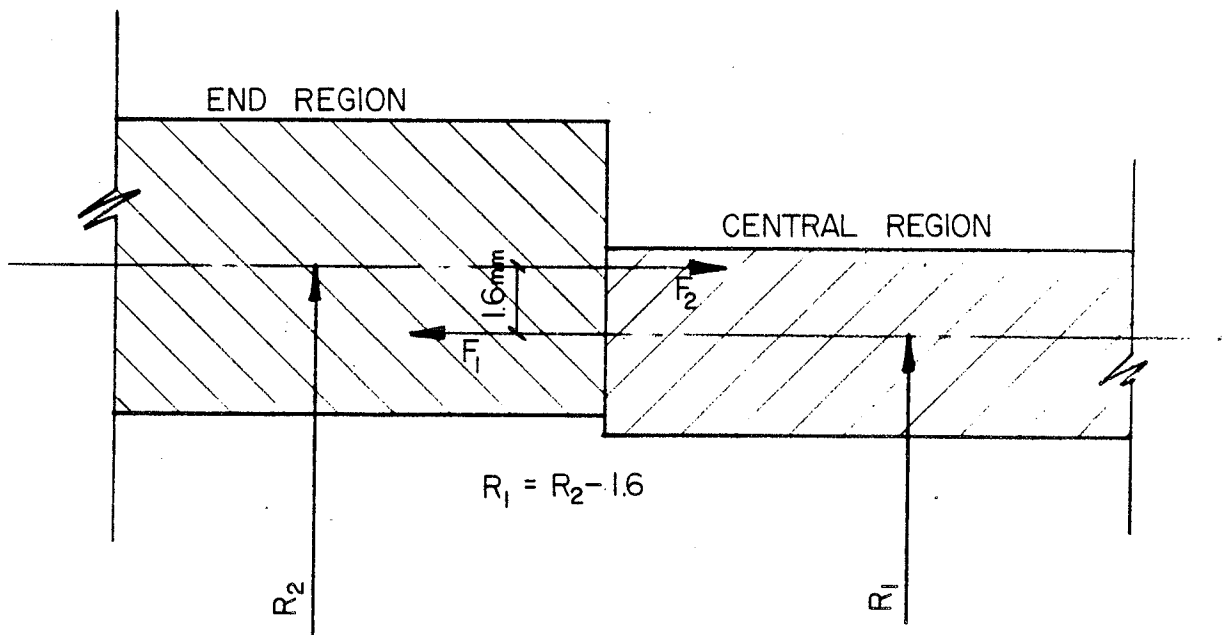


Figure 6.8: Mode Shape 1 B2S7.E1



DESIGNED CENTERLINE ALIGNMENT



EXPERIMENTAL ALIGNMENT

Figure 6.9: Shell Alignment

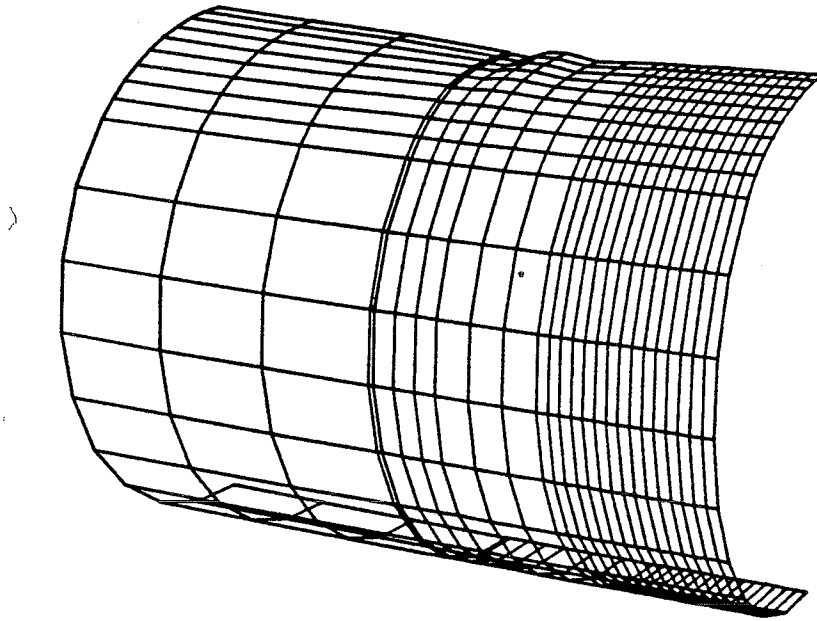


Figure 6.10: Local Buckling of B1S4.N1

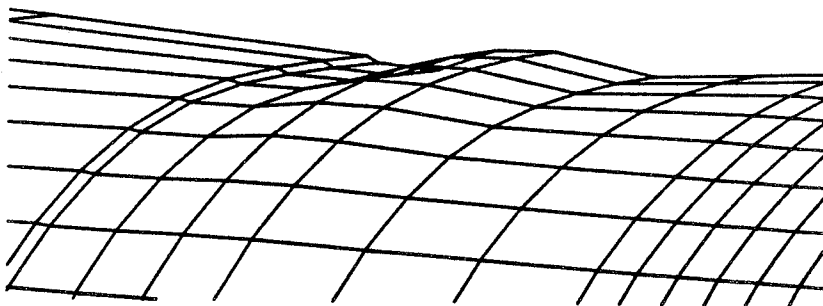


Figure 6.11: Buckled Region of B1S4.N1

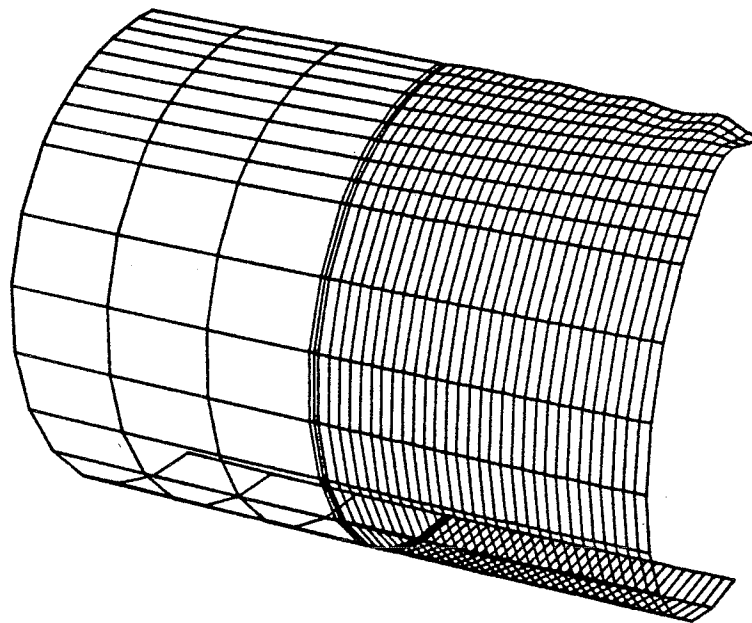


Figure 6.12: Failure Deformations of B1S7.N1

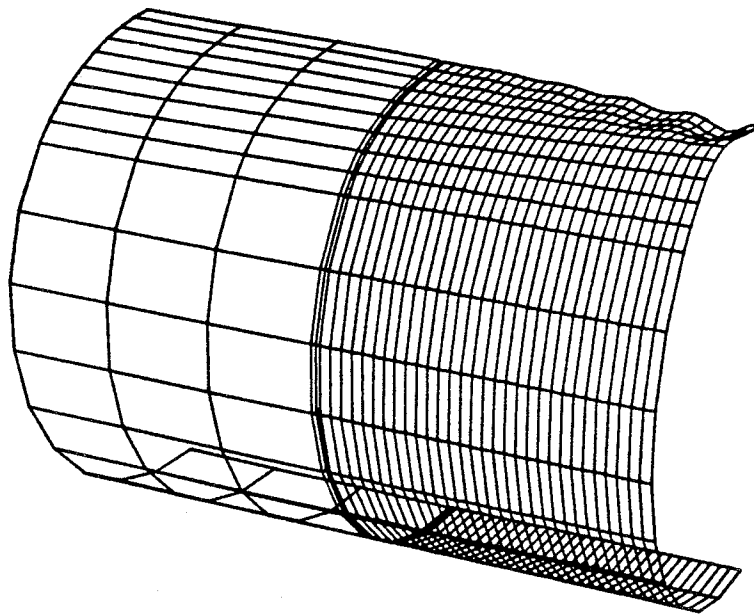


Figure 6.13: Failure Deformations of B2S7.N1

TABLE 6.3

Effect of Increased Nodal Imperfections on the Buckling Moment

Analysis	Extracted Scale Factor $a_1$	Applied Scaling Factor	Magnification	Limit Moment (kn-m)
B1S3.N1	0.00397	0.00397	1.00	3050
B1S3.N2	0.00397	0.01000	2.52	2540
B1S3.N3	0.00397	0.01500	3.78	2304
B1S3.N4	0.00397	0.02500	6.30	2110
EXPER.	nil	nil	nil	2143

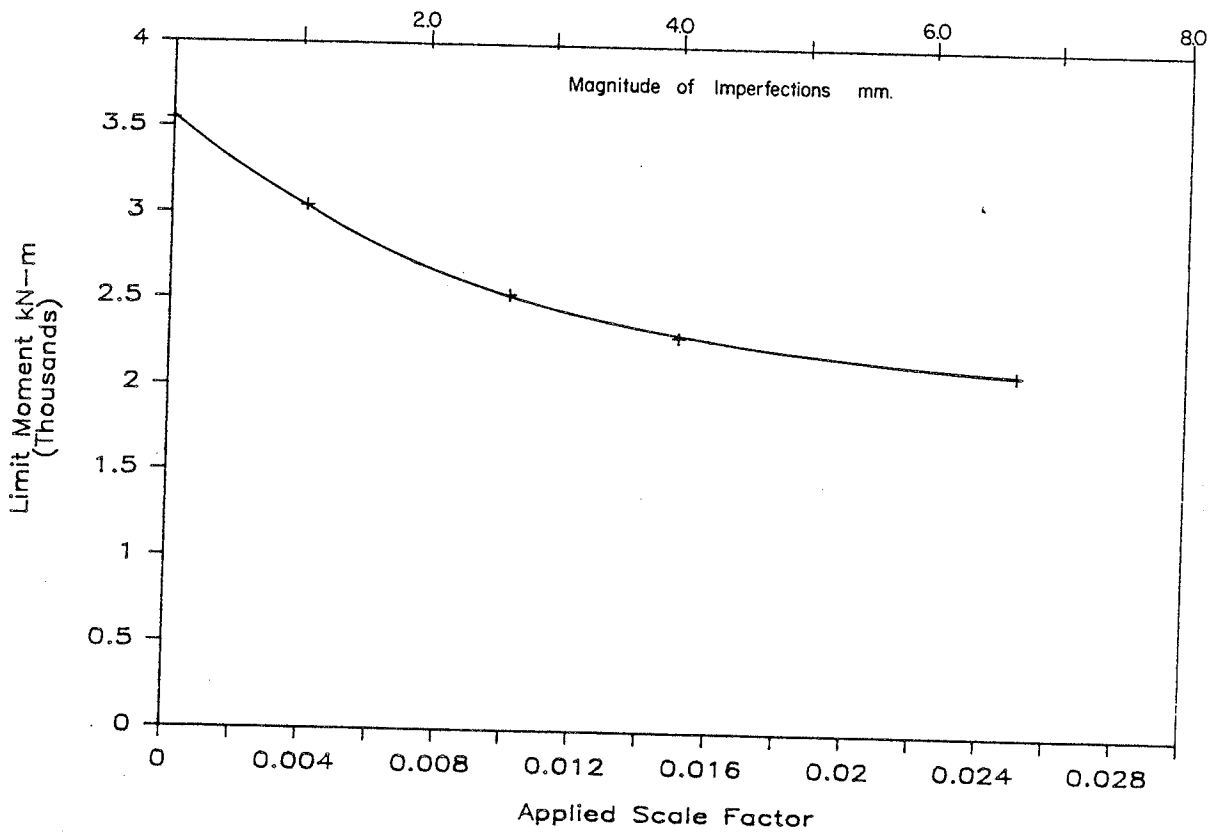


Figure 6.14: Scale Factor vs Moment B1S3

TABLE 6.4

Effect of Increased Nodal Imperfections on the Buckling Moment

Analysis	Extracted Scale Factor $a_1$	Applied Scaling Factor	Magnification	Limit Moment (kn-m)
B2S7.N1	0.01302	0.01302	1.00	1201
B2S7.N2	0.01302	0.05208	4.00	1012
B2S7.N3	0.01302	0.10416	8.00	920
B2S7.N4	0.01302	0.20832	16.00	850
EXPER.	nil	nil	nil	1030

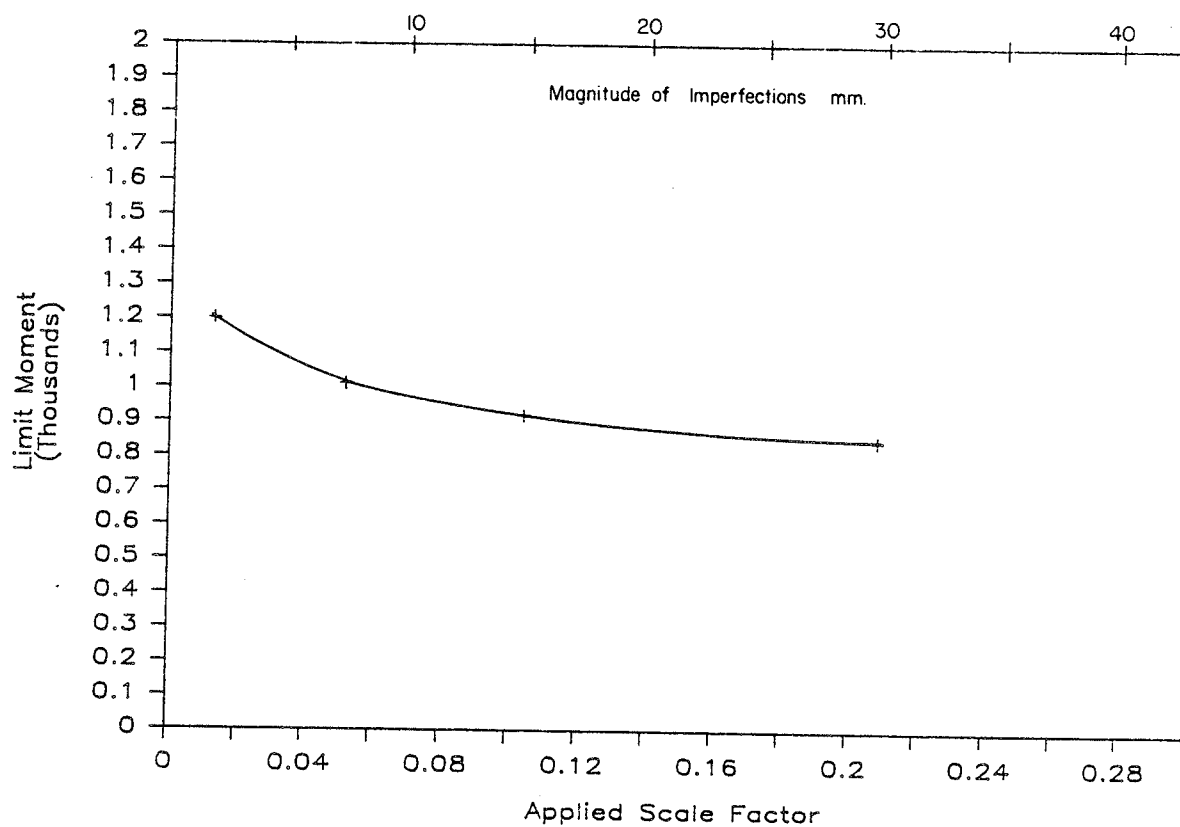


Figure 6.15: Scale Factor vs Moment B2S7

## Chapter VII

### DISCUSSION

#### 7.1 INTRODUCTION

In this chapter the results of the F.E.M. analysis are discussed with reference to the experimental program of Stephens et al (7). The effect of geometric imperfections is assessed with respect to the method of incorporation and magnitude. The effectiveness of the NISA80 program is reviewed. Finally, reasons are suggested why the analytical program failed to reach the experimental limit point load.

#### 7.2 INITIAL IMPERFECTIONS

The experimental cylindrical shells possessed a given displacement pattern of initial imperfections. The analytical procedure used those initial imperfections in order to determine a scale factor, which in turn was applied to the mode-shape 1 eigenvector displacements. Although small, the actual imposed pattern was severe since the initial shell configuration already followed the worst configuration possible. Since it is unlikely the real shell would possess this configuration, this introduces a biased failure pattern. The imposed nodal imperfections were as much as an

order of magnitude smaller than the observed quantities, but this did not outweigh the sensitivity of the eigenvalue displacement pattern. The scaling technique chosen was justified by its ease in repeated application to other shells of similar nature. It permits a consistent analysis procedure once a scale factor has been selected from a data bank of values.

The scaling method displayed consistency in similar analyses. In the four B2S7 series analyses an increased scale factor was employed for each successive analysis. As shown in figure 6.15, an increase in the scale factor led to a decrease in the limit point load obtained. This curve seems to imply that, after a certain magnitude of nodal imperfections are incorporated, only a very small decrease in the limit point load would be achieved with a further increase in the imperfections.

A shortcoming of the scaling method is related to the preferred failure pattern achieved with this method. In the experimental program failure was observed in a region close to the circumferential weld. For a cylindrical shell subjected to pure flexure, the eigenvalue solution consistently produced a mode-shape 1 displacement pattern with a concentrated region of maximum values located near the centerline section. This resulted in only very minor initial imperfections in the circumferential weld area. In the BLS4.N1 analysis, no initial imperfections were incorporated and

failure was observed in a region near the circumferential weld, possibly due to the eccentric junction of the end and central shell region. Although the eigenvalue solution of BLS4 again yielded the typical preferred configuration mentioned above, the results of the nonlinear solution suggest a bias may be introduced here.

### 7.3 ACHIEVING THE LIMIT POINT LOAD

The ultimate objective of this analysis was to test whether nonlinear finite element methods can successfully predict the experimental limit point load of a given cylindrical shell. Although, the results of this investigation suggest this is possible, certain modifications to the modelling system must first be made.

For cylindrical shells subjected to pure flexure, there is no stress gradient along the length of the shell. This suggests that a uniform mesh configuration should be used for all analysis.

The analytical modelling of large-scale experimental programs is restrictive because of the heavy demand placed on resources. The average nonlinear analysis required 12 time steps with approximately 2 to 3 iterations required per step. The average total CPU time required ranged between 6.5 and 7.5 hours. The above data is based on using the University of Manitoba Amdahl 670 computer. Eigenvalue

solutions were not as dependent on CPU time, but very high Input/Output counts were needed for a single solution of the S7 mesh configuration. Additional mesh refinement is usually limited by the available system resources and cost. Surprisingly though, an increase from the 494 nodes corresponding to the S3 configuration to the 703 node mesh corresponding to S7 resulted in only a slight increase in the overall cost of the nonlinear solution. The refined mesh pattern S7 required 26% more CPU per iteration, but the number of time steps and iterations per step decreased, resulting in a total cost comparable with the S3 analysis.

Throughout the analysis the NISA80 program provided consistent results. Refined mesh patterns repeatedly yielded better solutions. Increased nodal imperfections led to lower limit point loads. The program was easily restarted at any given time step. The load path traced was smooth and void of fluctuations near the limit point load.

The limit point loads predicted by NISA80 were higher than the experimental values. It is felt the major discrepancy between results is linked to the omission of residual stresses. As discussed previously, the calculation of residual stresses is extremely complex. It is dependent on the material type, fabrication technique, and size of specimen. It is certain that forming and welding processes used in the fabrication of the experimental specimen induced residual stress concentrations in the vicinity of the junction

between central and end section of the shell. An estimation of the magnitude of these stresses is needed to obtain accurate results. Once determined, a system must be developed to incorporate these initial stresses into the nonlinear finite element program.

Chapter VIII  
CONCLUSIONS AND RECOMMENDATIONS

8.1 CONCLUSIONS

1. Cylindrical shells subjected to pure bending are not as imperfection sensitive as the same cylindrical shells subjected to pure axial load.
2. Very large increases in initial imperfections cause only very moderate reductions in the limit moment.
3. The NISA80 program can effectively analyze the buckling behaviour of thin-walled cylindrical shells subjected to pure bending.
4. The eigenmode scaling technique for incorporating initial imperfections into the analysis resulted in predicted limit moments some 15-20% larger than were found experimentally.
5. Uniform mesh patterns should be employed for all all pure flexure analysis.
6. The discrepancies between analytical and experimental limit moments may be due to the presence of residual stresses which were not considered in the analyses.

## 8.2 RECOMMENDATIONS

1. Future investigations should study the lower imperfection sensitivity displayed by cylindrical shells subjected to pure bending.
2. Future analytical studies should seek a means of incorporating residual stresses into the nonlinear finite element analysis.
3. An investigation of plasticity reduction factors for nonhomogenous material behaviour caused by residual stresses should be conducted.
4. Further analytical study is needed to investigate the buckling of thin-walled cylindrical shells subjected to pure bending.

Appendix A  
MOMENT-CURVATURE

TABLE A.1

## Moment vs Curvature BLS3.N1

Step	Moment kN-m	Node 400		Node 418		Curvature $d\phi/ds \times 10^6$
		u $\times 10^3$	w $\times 10^3$	u $\times 10^3$	w $\times 10^3$	
1	359	-173.4	-271.6	172.3	-264.1	0.2472
2	717	-346.8	-547.2	343.4	-523.8	0.4935
3	1073	-520.1	-827.0	513.2	-779.3	0.7391
4	1428	-693.3	-1111.6	681.7	-1030.7	0.9835
5	1780	-866.4	-1401.5	848.8	-1278.0	1.2270
6	2130	-1039.4	-1697.4	1014.4	-1521.3	1.4690
7	2478	-1211.9	-2000.4	1178.1	-1760.5	1.7097
8	2637	-1291.4	-2144.1	1252.7	-1869.1	1.8207
9	2792	-1370.5	-2293.0	1325.9	-1976.0	1.9290
10	2878	-1415.1	-2382.5	1366.1	-2035.2	1.9896
11	2952	-1457.0	-2479.8	1401.2	-2088.6	2.0448
12	2984	-1476.4	-2529.7	1416.4	-2112.5	2.0696
13	3009	-1493.3	-2679.6	1428.2	-2132.1	2.0902
14	3029	-1506.1	-2628.5	1437.6	-2148.6	2.1061
15	3043	-1520.9	-2675.9	1444.6	-2163.8	2.1218
16	3057	-1550.9	-2827.1	1451.8	-2185.7	2.1486
17	3051	-1563.3	-2932.0	1445.0	-2187.8	2.1527
18	3012	-1569.9	-3027.0	1431.8	-2182.2	2.1481

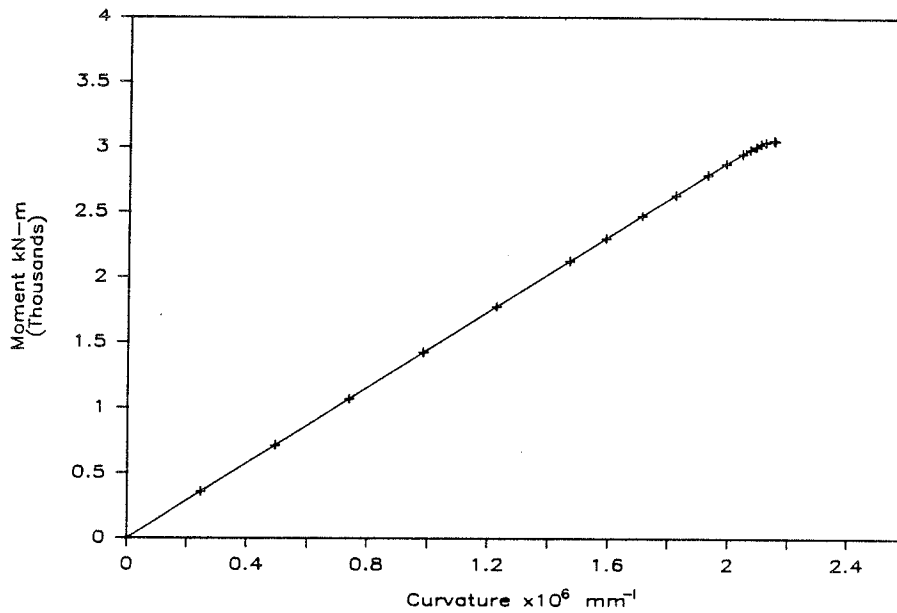


Figure A.1: Moment vs Curvature BLS3.N1

TABLE A.2

## Moment vs Curvature B1S3.N2

Step	Moment kN-m	Node 400		Node 418		Curvature $d\phi/ds \times 10^6$
		$u \times 10^3$	$w \times 10^3$	$u \times 10^3$	$w \times 10^3$	
1	359	-176.3	-293.6	172.0	-265.3	0.2491
2	714	-352.3	-594.7	342.0	-525.4	0.4967
3	1066	-527.9	-904.4	509.7	-780.1	0.7422
4	1411	-702.8	-1233.8	674.4	-1028.9	0.9852
5	1751	-876.3	-1154.6	835.5	-1274.2	1.2232
6	2077	-1045.9	-1902.0	989.7	-1503.8	1.4563
7	2358	-1205.8	-2281.0	1123.0	-1709.6	1.6661
8	2479	-1297.7	-2591.4	1181.2	-1812.3	1.7739
9	2526	-1358.8	-2869.7	1204.4	-1860.8	1.8345
10	2539	-1415.5	-3187.6	1212.3	-1907.3	1.8810
11	2530	-1463.3	-3493.0	1209.2	-1932.4	1.9134

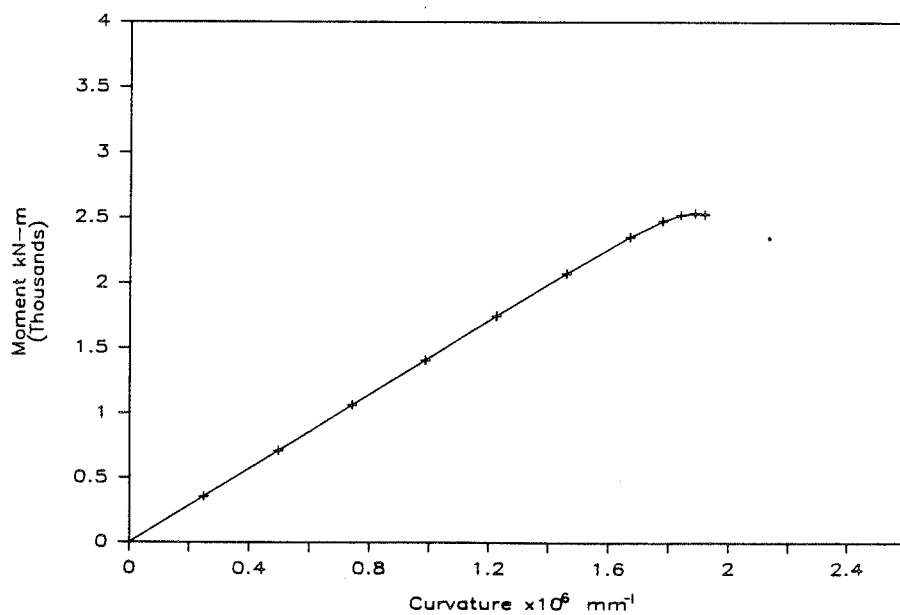


Figure A.2: Moment vs Curvature B1S3.N2

TABLE A.3

Moment vs Curvature BLS3.N3

Step	Moment kN-m	Node 400		Node 418		Curvature $d\phi/ds \times 10^6$
		u $\times 10^3$	w $\times 10^3$	u $\times 10^3$	w $\times 10^3$	
1	359	-180.3	-323.8	171.5	-266.8	0.2516
2	708	-359.5	-658.4	339.3	-526.4	0.4992
3	1049	-536.8	-1004.8	502.3	-777.7	0.7433
4	1379	-711.2	-1363.6	659.5	-1019.6	0.9806
5	1691	-880.7	-1736.4	807.8	-1248.7	1.2086
6	1962	-1038.2	-2125.1	937.1	-1452.5	1.4134
7	2116	-1143.6	-2444.9	1010.9	-1577.2	1.5418
8	2206	-1224.4	-2746.7	1054.3	-1661.4	1.6310
9	2257	-1290.3	-3033.0	1079.8	-1721.6	1.6970
10	2291	-1359.8	-3370.7	1097.5	-1777.2	1.7594
11	2306	-1423.3	-3700.7	1106.4	-1821.6	1.8110
12	2304	-1481.1	-4025.3	1106.8	-1854.7	1.8536
13	2290	-1535.7	-4344.8	1102.2	-1881.3	1.8897
14	2276	-1590.4	-4661.7	1097.1	-1907.4	1.9257

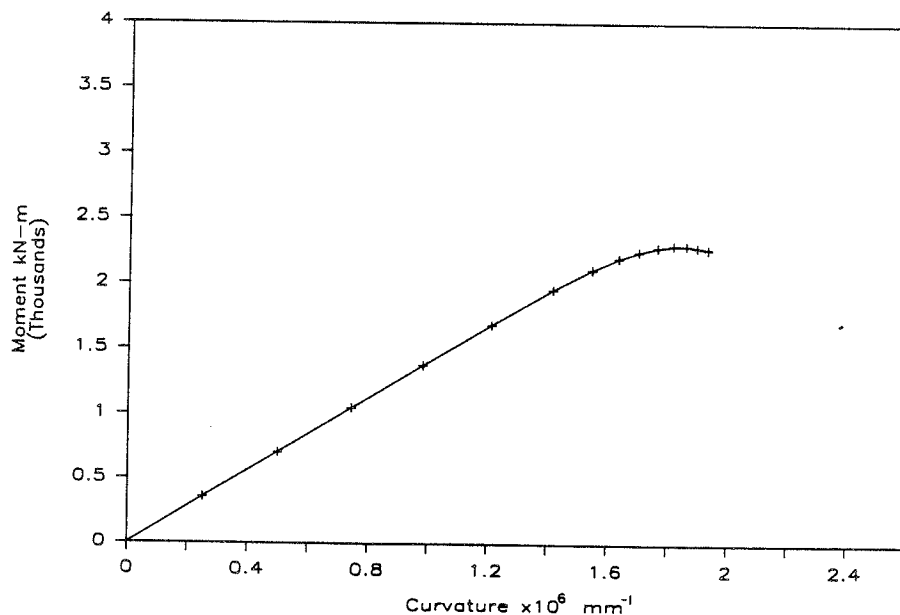


Figure A.3: Moment vs Curvature BLS3.N3

TABLE A.4

## Moment vs Curvature BLS3.N4

Step	Moment kN-m	Node 400		Node 418		Curvature $d\phi/ds \times 10^6$
		u $\times 10^3$	w $\times 10^3$	u $\times 10^3$	w $\times 10^3$	
1	352	-191.7	-403.1	169.5	-270.9	0.2584
2	687	-378.3	-817.3	330.1	-527.7	0.5067
3	1000	-558.6	-1240.7	480.4	-769.1	0.7428
4	1289	-731.1	-1670.7	619.0	-993.6	0.9960
5	1543	-891.7	-2103.8	740.4	-1194.6	1.1680
6	1743	-1033.8	-2532.5	836.5	-1361.7	1.3387
7	1850	-1129.6	-2867.8	888.5	-1462.9	1.4447
8	1946	-1234.3	-3267.7	935.5	-1564.9	1.5540
9	2011	-1328.9	-3657.3	968.6	-1648.6	1.6454
10	2054	-1416.9	-4039.5	990.3	-1717.5	1.7244
11	2074	-1482.9	-4347.4	1001.8	-1765.4	1.7801
12	2096	-1564.5	-4722.6	1014.0	-1822.0	1.8478
13	2110	-1644.7	-5098.2	1022.6	-1874.2	1.9118
14	2109	-1707.0	-5409.2	1023.7	-1908.5	1.9576
15	2106	-1783.8	-5792.0	1024.3	-1949.9	2.0135
16	2101	-1861.3	-6176.2	1024.2	-1990.7	2.0694
17	2095	-1939.1	-6564.3	1023.1	-2030.1	2.1250
18	2083	-2016.4	-6958.1	1019.7	-2066.2	2.1785

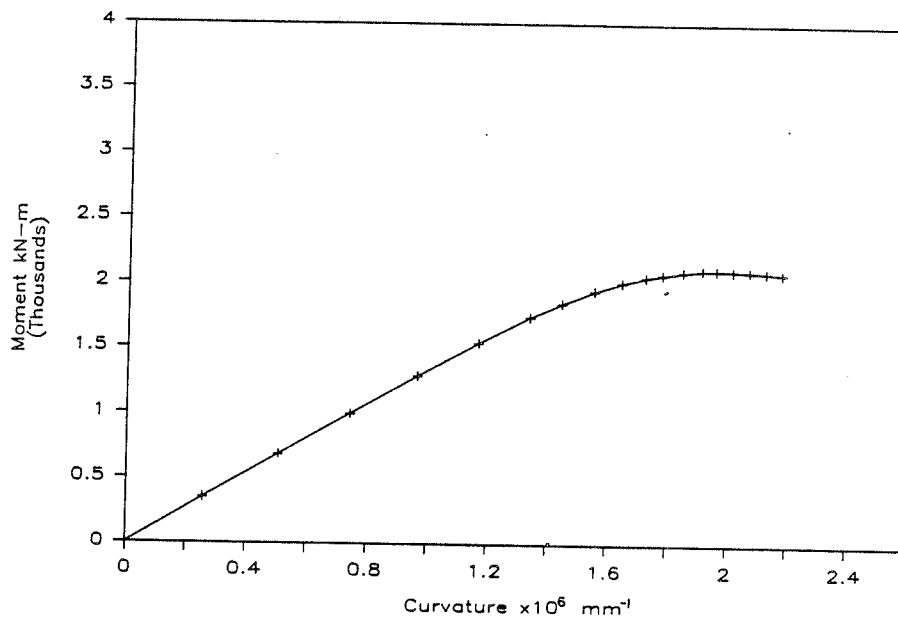


Figure A.4: Moment vs Curvature BLS3.N4

TABLE A.5

## Moment vs Curvature B1S4.N1

Step	Moment kN-m	Node 419		Node 437		Curvature $d\phi/ds \times 10^6$
		u $\times 10^3$	w $\times 10^3$	u $\times 10^3$	w $\times 10^3$	
1	359	-172.8	-270.1	171.9	-268.3	0.2465
2	718	-345.7	-543.6	342.6	-532.0	0.4923
3	1074	-518.5	-820.7	512.2	-791.3	0.7372
4	1430	-691.2	-1101.7	680.6	-1046.3	0.9812
5	1784	-863.9	-1386.6	847.8	-1297.2	1.2243
6	2136	-1036.4	-1676.6	1013.7	-1544.1	1.4664
7	2486	-1208.7	-1971.8	1178.3	-1787.3	1.7074
8	2832	-1380.4	-2273.4	1340.5	-2033.1	1.9464
9	3071	-1501.3	-2499.3	1452.1	-2216.7	2.1128
10	3372	-1679.2	-2947.0	1609.5	-2500.9	2.3530
11	3475	-1805.2	-3565.3	1706.8	-2739.0	2.5133
12	3485	-1887.1	-4133.9	1719.8	-2800.5	2.5820
13	3467	-1981.8	-4895.8	1714.1	-2838.3	2.6470
14	3435	-2069.4	-5672.7	1701.8	-2866.7	2.7023
15	3389	-2172.3	-6641.0	1683.7	-2896.2	2.7648

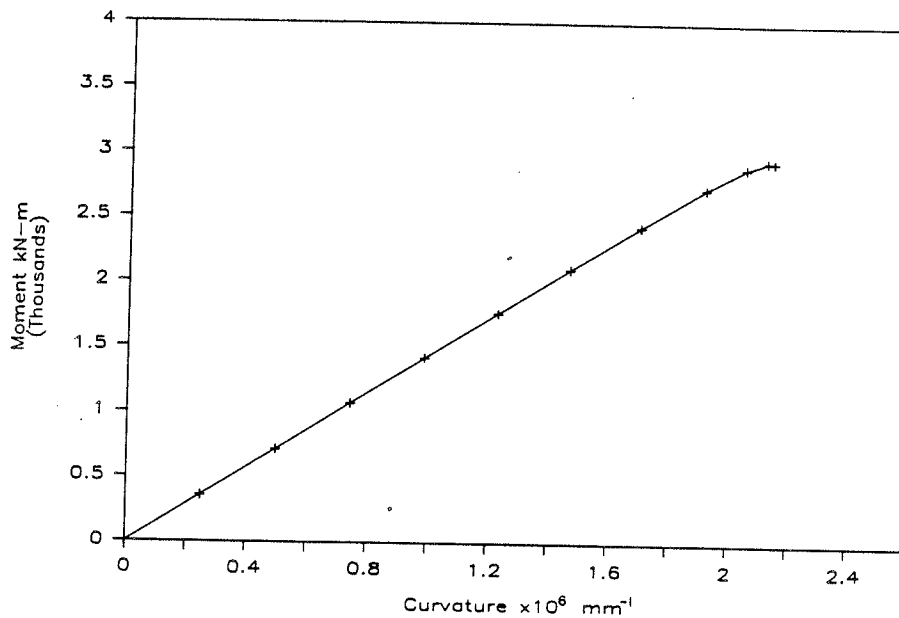


Figure A.5: Moment vs Curvature B1S4.N1

TABLE A.6

## Moment vs Curvature B1S5.N1

Step	Moment kN-m	Node 419		Node 437		Curvature $d\phi/ds \times 10^6$
		$u \times 10^3$	$w \times 10^3$	$u \times 10^3$	$w \times 10^3$	
1	359	-175.5	-311.7	172.5	-282.4	0.2488
2	716	-350.9	-631.1	343.3	-559.3	0.4965
3	1071	-526.1	-959.3	512.4	-830.9	0.7428
4	1421	-701.1	-1297.7	679.4	-1079.1	0.9876
5	1767	-875.7	-1648.4	844.1	-1357.7	1.2302
6	2108	-1049.0	-2018.5	1005.4	-1612.4	1.4689
7	2437	-1220.2	-2415.9	1161.1	-1861.7	1.7026
8	2732	-1384.5	-2889.2	1300.0	-2094.8	1.9190
9	2895	-1495.0	-3300.0	1377.1	-2239.5	2.0529
10	2950	-1565.4	-3637.3	1407.5	-2315.1	2.1244
11	2943	-1601.3	-3908.1	1401.8	-2333.7	2.1457

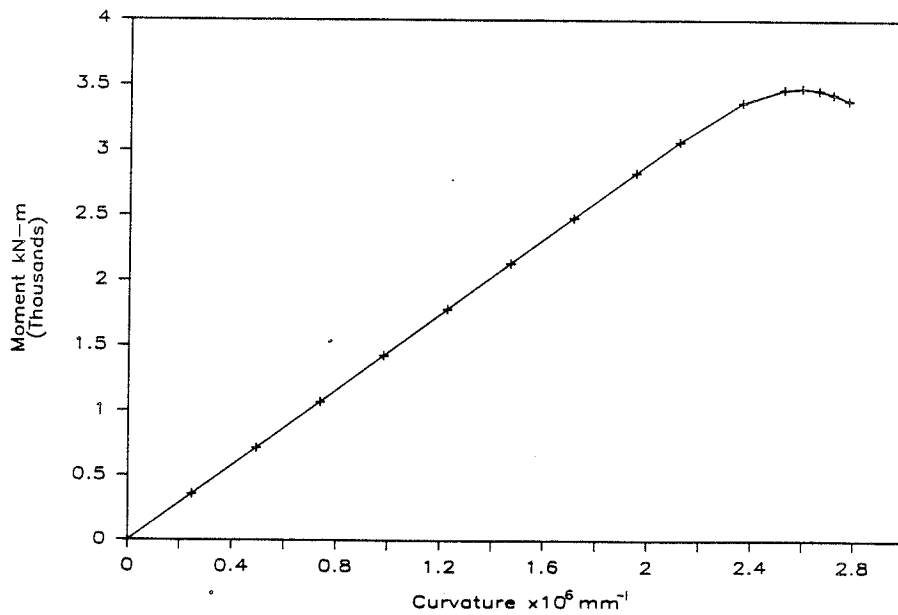


Figure A.6: Moment vs Curvature B1S5.N1

TABLE A.7

## Moment vs Curvature BlS7.N1

Step	Moment kN-m	Node 590		Node 608		Curvature $d\phi/ds \times 10^6$
		u $\times 10^3$	w $\times 10^3$	u $\times 10^3$	w $\times 10^3$	
1	357	-183.4	-344.0	172.1	-279.6	0.2543
2	708	-366.1	-701.0	340.7	-551.7	0.5056
3	1051	-547.5	-1070.2	505.0	-815.8	0.7529
4	1385	-727.1	-1458.7	664.4	-1071.2	0.9955
5	1706	-903.8	-1861.4	817.6	-1316.8	1.2317
6	2001	-1074.3	-2285.5	958.3	-1545.4	1.4545
7	2333	-1226.9	-2732.5	1069.4	-1735.9	1.6435
8	2367	-1332.1	-3094.5	1133.8	-1856.3	1.7652
9	2472	-1439.4	-3520.3	1185.3	-1966.8	1.8792
10	2522	-1513.0	-3845.7	1210.5	-2034.2	1.9503
11	2545	-1575.0	-4149.5	1222.7	-2083.3	2.0037
12	2538	-1625.8	-4432.6	1221.1	-2113.1	2.0393

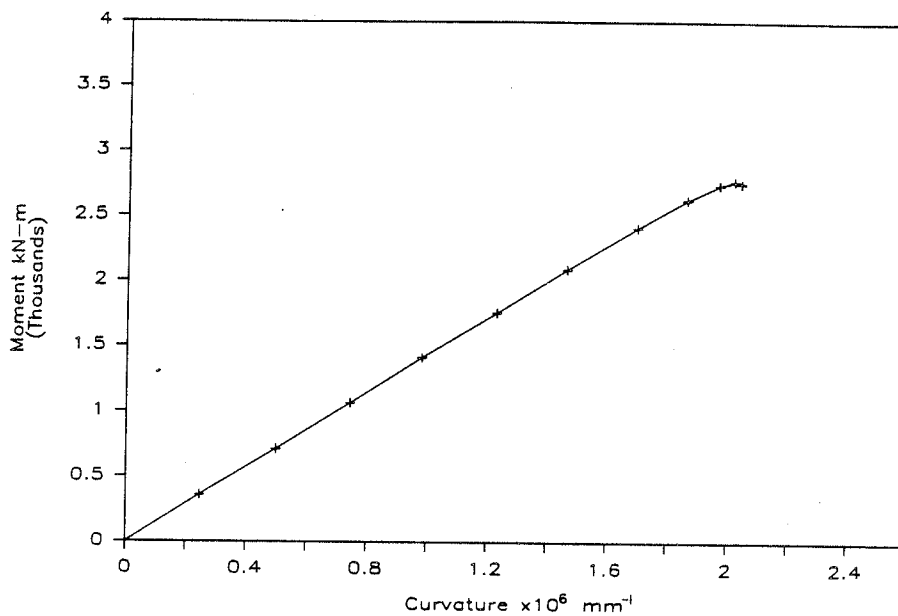


Figure A.7: Moment vs Curvature BlS7.N1

TABLE A.8

## Moment vs Curvature B1S7.N2

Step	Moment kN-m	Node 590		Node 608		Curvature $d\phi/ds \times 10^6$
		u $\times 10^3$	w $\times 10^3$	u $\times 10^3$	w $\times 10^3$	
1	358	-176.5	-317.8	172.4	-283.2	0.2495
2	714	-352.8	-644.5	342.8	-560.7	0.4975
3	1067	-529.0	-981.2	511.1	-832.4	0.7438
4	1415	-704.6	-1329.5	677.0	-1098.1	0.9880
5	1758	-879.5	-1691.7	839.8	-1357.5	1.2294
6	2092	-1052.6	-2074.9	998.4	-1609.9	1.4594
7	2409	-1221.9	-2490.5	1148.1	-1852.6	1.6944
8	2615	-1346.6	-2878.3	1245.6	-2021.8	1.8530
9	2752	-1440.4	-3247.2	1301.7	-2133.4	1.9598
10	2761	-1495.2	-3539.7	1316.6	-2184.3	2.0101
11	2717	-1517.9	-3765.1	1297.4	-2182.1	2.0115
12	2640	-1523.6	-3952.4	1262.2	-2155.6	1.9901

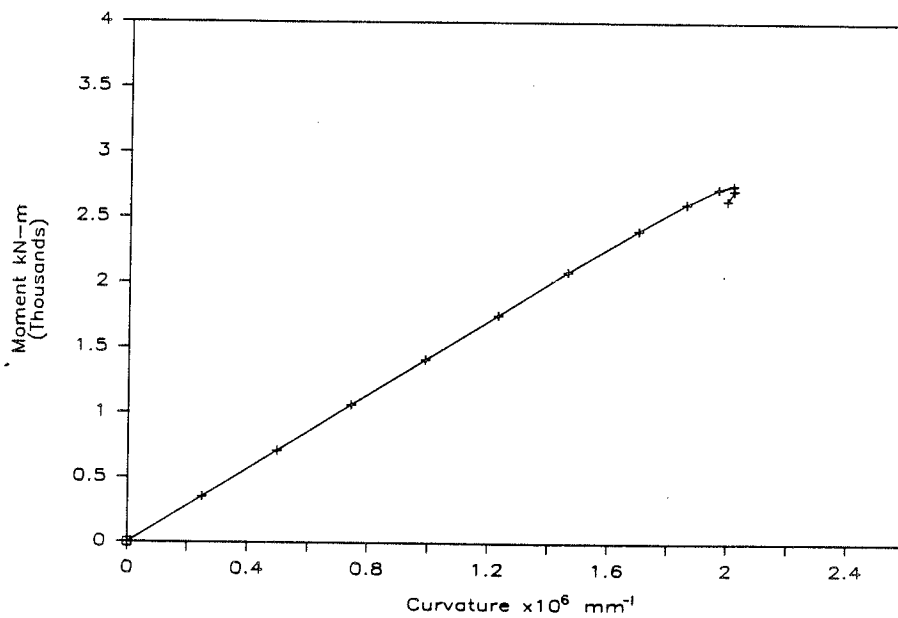


Figure A.8: Moment vs Curvature B1S7.N2

TABLE A.9

## Moment vs Curvature B1S7.N3

Step	Moment kN-m	Node 590		Node 608		Curvature $d\phi/ds \times 10^6$
		$u \times 10^3$	$w \times 10^3$	$u \times 10^3$	$w \times 10^3$	
1	359	-172.8	-313.3	172.4	-283.1	0.2469
2	715	-352.7	-634.9	342.9	-560.4	0.4975
3	1068	-528.7	-966.1	511.4	-832.0	0.7440
4	1416	-704.4	-1308.3	667.4	-1097.7	0.9813
5	1760	-879.3	-1663.6	840.4	-1357.3	1.2303
6	2095	-1052.7	-2038.2	993.4	-1609.8	1.4639
7	2413	-1222.6	-2441.9	1150.1	-1853.5	1.6976
8	2629	-1350.5	-2816.8	1252.3	-2029.0	1.8626
9	2744	-1443.9	-3180.9	1307.7	-2140.0	1.9694
10	2773	-1500.3	-3479.3	1321.9	-2190.3	2.0203
11	2755	-1536.9	-3745.0	1315.1	-2208.2	2.0419

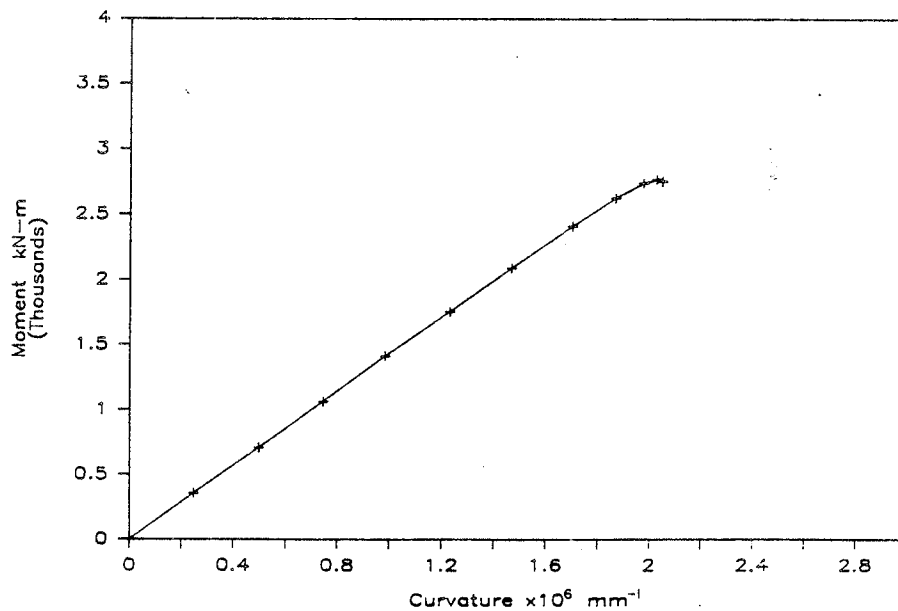


Figure A.9: Moment vs Curvature B1S7.N3

TABLE A.10

## Moment vs Curvature B2S3.N1

Step	Moment kN-m	Node 400		Node 418		Curvature $d\phi/ds \times 10^6$
		u $\times 10^3$	w $\times 10^3$	u $\times 10^3$	w $\times 10^3$	
1	191	-164.5	-402.1	137.3	-211.0	0.2167
2	363	-318.7	-810.2	260.7	-401.9	0.4160
3	515	-461.9	-1220.0	370.0	-572.9	0.5974
4	648	-594.1	-1628.1	465.7	-725.1	0.7613
5	759	-712.9	-2030.0	545.0	-855.1	0.9037
6	843	-816.8	-2420.8	605.8	-960.9	1.0220
7	903	-907.1	-2798.9	649.9	-1045.1	1.1190
8	949	-989.4	-3167.7	683.9	-1116.6	1.2030
9	984	-1065.9	-3528.5	710.3	-1178.8	1.2770
10	1008	-1137.2	-3883.4	728.9	-1231.8	1.3420
11	1020	-1202.5	-4232.6	738.4	-1273.7	1.3960
12	1028	-1267.1	-4578.8	746.1	-1314.0	1.4483
13	1033	-1319.7	-4860.0	751.5	-1346.2	1.4903
14	1040	-1384.4	-5203.8	757.5	-1385.5	1.5414
15	1044	-1449.5	-5552.2	762.4	-1423.8	1.5921
16	1043	-1501.7	-5846.3	763.2	-1451.4	1.6306
17	1042	-1566.8	-6210.4	764.5	-1486.1	1.6788
18	1040	-1632.4	-6577.8	767.3	-1520.6	1.7284

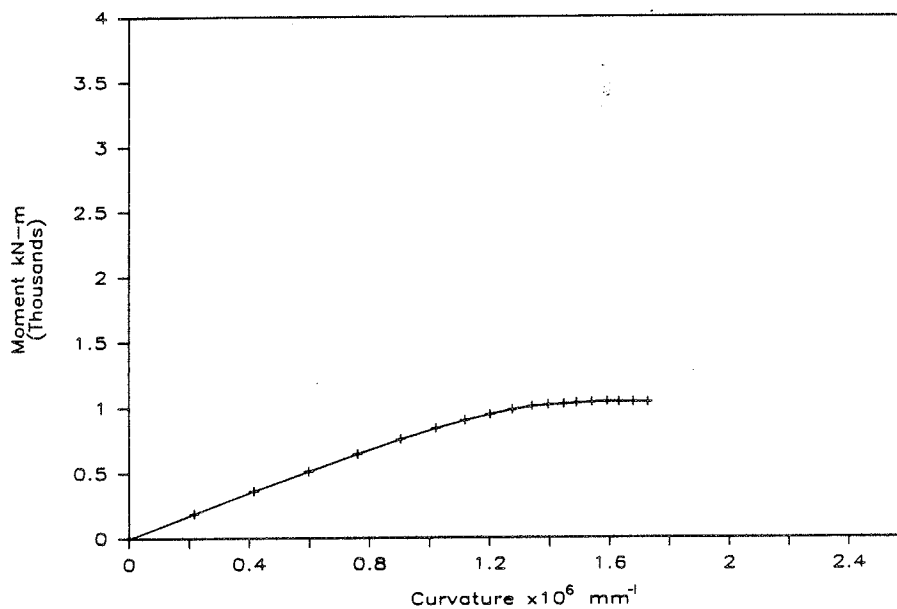


Figure A.10: Moment vs Curvature B2S3.N1

TABLE A.11  
Moment vs Curvature B2S7.N1

Step	Moment kN-m	Node 590		Node 608		Curvature $d\phi/ds \times 10^6$
		$u \times 10^3$	$w \times 10^3$	$u \times 10^3$	$w \times 10^3$	
1	197	-153.0	-306.7	141.7	-220.2	0.2115
2	387	-303.6	-630.7	278.0	-431.1	0.4176
3	568	-450.2	-972.6	407.1	-630.9	0.6156
4	735	-591.1	-1331.2	527.0	-816.7	0.8029
5	886	-723.6	-1705.7	635.2	-985.7	0.9759
6	1011	-841.9	-2088.4	724.6	-1128.5	1.1253
7	1086	-922.5	-2396.3	778.0	-1218.3	1.2217
8	1144	-1001.5	-2754.8	820.3	-1296.9	1.3091
9	1175	-1055.8	-3034.7	843.4	-1345.4	1.3649
10	1194	-1110.2	-3352.9	858.2	-1386.5	1.4149
11	1201	-1148.8	-3599.3	863.6	-1411.6	1.4467
12	1198	-1189.7	-3882.5	862.8	-1432.5	1.4758
13	1189	-1220.0	-4105.2	858.1	-1444.6	1.4944

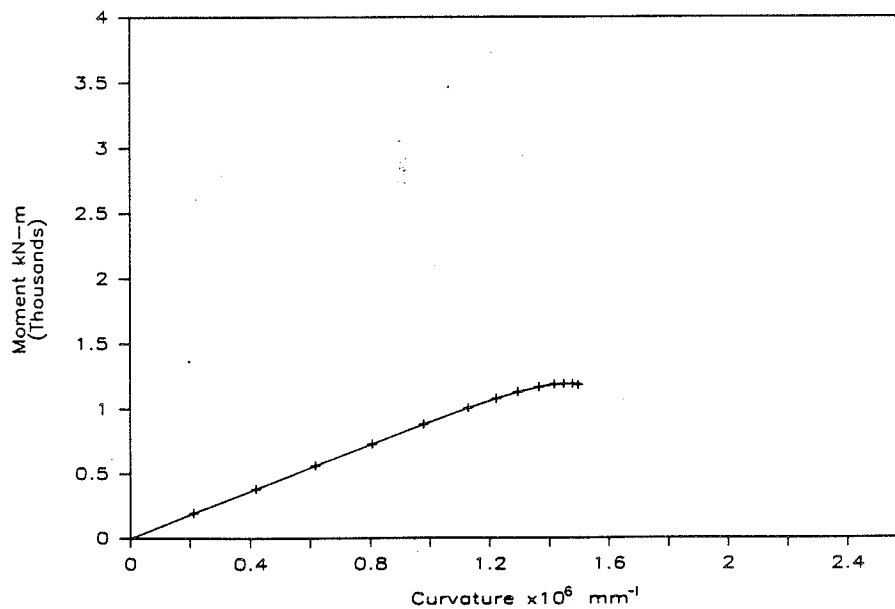


Figure A.11: Moment vs Curvature B2S7.N1

TABLE A.12

## Moment vs Curvature B2S7.N2

Step	Moment kN-m	Node 590		Node 608		Curvature $d\phi/ds \times 10^6$
		u $\times 10^3$	w $\times 10^3$	u $\times 10^3$	w $\times 10^3$	
1	190	-241.0	-867.1	139.6	-263.3	0.2733
2	363	-471.5	-1732.3	266.0	-507.6	0.5298
3	520	-692.7	-2595.7	381.5	-736.0	0.7721
4	663	-905.0	-3456.8	486.4	-949.7	1.0005
5	786	-1105.7	-4309.3	577.2	-1144.0	1.2106
6	882	-1292.0	-5150.9	649.2	-1313.7	1.3971
7	954	-1465.1	-5979.1	704.2	-1460.6	1.5619
8	994	-1623.0	-6786.1	735.8	-1576.7	1.6991
9	1010	-1744.5	-7427.3	750.9	-1656.7	1.7982
10	1012	-1858.8	-8067.4	754.7	-1720.0	1.8840
11	998	-1952.4	-8635.2	747.1	-1758.1	1.9467

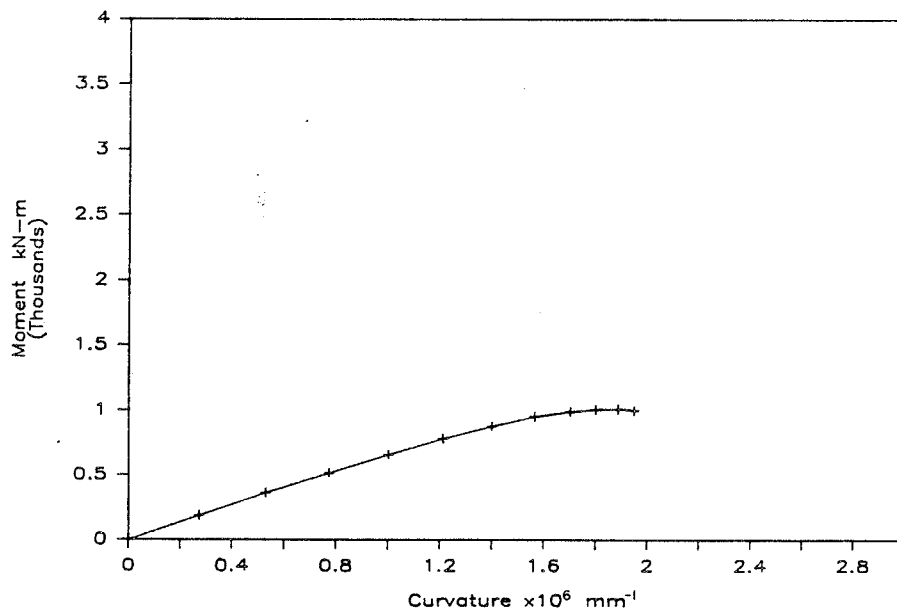


Figure A.12: Moment vs Curvature B2S7.N2

TABLE A.13

## Moment vs Curvature B2S7.N3

Step	Moment kN-m	Node 590		Node 608		Curvature $d\phi/ds \times 10^6$
		u $\times 10^3$	w $\times 10^3$	u $\times 10^3$	w $\times 10^3$	
1	192	-309.6	-1111.1	143.1	-311.0	0.3252
2	370	-608.5	-2227.0	275.2	-604.5	0.6351
3	533	-896.8	-3347.6	396.6	-881.3	0.9300
4	676	-1170.9	-4465.5	503.7	-1136.4	1.2048
5	789	-1425.7	-5569.2	589.3	-1360.3	1.4505
6	864	-1660.0	-6648.4	648.0	-1545.8	1.6624
7	904	-1839.7	-7511.4	680.4	-1674.1	1.8160
8	920	-2005.1	-8336.8	696.1	-1774.4	1.9475
9	907	-2156.7	-9127.5	690.2	-1839.6	2.0535

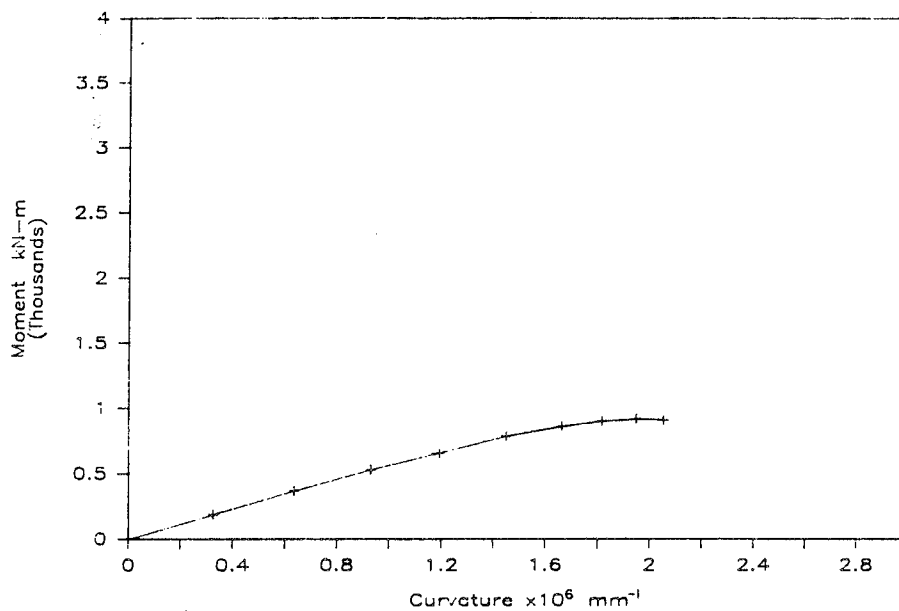


Figure A.13: Moment vs Curvature B2S7.N3

TABLE A.14

## Moment vs Curvature B2S7.N4

Step	Moment kN-m	Node 590		Node 608		Curvature $d\phi/ds \times 10^6$
		u $\times 10^3$	w $\times 10^3$	u $\times 10^3$	w $\times 10^3$	
1	192	-367.0	-1259.1	144.9	-350.0	0.3677
2	370	-722.1	-2523.6	278.9	-681.7	0.7195
3	533	-1065.4	-3793.6	402.5	-996.2	1.0557
4	675	-1393.6	-5065.3	510.7	-1286.8	1.3705
5	770	-1692.7	-6314.1	584.9	-1526.0	1.6402
6	812	-1915.8	-7304.7	620.2	-1682.0	1.8273
7	840	-2177.8	-8501.7	646.6	-1842.8	2.0365
8	849	-2383.6	-9447.3	658.0	-1953.5	2.1943
9	845	-2584.2	-10353.2	659.7	-2043.6	2.3415
10	840	-2787.0	-11247.5	660.6	-2129.7	2.4899
11	836	-2994.3	-12135.6	662.2	-2215.5	2.6421

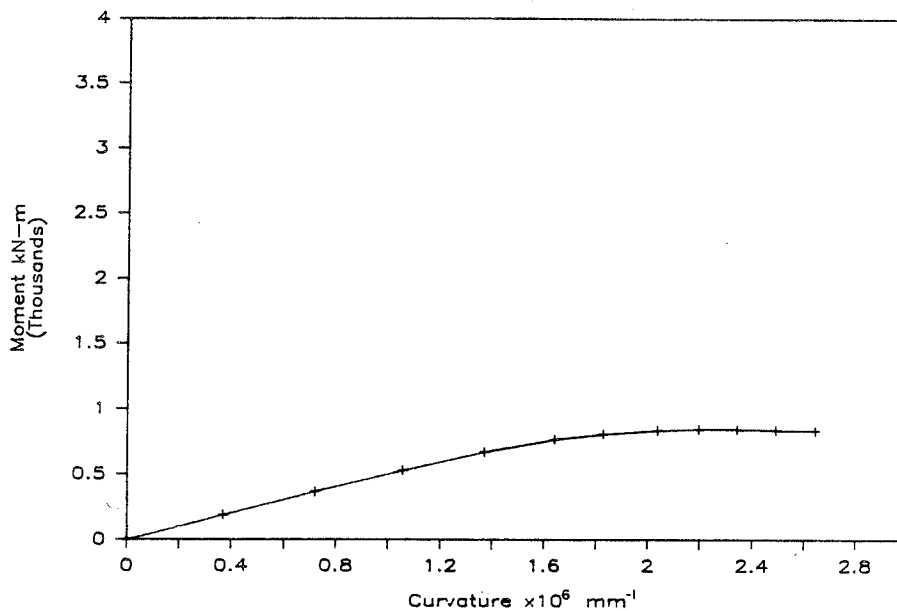


Figure A.14: Moment vs Curvature B2S7.N4

Appendix B  
SUPPORTING COMPUTER PROGRAMS

B.1 CYLINDER

F I L E        C Y L I N D R        F I L E

PROGRAM TO FIND THE LEAST SQUARES FIT OF A CYLINDRICAL SURFACE.

EXTERNAL CYLNDR

REAL\*8 TITLE

COMMON /HDR/ TITLE(10)

COMMON /CNTRL/ MX

READ 50, TITLE

50 FORMAT (10A8)

READ \*, MX

PRINT 100, TITLE, MX

100 FORMAT ('1'///' \*\*\*\*\*LEAST-SQUARES FIT OF A CYLINDER\*\*\*\*\*'//  
& 1X, 10A8//

& ' NUMBER OF SAMPLE POINTS . . . . .', I5)

NPOOL=18\*MX

CALL GETCOR (CYLNDR, 8\*NPOOL)

STOP

END

SUBROUTINE CYLNDR (A, NBYTES)

COMMON /CNTRL/ MX

REAL\*8 A(1)

NA=NBYTES/8

S T O R A G E    M A P

N1        X(MX)

N2        Y(MX)

N3        Z(MX)

N4        FP(MX,5)

N5        FO(MX)

N6        LI(MX)

N7        G(MX)

N8        H(MX,5)

N9        C(MX)

N10       CT(MX)

PARTITION THE STORAGE

N1=1

N2=N1+MX

N3=N2+MX

N4=N3+MX

N5=N4+5\*MX

N6=N5+MX

N7=N6+MX

N8=N7+MX

N9=N8+5\*MX

N10=N9+MX

N99=N10+MX

IF (N99-1.GT.NA) GO TO 9000

CALL CYL (MX, A(N1), A(N2), A(N3), A(N4), A(N5), A(N6), A(N7),  
& A(N8), A(N9), A(N10))

1000 STOP

```

9000 N99=8*(N99-1)
      NA=8*NA
      PRINT 9100, N99, NA
9100 FORMAT('-*****STORAGE REQUEST OF', I8, ' BYTES EXCEEDS AVAILABLE',
& ' STORAGE OF', I8, ' BYTES.')
      GO TO 1000
      END
      SUBROUTINE CYL (MX, X, Y, Z, FP, FO, LI, G, H, C, CT)
C     FPFORM
C     FOFORM
C     LIFORM
C     DUPL
C     TRNMLT
C     SUB
C     MULT
C     DAMULT
C     SYMTRI
C     SYMSLV
      IMPLICIT REAL*8 (A-H,O-Z)
      REAL*8 TITLE
      COMMON /HDR/ TITLE(10)
      DIMENSION X(MX), Y(MX), Z(MX), FP(MX,5), FO(MX,1), LI(1,MX),
& G(MX,1), H(MX,5), C(MX,1), CT(1,MX)
      DIMENSION P(5), A(5,5), B(5), DP(5)
      DATA LFP, LH, KP, KA, LA, KB, KDP, MP /8*5/
      DATA LFO, KLI, LG, LC, KCT, NP, LP, LB, LDP /9*1/
      REAL*8 LI
      EQUIVALENCE (X0,P(1)), (Y0,P(2)), (PHI,P(3)), (THETA,P(4)),
& (R,P(5))
      LOGICAL DEBUG
      REAL*8 DBUG/'DEBUG'/
      DEBUG=.FALSE.
      IF (TITLE(1).EQ.DBUG) DEBUG=.TRUE.
      PI=ACOS(-1.)
      KFP=MX
      KFO=MX
      LLI=MX
      KG=MX
      KH=MX
      KC=MX
      LCT=MX
C
C     READ PSI, Z, R AS MEASURED
C
      READ *, (X(I), Y(I), Z(MX-I+1), I=1,MX)
      PRINT 100, (I, X(I), Y(I), Z(I), I=1,MX)
100  FORMAT ('-POINT', 5X, 'ANGLE', 7X, 'Z', 7X, 'RADIUS'//
& (1X, I4, F11.2, F10.2, F11.3))
C
C     REVERSE CYLINDER
C
      XMAX=X(1)
      YMAX=Y(1)
      XMIN=XMAX
      YMIN=YMAX

```

```

DO 110 I=1,MX
XMAX=AMAX1(XMAX,X(I))
XMIN=AMIN1(XMIN,X(I))
YMAX=AMAX1(YMAX,Y(I))
YMIN=AMIN1(YMIN,Y(I))
110 CONTINUE
DO 120 I=1,MX
X(I)=XMAX-X(I)
Y(I)=YMAX-Y(I)
120 CONTINUE
C
C   COMPUTE X, Y AND Z COORDINATES
C
DO 200 I=1,MX
R=Z(I)
PSI=PI*X(I)/180.
Z(I)=Y(I)
X(I)=R*SIN(PSI)
Y(I)=R*COS(PSI)
200 CONTINUE
PRINT 300, (I, X(I), Y(I), Z(I), I=1,MX)
300 FORMAT ('-POINT', 7X, 'X', 9X, 'Y', 9X, 'Z'//
& (1X, I4, 3F11.3))
PRINT 5
5 FORMAT('- ', 37X, 'ITERATES'//16X, 'X0', 16X, 'Y0', 16X, 'PHI', 15X,
& 'THETA', 14X, 'RADIUS', 13X, 'SUM ERRORS**2'/1X)
NI=0
C SELECT INITIAL VALUES OF PARAMETERS
C
X0=0.0
Y0=0.0
PHI=0.1
THETA=0.0
C R IS AS LEFT ABOVE
C
C ITERATE PARAMETERS
3 IF(NI.GT.0)SO=S
CALL FPFORM (FP, KFP, LFP, MFP, NFP, X, Y, Z, MX, P, KP, LP, MP,
& NP)
IF (DEBUG) CALL DPRINT(FP,KFP,LFP,MFP,NFP,'G11.4/',11,0,'FP/','0')
CALL FOFORM (FO, KFO, LFO, MFO, NFO, X, Y, Z, MX, P, KP, LP, MP,
& NP)
IF (DEBUG) CALL DPRINT(FO,KFO,LFO,MFO,NFO,'G11.4/',11,0,'FO/','0')
CALL LIFORM (LI, KLI, LLI, MLI, NLI, X, Y, Z, MX, P, KP, LP, MP,
& NP)
IF (DEBUG) CALL DPRINT(LI,KLI,LLI,MLI,NLI,'G11.4/',11,0,'LI/','0')
CALL DAMULT(LI,KLI,LLI,MLI,NLI,FO,KFO,LFO,MFO,NFO,G,KG,LG,MG,NG)
IF (DEBUG) CALL DPRINT (G,KG,LG,MG,NG,'G11.4/',11,0,'G/','0')
CALL DAMULT(LI,KLI,LLI,MLI,NLI,FP,KFP,LFP,MFP,NFP,H,KH,LH,MH,NH)
IF (DEBUG) CALL DPRINT (H,KH,LH,MH,NH,'G11.4/',11,0,'H/','0')
CALL TRNMLT(FP,KFP,LFP,MFP,NFP,H,KH,LH,MH,NH,A,KA,LA,MA,NA)
IF (DEBUG) CALL DPRINT (A,KA,LA,MA,NA,'G11.4/',11,0,'A/','0')
CALL TRNMLT(FP,KFP,LFP,MFP,NFP,G,KG,LG,MG,NG,B,KB,LB,MB,NB)
IF (DEBUG) CALL DPRINT (B,KB,LB,MB,NB,'G11.4/',11,0,'B/','0')
CALL SYMSLV(A,KA,LA,MA,NA,DP,KDP,LDP,MDP,NDP,B,KB,LB,MB,NB)

```

```

IF (DEBUG) CALL DPRINT (A,KA,LA,MA,NA,'G11.4/',11,0,'A/','0')
IF (DEBUG) CALL DPRINT (B,KB,LB,MB,NB,'G11.4/',11,0,'B/','0')
CALL SUB(P,KP,LP,MP,NP,DP,KDP,LDP,MDP,NDP,P,KP,LP,MP,NP)
CALL MULT(H,KH,LH,MH,NH,DP,KDP,LDP,MDP,NDP,C,KC,LC,MC,NC)
CALL SUB(G,KG,LG,MG,NG,C,KC,LC,MC,NC,C,KC,LC,MC,NC)
CALL TRNMLT(C,KC,LC,MC,NC,G,KG,LG,MG,NG,S,1,1,MS,NS)
PHI=AMOD(PHI,2.*PI)
NI=NI+1
PRINT 400, NI, X0, Y0, PHI, THETA, R, S
400 FORMAT(I4,2X,6(3X,G15.8))
IF(NI.EQ.1)GO TO 3
IF(DABS(SO-S)/S.GT.1.E-8)GO TO 3
C END OF ITERATIVE PROCEDURE
PHID=180.*PHI/PI
THETAD=180.*THETA/PI
PRINT 4, X0, Y0, PHI, PHID, THETA, THETAD, R
4 FORMAT('-X0 . . . . .', G15.8/
& ' Y0 . . . . .', G15.8/
& ' PHI . . . . .', G15.8, 2X, '(', F6.1, ' DEGREES')'/
& ' THETA . . . . .', G15.8, 2X, '(', F6.1, ' DEGREES')'/
& ' RADIUS . . . . .', G15.8)
CALL DPRINT (FO,MX,1,MX,1,'G11.4/',11,0,
& 'ADJUSTED INITIAL DEFLECTIONS/','1')
RETURN
END
SUBROUTINE FPFOR (FP, KFP, LFP, MFP, NFP, X, Y, Z, MX, P,
& KP, LP, MP, NP)
DIMENSION FP(KFP,LFP), X(MX), Y(MX), Z(MX), P(KP)
X0=P(1)
Y0=P(2)
PHI=P(3)
THETA=P(4)
R=P(5)
CT=COS(THETA)
ST=SIN(THETA)
CP=COS(PHI)
SP=SIN(PHI)
DO 100 I=1,MX
DX=X(I)-X0
DY=Y(I)-Y0
A=2.*(DX*CT*CP+DY*CT*SP-Z(I)*ST)
B=2.*(-DX*SP+DY*CP)
C=SQRT(A*A+B*B)
FP(I,1)=(-A*CT*CP+B*SP)/C
FP(I,2)=(-A*CT*SP-B*CP)/C
FP(I,3)=(A*(-DX*CT*SP+DY*CT*CP)-B*(DX*CP+DY*SP))/C
FP(I,4)=(-A*(DX*ST*CP+DY*ST*SP+Z(I)*CT))/C
FP(I,5)=-1.
100 CONTINUE
MFP=MX
NFP=MP
RETURN
END
SUBROUTINE FOFOR (FO, KFO, LFO, MFO, NFO, X, Y, Z, MX, P, KP,
& LP, MP, NP)

```

```

DIMENSION FO(KFO), X(MX), Y(MX), Z(MX), P(KP)
X0=P(1)
Y0=P(2)
PHI=P(3)
THETA=P(4)
R=P(5)
CT=COS(THETA)
CP=COS(PHI)
ST=SIN(THETA)
SP=SIN(PHI)
DO 100 I=1,MX
DX=X(I)-X0
DY=Y(I)-Y0
A=DX*CT*CP+DY*CT*SP-Z(I)*ST
B=-DX*SP+DY*CP
FO(I)=SQRT(A*A+B*B)-R
100 CONTINUE
MFO=MX
NFO=1
RETURN
END
SUBROUTINE LIFORM (LI, KLI, LLI, MLI, NLI, X, Y, Z, MX, P, KP,
& LP, MP, NP)
REAL LI(KLI), P(KP), X(MX), Y(MX), Z(MX)
X0=P(1)
Y0=P(2)
PHI=P(3)
THETA=P(4)
R=P(5)
CT=COS(THETA)
CP=COS(PHI)
ST=SIN(THETA)
SP=SIN(PHI)
DO 100 I=1,MX
DX=X(I)-X0
DY=Y(I)-Y0
A=2.*(DX*CT*CP+DY*CT*SP-Z(I)*ST)
B=2.*(-DX*SP+DY*CP)
C2=A*A+B*B
LI(I)=C2/((A*CT*CP-B*SP)**2 + (A*CT*SP+B*CP)**2 + (A*ST)**2)
100 CONTINUE
MLI=1
NLI=MX
RETURN
END
SUBROUTINE DAMULT(D,KD,LD,MD,ND,A,KA,LA,MA,NA,B,KB,LB,MB,NB)
C FORM THE PRODUCT OF DIAGONAL MATRIX D WITH ANY COMPATIBLE MATRIX A.
C D MAY BE STORED AS A ROW OR AS A DIAGONAL.
IMPLICIT REAL*8 (A-H,O-Z)
DIMENSION D(KD,LD),A(KA,LA),B(KB,LB)
MB=ND
NB=NA
IF(MD.EQ.1)GO TO 25
DO 21 I=1,MA
DO 21 J=1,NA

```

```

21 B(I,J)=D(I,I)*A(I,J)
   GO TO 27
25 DO 26 I=1,MA
   DO 26 J=1,NA
26 B(I,J)=D(I,I)*A(I,J)
27 RETURN
   END
   SUBROUTINE DUPL(A,KA,LA,MA,NA,B,KB,LB,MB,NB)
C  MATRIX B IS SET EQUAL TO MATRIX A.
   IMPLICIT REAL*8 (A-H,O-Z)
   DIMENSION A(KA,LA),B(KB,LB)
   MB=MA
   NB=NA
   DO 1 I=1,MA
   DO 1 J=1,NA
1  B(I,J)=A(I,J)
   RETURN
   END
   SUBROUTINE SYMSLV(A,KA,LA,MA,NA,X,KX,LX,MX,NX,B,KB,LB,MB,NB)
C  THE SYSTEM AX=B IS SOLVED FOR X, WHERE A IS SYMMETRIC AND POSITIVE
C  DEFINITE.
   IMPLICIT REAL*8 (A-H,O-Z)
   DIMENSION A(KA,LA), X(KX,LX), B(KB,LB)
   CALL SYMTRI (A, KA, LA, MA, NA)
   CALL DUPL (B, KB, LB, MB, NB, X, KX, LX, MX, NX)
   IF(MA.EQ.1)GO TO 4
   NN=MA-1
   DO 1 J=1,NN
   K=J+1
   DO 1 I=K,MA
   DO 1 L=1,NB
1  X(I,L)=X(I,L)-A(I,J)*X(J,L)
C  BACK-SUBSTITUTION
4  DO 2 K=1,NX
   DO 2 II=1,MA
   I=MA-II+1
   IP1=I+1
   IF(IP1.GT.NA)GO TO 2
   DO 3 J=IP1,NA
3  X(I,K)=X(I,K)-A(I,J)*X(J,K)
2  X(I,K)=X(I,K)/A(I,I)
   RETURN
   END
   SUBROUTINE SYMTRI(A,KA,LA,MA,NA)
C  TRIANGULARIZATION OF A SYMMETRIC, POSITIVE DEFINITE MATRIX.
   IMPLICIT REAL*8 (A-H,O-Z)
   DIMENSION A(KA,LA)
   IF(MA.EQ.1)RETURN
   N=NA-1
   DO 1 J=1,N
   K=J+1
   DO 1 I=K,NA
   A(I,J)=(A(J,I)/A(J,J))
   DO 5 L=I,NA
5  A(I,L)=A(I,L)-A(I,J)*A(J,L)

```

```
1 CONTINUE
  RETURN
  END
  SUBROUTINE SUB (A,KA,LA,MA,NA,B,KB,LB,MB,NB,C,KC,LC,MC,NC)
  IMPLICIT REAL*8 (A-H,O-Z)
  DIMENSION A(KA,LA), B(KB,LB), C(KC,LC)
  MC=MA
  NC=NA
  DO 100 I=1,MA
  DO 100 J=1,NA
100 C(I,J)=A(I,J)-B(I,J)
  RETURN
  END
  SUBROUTINE MULT (A,KA,LA,MA,NA,B,KB,LB,MB,NB,C,KC,LC,MC,NC)
  IMPLICIT REAL*8 (A-H,O-Z)
  DIMENSION A(KA,LA), B(KB,LB), C(KC,LC)
  DO 200 I=1,MA
  DO 200 J=1,NB
  S=0.0
  DO 100 K=1,NA
100 S=S+A(I,K)*B(K,J)
200 C(I,J)=S
  MC=MA
  NC=NB
  RETURN
  END
  SUBROUTINE TRNMLT (A,KA,LA,MA,NA,B,KB,LB,MB,NB,C,KC,LC,MC,NC)
  IMPLICIT REAL*8 (A-H,O-Z)
  DIMENSION A(KA,LA), B(KB,LB), C(KC,LC)
  DO 200 I=1,NA
  DO 200 J=1,NB
  S=0.0
  DO 100 K=1,MB
100 S=S+A(K,I)*B(K,J)
200 C(I,J)=S
  MC=NA
  NC=NB
  RETURN
  END
```

B.2 GEN



```

30  CONTINUE
    A(1,1)=N
    A(1,2)=SSUMX
    A(2,1)=SSUMX
    A(2,2)=X2SUM
    B(1,1)=SSUMY
    B(2,1)=XYSSUM
    KA=2
    LA=2
    MA=2
    NA=2
    KX=2
    LX=1
    MX=2
    NX=1
    KB=2
    LB=1
    MB=2
    NB=1
    CALL SYMSLV(A,KA,LA,MA,NA,X,KX,LX,MX,NX,B,KB,LB,MB,NB)
    PRINT 50,SSUMX,X2SUM,SSUMY,XYSSUM,X(1,1),X(2,1)
50  FORMAT(' ',//,T10,5F16.3,5X,F12.7)
    BB(I)=X(1,1)
    RMM(I)=X(2,1)
20  CONTINUE
    XX(1)=0.0
    XX(2)=228.6
    XX(3)=685.8
    XX(4)=914.4
    XX(5)=2743.0
    XX(6)=2971.6
    XX(7)=3429.0
    XX(8)=3657.6
    DO 31 I=1,4
31  XF(I)=XX(I)
    DO 32 I=5,11
32  XF(I)=X1(I-4)
    DO 33 I=12,15
33  XF(I)=XX(I-7)
    PRINT 203
203 FORMAT(' '///'** INTERPOLATED DATA LEVELS **'///)
    PRINT 78,(XX(I),I=1,8)
78  FORMAT(' ',8F12.3///)
    DO 250 I=1,8
        DO 300 J=1,M
            Y(J,I)=RMM(J)*XX(I) + BB(J)
300  CONTINUE
250 CONTINUE
    PRINT 708,TITLE
708 FORMAT('1'///'*****GENERATORS EXTRAPOLATED TO PRODUCE END DATA'//
& 1X,10A8//)
    DO 400 I=1,M
        PRINT 77,(Y(I,J),J=1,8)
400 CONTINUE
77  FORMAT(' ',8F8.3)

```

```

STOP
END
SUBROUTINE SYMSLV(A,KA,LA,MA,NA,X,KX,LX,MX,NX,B,KB,LB,MB,NB)
C THE SYSTEM AX=B IS SOLVED FOR X, WHERE A IS SYMMETRIC AND POSITIVE
C DEFINITE.
  IMPLICIT REAL*8 (A-H,O-Z)
  DIMENSION A(KA,LA), X(KX,LX), B(KB,LB)
C PRINT 909
C909 FORMAT('1',10X,12H @@@@@@@@@@@@ )
C PRINT*,A
C PRINT*,B
  CALL SYMTRI (A, KA, LA, MA, NA)
  CALL DUPL (B, KB, LB, MB, NB, X, KX, LX, MX, NX)
  IF(MA.EQ.1)GO TO 4
  NN=MA-1
  DO 1 J=1,NN
  K=J+1
  DO 1 I=K,MA
  DO 1 L=1,NB
  1 X(I,L)=X(I,L)-A(I,J)*X(J,L)
C BACK-SUBSTITUTION
  4 DO 2 K=1,NX
  DO 2 II=1,MA
  I=MA-II+1
  IP1=I+1
  IF(IP1.GT.NA)GO TO 2
  DO 3 J=IP1,NA
  3 X(I,K)=X(I,K)-A(I,J)*X(J,K)
  2 X(I,K)=X(I,K)/A(I,I)
  RETURN
  END
SUBROUTINE SYMTRI(A,KA,LA,MA,NA)
C TRIANGULARIZATION OF A SYMMETRIC, POSITIVE DEFINITE MATRIX.
  IMPLICIT REAL*8 (A-H,O-Z)
  DIMENSION A(KA,LA)
  IF(MA.EQ.1)RETURN
  N=NA-1
  DO 1 J=1,N
  K=J+1
  DO 1 I=K,NA
  A(I,J)= (A(J,I)/A(J,J))
  DO 5 L=I,NA
  5 A(I,L)=A(I,L)-A(I,J)*A(J,L)
  1 CONTINUE
  RETURN
  END
SUBROUTINE DUPL(A,KA,LA,MA,NA,B,KB,LB,MB,NB)
C MATRIX B IS SET EQUAL TO MATRIX A.
  IMPLICIT REAL*8 (A-H,O-Z)
  DIMENSION A(KA,LA),B(KB,LB)
  MB=MA
  NB=NA
  DO 1 I=1,MA
  DO 1 J=1,NA
  1 B(I,J)=A(I,J)

```

RETURN  
END

B.3 SEAM

C  
C  
C  
C  
C  
C  
C  
C  
C  
C  
C  
C  
C

## F I L E        S E A M        F I L E

\*\*\*\*\*

FILE SEAM IS USED TO INCORPORATE THE CIRCUMFERENTIAL WELD DEPRESSIONS AFTER THE CYLINDER HAS BEEN ADJUSTED FOR AXIS TILT AND THE GENERATORS HAVE BEEN EXTENDED TO THE END SHELL REGIONS.

\*\*\*\*\*

```

IMPLICIT REAL*8 (A-H,O-Z)
DIMENSION PP(17,8),A(17,8),B(17,2),TITLE(10)
M=17
N=8
READ 707,TITLE
707 FORMAT (10A8)
PRINT 709,TITLE
709 FORMAT('1'///'*** PGM=SEAM INCORPORATES WELD DEPRESSIONS ***'///
& 1X,10A8)
DO 99 I=1,M
READ *,(A(I,J),J=1,N)
99 CONTINUE
27 FORMAT(8F8.3)
READ*,B
PRINT 1
1 FORMAT(' ',///,33H INITIAL VALUES W/O SEAM ADJUST )
DO 10 I=1,M
PRINT 2,(A(I,J),J=1,N)
10 CONTINUE
2 FORMAT(' ',8F8.3)
PRINT 3
3 FORMAT(' ',////,18H SEAM DEPRESSIONS )
DO 15 I=1,M
PRINT 2,(B(I,J),J=1,2)
15 CONTINUE
DO 20 I=1,M
DO 25 J=1,3
PP(I,J)=A(I,J)
K=J+5
25 PP(I,K)=A(I,K)
PP(I,4)=A(I,4) - B(I,1)
PP(I,5)=A(I,5) - B(I,2)
20 CONTINUE
PRINT 4
4 FORMAT(' ',////,32H FINAL ADJUSTED END CONDITIONS )
DO 30 I=1,M
PRINT 2,(PP(I,J),J=1,N)
30 CONTINUE
STOP
END

```

B.4 GRAPH

B.5 PLOTSUR



B.6 MODE1



```

102 FORMAT(' ',///, 8H Y(I) = )
PRINT*,Y
C
C
C      MATRIX FF : ORIGINAL DATA SHOWN FOR DISPLAY
C      MATRIX AA : MIDDLE SECTION ADJUSTED DATA POINTS
C      MATRIX PP : END REGIONS & SEAMS
C                  COL 1:3 END1 COL 4&5 SEAMS COL 6:8 END2
C
C
C*****
C      N O T E   MUST USE THIS DO LOOP TO READ IN THE
C                  ORIGINAL DATA FOR SPECIMEN B2
C
C      DO 713 I=1,16
C      READ*(FF(I,J),J=1,7)
C 713 CONTINUE
C
C*****
C      READ*,FF
C      READ*,AA
C      DO 41 I=1,M1
C          READ*(PP(I,J),J=1,N1)
C 41      CONTINUE
C      DO 42 I=1,NUMNP
C          READ*(EGG(I,J),J=1,4)
C 42 CONTINUE
C      NUMN2=NUMNP*2
C      DO 43 I=1,NUMNP
C          JI=(NUMNP + I)
C          TEGG(I)=EGG(I,3)
C          TEGG(JI)=EGG(I,4)
C 43 CONTINUE
C
C*****
C      CALCULATE THE SUMMATION OF THE EIGENVECTOR DISPLACEMENT
C      MATRIX SQUARED
C
C      ZSUM=0.0
C      DO 44 I=1,NUMN2
C 44      ZSUM=ZSUM+(TEGG(I)*TEGG(I))
C
C      CALL D1TA(BB,FF,MF,TF,AA,PP,F,M,N,DE)
C*****
C      *****
C      ***
C      *** THESE RECORDS ARE FOR INTERPOLATING
C      *** THE MESH NODAL POINTS
C      ***
C      ***
C      ***
C      ***

```







```

PRINT 29
29 FORMAT(' ',///,38H AXIAL DIRECTION YL THETA DIRECTION ,
* 14H THETA DEGREES ,
* 5X,48H INTERPOLATED IMPERFECTIONS (MEASURED RADIALY) )
301 CONTINUE
DO 300 J=1,NYL
    JK=(J-1)*NXL
    DO 305 I=1,NXL
        JI=JK + I
        II=NUMNP + JK + I
        V(JI)=FL(I,J)*SIN(THETA(I))
        V(II)=FL(I,J)*COS(THETA(I))
        IF(K .NE. 2) GO TO 305
        PRINT 306,YL(J),XL(I),XL1(I),FL(I,J),V(JI),V(II),K
305 CONTINUE
300 CONTINUE
306 FORMAT(' ',T5,F15.4,,5X,F10.7,5X,F10.3,10X,F15.4,
* 10X,F15.4,5X,F15.4,5X,I3)
65 FORMAT(' ',///,T5,19F6.3)
IF (K .NE. 2) GO TO 635
C WRITE(6,632)
C 632 FORMAT(' ',1X,'NODAL DISP COMPONENTS'//)
C DO 671 J=1,190
C J2=J+190
C J3=J+380
C J4=J+570
C J5=J+760
C 671 WRITE(6,633) J,V(J),J2,V(J2),J3,V(J3),J4,V(J4),
C * J5,V(J5)
633 FORMAT(' ',2X,I3,2X,F7.3,4X,I3,2X,F7.3,4X,I3,2X,F7.3,
* 4X,I3,2X,F7.3,4X,I3,2X,F7.3)
635 CONTINUE
C *****
C
C CALCULATE THE PRODUCT OF THE EIGENVECTOR TIMES THE
C INTERPOLATED NODAL IMPERFECTIONS
C
C
C YSUM=0.0
DO 500 J=1,NUMN2
    YSUM=YSUM+ (TEGG(J)*V(J))
500 CONTINUE
C *****
C
C PRINT 604,YSUM,ZSUM
604 FORMAT(' ',10X,F15.4,5X,F15.4)
A1(K)=YSUM/ZSUM
63 CONTINUE
PRINT 505
505 FORMAT(' ',///,1X,' CONTRIBUTION OF THE FIRST MODE'/)
DO 507 KI=1,16
    PRINT 506,A1(KI)
507 CONTINUE
506 FORMAT(' ',15X,3F10.5)

```



B.7 ADDDISP

```

C
C           *   F I L E   A D D I S P   F I L E   *
C
C *****
C
C FILE ADDDISP PERFORMS THE FOLLOWING FUNCTIONS:
C     1) MULTIPLIES THE EXTRACTED SCALE FACTOR TIMES
C         THE CORRESPONDING RADIAL COMPONENT OF THE
C         EIGENVECTOR
C     2) ADDS THE CALCULATED NODAL DISPLACEMENTS
C         TO THE NODAL COORDINATES
C
C *****
C
C REAL*8 FIELD(80),VV(475,4),V(475),XI(19),THETA(19),R(475)
C INTEGER FMT1(6)/'(5A8', ' ',A5,',', 'F10.', ' ', ' ', '3A8', ' ',A1)'/
C INTEGER SETFMT
C NUMNP=475
C PI=ACOS(-1.0)
C
C *****
C
C           SCALE FACTOR "A1"
C
C *****
C
C           A1=-0.00397
C
C *****
C
C           READ IN THE EIGENVECTOR
C
C           VV(NUMNP,4)
C           COL 11 : NODE NUMBER
C           12 : X-DISPLACEMENT (NOT USED)
C           13 : Y-DISPLACEMENT
C           14 : Z-DISPLACEMENT
C
C *****
C
C           DO 500 I=1,NUMNP
C             READ*,(VV(I,J),J=1,4)
C 500 CONTINUE
C
C *****
C
C           SCALE THE EIGENVECTOR & CONVERT TO POLAR COORD
C
C *****
C
C           PRINT 4000
C           XI(1)=90.0
C           DO 99 II=2,10
C 99  XI(II)=XI(II-1) - 5.
C           DO 98 IJ=11,19

```

```

98  XI(IJ)=XI(IJ-1) - 15.
    DO 62 I=1,19
62  THETA(I)=XI(I)*PI/180.
    ICNT=NUMNP/19
    DO 600 I=1,ICNT
    DO 625 J=1,19
    JI=(I-1)*19 + J
    TEMP1=VV(JI,3)*COS(THETA(J))
    TEMP2=VV(JI,4)*SIN(THETA(J))
    R(JI)=TEMP1 +TEMP2
    V(JI)=R(JI)*A1
    PRINT 5000,JI,XI(J),TEMP1,TEMP2,R(JI),V(JI)
625 CONTINUE
600 CONTINUE
4000 FORMAT('1',///,1X,'NODE',5X,'THETA',8X,'Y-COMP',8X,'Z-COMP',8X,
* 'RADIAL DISP',4X,'SCALED DISP',//)
5000 FORMAT(' ',1X,I3,5X,F5.1,5X,F10.5,5X,F10.5,5X,F10.5)
C
C*****
C
C          READ IN POLAR COORDINATE "R"
C          ADD THE COMPUTED DISPLACEMENT V(I)
C
C*****
C
    DO 1000 I=1,NUMNP
        READ (5,900) (FIELD(J),J=1,6), Y, (FIELD(J),J=7,10)
900  FORMAT(5A8, A5, F10.0, 3A8, A1)
        Y = Y + V(I)
        FMT1(4)=SETFMT (10,Y,1)
        WRITE (6,FMT1) (FIELD(J),J=1,6), Y, (FIELD(J),J=7,10)
1000 CONTINUE
    STOP
    END
C
C
C*****
C
C          FUNCTION SETFMT
C
C*****
C
    INTEGER FUNCTION SETFMT (KF, X, N)
    DIMENSION X(N)
    XMIN=0.0
    XMAX=0.0
    DO 100 I=1,N
    XMAX=AMAX1(XMAX,X(I))
    XMIN=AMIN1(XMIN,X(I))
100  CONTINUE
    IMAX=XMAX
    IMIN=ABS(XMIN)
    IMIN=IMIN*10
    I=KF-1
300  IMAX=IMAX/10

```

```
IMIN=IMIN/10  
I=I-1  
IF (IMAX.NE.0 .OR. IMIN.NE.0) GO TO 300  
SETFMT=ITOA(I)  
RETURN  
END
```

B.8 LOADS

\*\*\* FILE LOADS FILE \*\*\*

\*\*\*\*\*  
 FILE LOADS IS USED TO CALCULATE THE CONSISTANT LOAD VECTOR  
 SCALE FACTORS FOR THE GIVEN SHELL GEOMETRY

\*\*\*\*\*

```

REAL S(19), Q(19), PSI(4,4)
REAL PHI(19)/90., 85., 80., 75., 70., 65., 60., 55., 50.,
& 45., 30., 15., 0., -15.,
& -30., -45., -60., -75., -90./
INTEGER NODE(19), IDIRN, NCUR
NLOADS=19
NELS=6
NODINC=1
NODE1=666
PI=ARCOS(-1.)
RAD=PI/180.
R=763.3/1000.
PIR=PI*R
DO 100 I=1,NLOADS
  NODE(I)=NODINC*I-1+NODE1
  S(I)=SIN(RAD*PHI(I))
  Q(I)=0.0
100 CONTINUE
  CALL DPRINT (PHI,NLOADS,1,NLOADS,1,'F5.0/',0,'PHI/',1')
  CALL DPRINT (S,NLOADS,1,NLOADS,1,'F10.6/',0,'S/',1)
  PSI(1,1)=128./1680.
  PSI(2,1)=99./1680.
  PSI(1,2)=PSI(2,1)
  PSI(3,1)=-36./1680.
  PSI(1,3)=PSI(3,1)
  PSI(4,1)=19./1680.
  PSI(1,4)=PSI(4,1)
  PSI(2,2)=648./1680.
  PSI(3,2)=-81./1680.
  PSI(2,3)=PSI(3,2)
  PSI(4,2)=PSI(3,1)
  PSI(2,4)=PSI(4,2)
  PSI(3,3)=PSI(2,2)
  PSI(4,3)=PSI(2,1)
  PSI(3,4)=PSI(4,3)
  PSI(4,4)=PSI(1,1)
  CALL DPRINT (PSI,4,4,4,4,'F9.6/',9,1,'PSI/',1)
  N=-3
  DO 500 M=1,NELS
    N=N+3
    DPHI=(PHI(N+1)-PHI(N+4))*RAD
    PRINT 250, M, DPHI
250 FORMAT ('0M =', I2, 5X, 'DPHI =', E14.6)

```

```
DO 400 I=1,4
SUM=0.0
DO 300 J=1,4
SUM=SUM+PSI(I,J)*S(N+J)
300 CONTINUE
Q(N+I)=Q(N+I)-DPHI*SUM/PIR
400 CONTINUE
500 CONTINUE
PRINT 600, (NODE(I), Q(I), I=1,NLOADS)
600 FORMAT ('-NODE      FORCE'/(1X, I4, E15.6))
C
C COMPUTE RESULTANT MOMENT AS A CHECK
C
SUM=0.0
DO 1000 I=1,NLOADS
SUM=SUM-Q(I)*S(I)
1000 CONTINUE
SUM=R*SUM
PRINT 1200, SUM
1200 FORMAT ('-RESULTANT MOMENT = ', E22.15)
FACTOR=0.5/SUM
DO 1300 I=1,NLOADS
1300 Q(I)=Q(I)*FACTOR
IDIRN=1
NCUR=1
PRINT 1400, (NODE(I),IDIRN,NCUR, Q(I), I=1,NLOADS)
1400 FORMAT ('-NODE      CORRECTED FORCE'/(1X, I4, 2I5, F10.8))
STOP
END
```

B.9 NISAPLOT

```

C*****
C
C   N I S A P L O T   ( U   O F   M   V E R S I O N )
C
C       LAST UPDATE:   JUNE 1/84   BY   DJP
C
C*****
C   EXTERNAL PARTN
C   COMMON /CNTL/ NUMNP, MXFIGS, MXNODS, MXLINK, NUMEL, NUMFIG
C   COMMON /IO/ NT1, NT2
C   NT1=1
C   NT2=2
C
C*****
C
C       REQUIRED INPUT
C
C   FIRST INPUT CARD
C       * NUMNP       - NUMBER OF NODAL POINTS
C       * NTPYPE1     - NUMBER OF TRUSS ELEMENTS
C       * NTYPE7      - NUMBER OF SHELL ELEMENTS
C
C   SECOND INPUT CARD
C       * NUMNP       -NUMBER OF NODAL POINTS
C
C   THIRD INPUT CARD
C       * EMBED ELEMENT COORDS DIRECT FROM NISA DATA FILE
C
C   FORTH INPUT CARD
C       * NTYPE       - ELEMENT TYPE (NPAR(1))
C       * NEL         - NUMBER OF THESE ELEMENTS TO BE PLOTTED
C       * IEL         - NUMBER OF NODES PER ELEMENT
C
C   FIFTH INPUT CARD
C       * EMBED ELEMENT INFO BLOCK DIRECT FROM NISA INPUT(2*NEL)
C
C   SIXTH INPUT CARD
C       * REPEAT 4TH & 5TH CARDS FOR OTHER TWO ELEMENT GROU@S
C*****
C
C   READ (NT1,*,END=9000) NUMNP, NTYPE1, NTYPE7
C   NUMEL=NTYPE1+NTYPE7
C   MXFIGS=NTYPE1+3*NTYPE7
C
C   MXFIGS IS THE NUMBER OF CLOSED FIGURES TO BE PLOTTED
C
C   MXNODS=12
C
C   S T O R A G E   M A P
C
C   N1   X(NUMNP)           R8
C   N2   Y(NUMNP)           R8
C   N3   Z(NUMNP)           R8

```

```

C      N3A  DX(NUMNP)           R8      X-TRANSLATION
C      N3B  DY(NUMNP)           R8      Y-TRANSLATION
C      N3C  DZ(NUMNP)           R8      Z-TRANSLATION
C      N4   IELS(MXFIGS)        I4      NUMBER OF NODES PER ELEMENT
C      N5   NOD(MXNODS,MXFIGS)  I4      INCIDENCE TABLE
C      N6   LINKS(MXLINK,2)     I4
C
      MXLINK=2*NTYPE1+28*NTYPE7
      NA=8*6*NUMNP + 4*(MXFIGS+1) + 4*MXNODS*(MXFIGS+1) +
& 4*2*MXLINK
      CALL GETCOR (PARTN,NA)
9000  STOP
      END
      SUBROUTINE PARTN (A,NNA)
      REAL*8 A(1)
      COMMON /CNTL/ NUMNP, MXFIGS, MXNODS, MXLINK, NUMEL, NUMFIG
      NA=NNA/8
C
C      PARTITION STORAGE
C
      N1=1
      N2=N1+NUMNP
      N3=N2+NUMNP
      N3A=N3+NUMNP
      N3B=N3A+NUMNP
      N3C=N3B+NUMNP
      N4=N3C+NUMNP
      N5=N4+(MXFIGS+1)/2
      N6=N5+(MXNODS*MXFIGS+1)/2
      N7=N6+(2*MXLINK+1)/2
      N50=N7
C
      CALL FEMPLT (A(N1), A(N2), A(N3), A(N3A), A(N3B), A(N3C),
& A(N4), A(N5), A(N6))
      RETURN
      END
      SUBROUTINE FEMPLT (X, Y, Z, DX, DY, DZ, IELS, NOD, LINKS)
      COMMON /CNTL/ NUMNP, MXFIGS, MXNODS, MXLINK, NUMEL, NUMFIG
      DIMENSION X(NUMNP), Y(NUMNP), Z(NUMNP), IELS(MXFIGS),
& NOD(MXNODS,MXFIGS), LINKS(MXLINK,2)
      DIMENSION DX(NUMNP), DY(NUMNP), DZ(NUMNP)
C
C*****
C
C      NEXT LINE ADDED BY DJP MARCH 15/84
C
      REAL*8 DUMMY(10),DUMX(1)
C*****
C
      CALL INPUTM (X, Y, Z, IELS, NOD)
      CALL INPUTD (DX, DY, DZ)
      CALL LINK (IELS, NOD, LINKS, NLINKS)
      CALL OUTPUT (X, Y, Z, NLINKS, LINKS, DX, DY, DZ)
      RETURN

```

```

END
SUBROUTINE INPUTM (X, Y, Z, IELS, NOD)
COMMON /CNTL/ NUMNP, MXFIGS, MXNODS, MXLINK, NUMEL, NUMFIG
COMMON /IO/ NT1, NT2
DIMENSION X(NUMNP), Y(NUMNP), Z(NUMNP), IELS(MXFIGS),
& NOD(MXNODS,MXFIGS), INOD(16), INOD1(4)
C
C*****
C
C          NEXT LINE ADDED BY DJP MARCH 15/84
C
C          REAL*8 DUMMY(10),DUMX(1)
C
C*****
C          RAD=ARCOS(-1.)/180.
C
C          INPUT NODAL COORDINATES
C
C          READ (NT1,*) NNP
C          DO 300 I=1,NUMNP
C          READ (NT1,200) X(I), Y(I), Z(I), KODE
200  FORMAT (35X, 3F10.0, 5X, I2)
C          IF (KODE.EQ.0) GO TO 300
C          R=Y(I)
C          PHI=RAD*Z(I)
C          Y(I)=R*COS(PHI)
C          Z(I)=R*SIN(PHI)
300  CONTINUE
C
C          INPUT AND REORGANIZE INCIDENCE TABLE
C
C          I2=0
C          NUMFIG=0
400  IF (NUMEL.LE.0) GO TO 9000
C          I1=I2+1
C          READ (NT1,*,END=9000) NTYPE, NEL, IEL
C          NUMEL=NUMEL-NEL
C          GO TO (1000,2000,3000,4000,5000,6000,7000), NTYPE
C
C          TRUSS ELEMENTS (2 NODES PER ELEMENT)
C
C          1000 I2=I1+NEL-1
C          DO 1500 I=I1,I2
C          NUMFIG=NUMFIG+1
C          IELS(I)=IEL
C          READ (NT1,1100) (NOD(J,I), J=1,IEL)
1100  FORMAT (5X, 2I5)
1500  CONTINUE
C          GO TO 400
C
C          ELEMENT TYPE 2
C
C          2000 GO TO 9900
C

```

```

C     ELEMENT TYPE 3
C
3000 GO TO 9900
C
C     ELEMENT TYPE 4
C
4000 GO TO 9900
C
C     ELEMENT TYPE 5
C
5000 GO TO 9900
C
C     ELEMENT TYPE 6
C
6000 GO TO 9900
C
C     ELEMENT TYPE 7 (PLATE/SHELL ELEMENT)
C
7000 K=IEL/4 + IEL - 4*(IEL/4)
      GO TO (7200,7400,7600,7800), K
C
C     4-NODE ELEMENT
C
C*****
C
C           4 NODE ELEMENT ADDED BY DJP  APR/84
C
C
7200 I2=I1+NEL-1
      DO 7300 I=I1,I2
          NUMFIG=NUMFIG+1
          READ (NT1,7830) DUMX
          READ (NT1,7860) INOD1
          IELS(I)=4
          NOD(1,I)=INOD1(1)
          NOD(2,I)=INOD1(2)
          NOD(3,I)=INOD1(3)
          NOD(4,I)=INOD1(4)
7860 FORMAT (4I4)
7300 CONTINUE
7830 FORMAT(A8)
      GO TO 400
C
C     8-NODE ELEMENT
C
7400 GO TO 9900
C
C     9-NODE ELEMENT
C
7600 GO TO 9900
C
C     16-NODE ELEMENT
C
7800 I2=I1+3*NEL-1
      DO 7900 I=I1,I2,3

```

NUMFIG=NUMFIG+3

```

C
C*****
C
C           NEXT LINE ADDED BY DJP MARCH 15/84
C
C           READ (NT1,7825) DUMMY
7825 FORMAT (10A8)
C
C*****
C
C           READ (NT1,7850) INOD
           IELS(I)=12
           IELS(I+1)=8
           IELS(I+2)=8
           NOD(1,I)=INOD(1)
           NOD(2,I)=INOD(5)
           NOD(3,I)=INOD(6)
           NOD(4,I)=INOD(2)
           NOD(5,I)=INOD(7)
           NOD(6,I)=INOD(8)
           NOD(7,I)=INOD(3)
           NOD(8,I)=INOD(9)
           NOD(9,I)=INOD(10)
           NOD(10,I)=INOD(4)
           NOD(11,I)=INOD(11)
           NOD(12,I)=INOD(12)
           NOD(1,I+1)=INOD(12)
           NOD(2,I+1)=INOD(13)
           NOD(3,I+1)=INOD(14)
           NOD(4,I+1)=INOD(7)
           NOD(5,I+1)=INOD(8)
           NOD(6,I+1)=INOD(15)
           NOD(7,I+1)=INOD(16)
           NOD(8,I+1)=INOD(11)
           NOD(1,I+2)=INOD(6)
           NOD(2,I+2)=INOD(14)
           NOD(3,I+2)=INOD(15)
           NOD(4,I+2)=INOD(9)
           NOD(5,I+2)=INOD(10)
           NOD(6,I+2)=INOD(16)
           NOD(7,I+2)=INOD(13)
           NOD(8,I+2)=INOD(5)
7850 FORMAT (16I4)
7900 CONTINUE
           GO TO 400
C
C           9000 RETURN
C
C           DESTINATION FOR CURRENTLY UNSUPPORTED OPTIONS
C
C           9900 PRINT 9910
           9910 FORMAT (' OPTION NOT CURRENTLY SUPPORTED' )
           STOP
           END

```

```

SUBROUTINE LINK (IELS, NOD, LINKS, NLINKS)
COMMON /CNTL/ NUMNP, MXFIGS, MXNODS, MXLINK, NUMEL, NUMFIG
DIMENSION IELS(MXFIGS), NOD(MXNODS,MXFIGS), LINKS(MXLINK,2)
L=0
DO 1000 I=1,NUMFIG
  IEL=IELS(I)
  DO 200 J=1,IEL
    L=L+1
    K=MOD(J,IEL)+1
    NJ=NOD(J,I)
    NK=NOD(K,I)
    LINKS(L,1)=MIN0(NJ,NK)
    LINKS(L,2)=MAX0(NJ,NK)
  200 CONTINUE
1000 CONTINUE
C   CALL PRINT4 (LINKS,MXLINK,2,L,2,'I4/',1,'BEFORE SORTING/','1')
  CALL SORT (LINKS(1,2), LINKS(1,1), L)
C   CALL PRINT4 (LINKS,MXLINK,2,L,2,'I4/',1,'FIRST SORT/','1')
  CALL SORT (LINKS(1,1), LINKS(1,2), L)
C   CALL PRINT4 (LINKS,MXLINK,2,L,2,'I4/',1,'SECOND SORT/','1')
C
C   NOW ELIMINATE DUPLICATE LINKS
C
  I=1
2000 J=I+1
2200 IF (J.GT.L) GO TO 3000
  IF (LINKS(I,1).NE.LINKS(J,1) .OR. LINKS(I,2).NE.LINKS(J,2))
    &   GO TO 2600
  DO 2400 K=J,L
    LINKS(K-1,1)=LINKS(K,1)
    LINKS(K-1,2)=LINKS(K,2)
  2400 CONTINUE
  L=L-1
  GO TO 2200
2600 I=I+1
  GO TO 2000
3000 CONTINUE
C   CALL PRINT4 (LINKS,MXLINK,2,L,2,'I4/',1,'AFTER COMPRESSING/','1')
  NLINKS=L
  RETURN
  END
SUBROUTINE SORT (LINK1, LINK2, L)
DIMENSION LINK1(L), LINK2(L)
LM1=L-1
DO 800 I=1,LM1
  K=LINK1(I)
  IP1=I+1
  DO 700 J=IP1,L
    IF (LINK1(J).GT.K) GO TO 700
    LINK1(I)=LINK1(J)
    LINK1(J)=K
  K=LINK1(I)
  M=LINK2(I)
  LINK2(I)=LINK2(J)
  LINK2(J)=M

```

```

700 CONTINUE
800 CONTINUE
  RETURN
  END
  SUBROUTINE OUTPUT (X, Y, Z, NLINKS, LINKS, DX, DY, DZ)
  COMMON /CNTL/ NUMNP, MXFIGS, MXNODS, MXLINK, NUMEL, NUMFIG
  COMMON /IO/ NT1, NT2
  LOGICAL FLAG1
  COMMON /FLAGS/ FLAG1
  DIMENSION X(NUMNP), Y(NUMNP), Z(NUMNP), LINKS(MXLINK,2)
  DIMENSION DX(NUMNP), DY(NUMNP), DZ(NUMNP)
  REWIND NT2
  WRITE (NT2) NUMNP, NLINKS
  DO 100 I=1,NUMNP
  WRITE (NT2) X(I), Y(I), Z(I)
100 CONTINUE
  DO 200 I=1,NLINKS
  WRITE (NT2) LINKS(I,1), LINKS(I,2)
200 CONTINUE
  IF (.NOT.FLAG1) GO TO 400
  DO 300 I=1,NUMNP
  WRITE (NT2) DX(I), DY(I), DZ(I)
300 CONTINUE
400 RETURN
  END
  SUBROUTINE INPUTD (DX, DY, DZ)

```

C  
C  
C

```

INPUT THE CARTESIAN COMPONENTS OF THE NODAL DISPLACEMENTS

COMMON /CNTL/ NUMNP, MXFIGS, MXNODS, MXLINK, NUMEL, NUMFIG
COMMON /IO/ NT1, NT2
LOGICAL FLAG1
COMMON /FLAGS/ FLAG1
DIMENSION DX(NUMNP), DY(NUMNP), DZ(NUMNP)
FLAG1=.FALSE.
READ (NT1,*,END=100) (DX(I), DY(I), DZ(I), I=1,NUMNP)
FLAG1=.TRUE.
100 RETURN
  END

```

## BIBLIOGRAPHY

1. Yamaki, N., Elastic stability of circular cylindrical shells, Elsevier Science Publishers B.V., Amsterdam, Netherlands, 1984.
2. Troitsky, M.S., Tubular Steel Structures - Theory and Design, The James F. Lincoln Arc Welding Foundation, Cleveland, Ohio, 1982.
3. Canadian Standards Association, Cold-Formed Steel Structural Members, CSA Standard S136-1974, 1974.
4. American Iron and Steel Institute, Specifications for the Design of Light Gauge Cold-Formed Steel Structural Members, 1980.
5. American Society of Mechanical Engineers, Metal Containment Shell Buckling Design Methods, Case N-284 of the ASME Boiler and Pressure Vessel Code, 1980.
6. Baker, E.H., and Kovalevsky, L., and Rish, F.L., Structural Analysis of Shells, McGraw Hill, Huntington, New York, 1961, pp.220-278.
7. Stephens M.J., and Kukak, G.L., and Montgomery, C.J., Local Buckling of Thin-Walled Tubular Steel Members, Department of Civil Engineering, University of Alberta, Edmonton, Alberta, Structural Engineering Report No. 103, February, 1982.
8. von Karmam, T., The Influences of Curvature on the Buckling Characteristics of Structures, J. Aeron. Sci., Vol. 7, No. 7, 1940.
9. Flugge, W., Die Stabilitat der Kreiszyllinderschale, Ingenieur-Archiv., Vol. 3, 1932; later reference in: Stresses in Shells, Springer-Verlag, New York, New York, 1973, pp. 452-459.
10. Timoshenko, S., and Gere, J., Theory of Elastic Stability, McGraw Hill, New York, New York, 1961, pp. 482-485, 541.
11. Seide, P., and Weingarten, V.I., On the Buckling of Circular Cylindrical Shells Under Pure Bending, Trans. ASME, Vol 83, Series E, March, 1961, pp. 112-116.

12. Brazier, L.G., On the Flexure of Thin Cylindrical Shells and Other Thin Sections, Proceedings of the Royal Society of London, Series A, Vol. 116, 1927.
13. National Aeronautics and Space Administration, Buckling of Thin-Walled Circular Cylinders, NASA Space Vehicle Design Criteria (Structures), NASA SP-8007, 1968.
14. Gerrard, G., Compressive and Torsional Buckling of Thin-Walled Cylinders in the Yield Region, NACA TN-3726, 1956.
15. Masubuchi, K., Analysis of Welded Structures, Pergamon Press, New York, New York, 1980.
16. Weingarten, V.E., and Morgan, E.J., and Seide, P., Final Report on Development of Design Criteria for Elastic Stability of Thin Shell Structures, Space Technology Laboratories, Inc., STL/TR-60-0000-19425, 1960.
17. Gerrard, G., and Becker, H., Handbook of Structural Stability, part III, Buckling of Curved Plates and Shells, NACA, TN 3783, 1957. Weingarten, V.E., and Morgan, E.J., and Seide, P., Elastic Stability of Thin-Walled Cylindrical and Conical Shells Under Axial Compression, AIAA J., Vol. 3, No. 3, 1965.
18. Donnell, L.H., A New Theory for the Buckling of Thin Cylinders Under Axial Compression and Bending, Trans. ASME, Vol. 56, 1934, AER-56-12.
19. von Karman, T., and Tsien, H.S., The Buckling of Thin Cylindrical Shells Under Axial Compression, J. Aeron. Sci., Vol. 8, No. 8, 1941.
20. Koiter, W.T., On the Stability of Elastic Equilibrium, Thesis, Technical University Delft, Amsterdam, 1945; English Translation: Air Force Flight Dynamics Laboratory, Air Force Systems Command, Wright-Patterson Air Force Base, Ohio, Technical Report AFFDL-TR-70-25, 1970.
21. Almroth, B.O., Influence of Imperfections and Edge Constraint on the Buckling of Axially Compressed Cylinders, NASA CR-432, 1966.
22. Tennyson, R.C., and Muggeridge, D.B., Buckling of Axisymmetric Imperfect Circular Cylindrical Shells Under Axial Compression, AIAA J., Vol. 7, No. 11, 1966.

23. Koiter, W.T., Elastic Stability and Postbuckling Behaviour, Proc. of the Sympos. on Nonlinear Problems, Ed., Langer, R. E., Univeristy of Wisconsin Press, 1963, p. 257.
24. Bathe, K.J., Finite Element Procedures in Engineering Analysis, Englewood Cliffs, N. J., Prentice-Hall, 1982.
25. Bathe, K.J., and Bolourchi, S. , A Geometric and Material Nonlinear Plate and Shell Element, Computers & Structures, Vol. 11, No. 1-2, February 1980, pp. 23-48.
26. Malvern, L. E., Introduction to the Mechanics of a Continous Medium, Prentice-Hall, Englewood Cliffs, New Jersey, 1969, pp.220-263.
27. Fung, Y. C ., Foundations of Solid Mechanics, Prentice-Hall, Englewood Cliffs, New Jersey, 1965, pp.91-115.
28. Ramm, E., Strategies for Tracing Nonlinear Response Near Limit Points, Europe-U.S.-Workshop:, 'Nonlinear Finite Element Analysis in Structural Mechanics', Bochum, July 28-31, 1980.
29. Ramm, E., A plate/shell element for large deflections and rotations Formulations and Computational Algorithms in Finite Element Analysis, Bathe, K.J., and Oden, J.T., and Wunderlich, W., (eds.), M.I.T. Press, 1977.
30. Krakeland, B., Large displacement analysis of shells considering elastic-plastic and elasto-visoplastic materials, Report No. 776, The Norwegian Institute of Technology, The University of Trondheim, Norway, December 1977.
31. Riks, E., The Application of Newton's Method to the Problem of Elastic Stability, J. Appl. Mech., Vol. 39, 1972, pp. 1060-1066.
32. Riks, E., An Incremental Approach to the Solution of Snapping and Buckling Problems, Int. J. Solid Struct., Vol. 15, 1979, pp. 529-551.
33. Wempner, G.A., Discrete Approximations Related to Nonlinear Theories of Solids, Int. J. Solid Struct., Vol. 7, 1971, pp. 1581-1591.

34. Crisfield, M.A., A Fast Incremental/Iterative Solution Procedure that Handles 'Snap-Through', Proc. Symp. on 'Computational Methods in Nonlinear Structural and Solid Mech.', Washington, D.C., October, 1980.
35. Wessels, M., Das statische und dynamische Durchschlags-problem der imperfekten flachen Kugelschale bei elastischer rotations symmetrischer Verformung, Dissertation, TU Hannover, 1977, Mitteil. Nr. 23 des Instituts fur Staik.
36. Hutchinson, J., Axial Buckling of Pressurized Imperfect Cylindrical Shells, AIAA Journal, Vol 3, No. 8, Aug. 1965, pp. 1461-1466.
37. Deming, W.E., Statistical Adjustment of Data, Dover Publications, New York, New York, 1964.
38. International Mathematical and Statistical Library Edition 9, Interpolation:Approximation:Smoothing, IMSL Inc., Edited by, Computer Center, University of Manitoba, 1983.
39. de Boor, C., A Practical Guide to Splines, Springer-Verlag, Inc., New York, New York, 1978.
40. Pinkney, R.B., and Stephens, M.J., and Murray, D.W., and Kulak, G. L., Use of measured imperfections to predict the buckling of axially loaded cylindrical shells, Canadian Journal of Civil Engineering, Vol. 10, No. 4, December 1983, pp. 662-669.
41. Kula, E., and Weiss, V., Residual Stress and Stress Relaxation, Pleunum Press, New York, New York, 1982.
42. Blodgett, O.W., Design of Welded Steel Structures, The James F. Lincoln Arc Welding Foundation, Cleveland, Ohio, 1966.
43. Arbocz, J., The Imperfection Data Bank, A Means to Obtain Realistic Buckling Loads, Buckling of Shells: A State-of-the-Art Colloquim, Institut fur Baustatik, University of Stuttgart, May 6-7,1982.
44. Troitsky, M.S., Design Guidelines for Steel Tubular Thin-Walled Structures, 4th Progress Report, Canadian Steel Industries Construction Council Project No. 724, January, 1974.